Copyright Warning & Restrictions

The copyright law of the United States (Title 17, United States Code) governs the making of photocopies or other reproductions of copyrighted material.

Under certain conditions specified in the law, libraries and archives are authorized to furnish a photocopy or other reproduction. One of these specified conditions is that the photocopy or reproduction is not to be "used for any purpose other than private study, scholarship, or research." If a, user makes a request for, or later uses, a photocopy or reproduction for purposes in excess of "fair use" that user may be liable for copyright infringement,

This institution reserves the right to refuse to accept a copying order if, in its judgment, fulfillment of the order would involve violation of copyright law.

Please Note: The author retains the copyright while the New Jersey Institute of Technology reserves the right to distribute this thesis or dissertation

Printing note: If you do not wish to print this page, then select "Pages from: first page # to: last page #" on the print dialog screen

ABSTRACT

AN INVESTIGATION OF THE EFFECT OF SONIC FREQUENCY IN THE REMOVAL OF VOLATILE ORGANIC COMPOUNDS FROM SOILS USING A SIREN-PNEUMATIC FRACTURING COUPLED TECHNIQUE

by
Chin-Yu Lin

This study investigates the effect of frequency from sonic energy coupled with soil fracturing for the removal of volatile organic compounds from low permeability soils. The laboratory experiments consisted of a test cell, 12 ½ inches by 12 ½ inches and 23 ¾ inches high, containing a ½ inch geotextile made to simulate the fracture. The pneumatic sound generator used was a siren type generator designed and built at NJIT.

Laboratory experiments were performed using the NJIT siren at frequencies of 2957, 6637, 10317, 13997 Hertz and baseline tests with no sound energy were also conducted. The free moisture content was measured by weight loss over time and the concentration of the contaminant was measured by using gas chromatography with a Flame Ionization Detector. These measurements were monitored frequently throughout the experiments. The results of this study at different frequencies were analyzed and correlated and were also compared with the results obtained by Fernandez (1997) using the NJIT siren and the whistle. The measurements agreed with those of Fernandez and showed a slight increase in the removal rate constant with a rise in frequency but this improvement was not significant.

It was concluded that within the range of frequencies studied, no significant improvement in removal rate can be attributed to frequency. It is recommended that the siren should be reconfigured to operate at higher frequencies (20 kHz) and much higher sound intensities (> 145 dB).

AN INVESTIGATION OF THE EFFECT OF SONIC FREQUENCY IN THE REMOVAL OF VOLATILE ORGANIC COMPOUNDS FROM SOILS USING A SIREN- PNEUMATIC FRACTURING COUPLED TECHNIQUE

by
Chin-Yu Lin

A Thesis
Submitted to the Faculty of
New Jersey Institute of Technology
In Partial Fulfillment of the Requirements for the Degree of
Master of Science in Environmental Science

Department of Chemical Engineering, Chemistry and Environmental Science

January 1999

APPROVAL PAGE

AN INVESTIGATION OF THE EFFECT OF SONIC FREQUENCY IN THE REMOVAL OF VOLATILE ORGANIC COMPOUNDS FROM SOILS USING A SIREN- PNEUMATIC FRACTURING COUPLED TECHNIQUE

Chin-Yu Lin

Dr. Deran Hanesian, Thesis Advisor — Date
Professor of Chemical Engineering, NJIT

Dr. Angelo J. Perna, Committee Member — Date
Professor of Chemical and Environmental Engineering, NJIT

Dr. John R. Schuring, Committee Member — Date
Professor of Civil and Environmental Engineering, NJIT

BIOGRAPHICAL SKETCH

Author: Chin-Yu Lin

Degree: Master of Science

Date: January 1999

Undergraduate and Graduate Education:

- Master of Science in Environmental Science
  New Jersey Institute of Technology
  Newark, New Jersey, 1999

- Bachelor of Science in Chemical Engineering
  New Jersey Institute of Technology
  Newark, New Jersey, 1996

Major: Environmental Science

To thesis is dedicated to David
and my family

ACKNOWLEDGEMENT

I wish to give express my deepest appreciation to my advisor, Dr. Deran Hanesian for his inspiration and guidance as well as his patience and knowledge in making the completion of this research work possible.

I thank Dr. Angelo Perna and Dr. John Schuring for serving as members of the committee, and for their motivation, support and help throughout this research project. Special thanks are also extended to Jannina Alvarez, Clint Brockway, Hugo Fernandez, and Tom Boland for their valuable knowledge and technical help in the laboratory.

I thank the members of the Pneumatic Fracturing Team, Heather Hall, Michael Galbraith and Brian Sielski for their support, encouragement and help.

Finally, I wish to acknowledge my fiancé, Dr. David Nassimi and my family for their love, support, and encouragement throughout the pursuit of this degree.

TABLE OF CONTENTS

TABLE OF CONTENTS

(Continued)

Chapter **Page**

LIST OF TABLES

LIST OF FIGURES

LIST OF SYMBOLS

A = Exposed Surface Area for Drying (m^2 or ft^2)

a = Proportionality Constant

B = Sound Intensity Level (dB)

dt = Differential Change in Time (hours, minutes or seconds)

dx = Differential Change in Free Moisture Content $\left(\frac{kg\ H_2O}{kg\ dry\ Solid}\ or\ \frac{lb_m\ H_2O}{lb_m\ Dry\ Solid}\right)$

g_c = Gravitational Conversion Factor $\left(1.0\frac{kg \cdot m}{N \cdot s^2}\ or\ 32.2\frac{lb_m \cdot ft}{lb_f \cdot s^2}\right)$

f = Frequency of the Sound Wave (h^{-1} or m^{-1} or s^{-1})

I = Intensity (Newton-meters per m^2 or Joules per second or Watts per m^2)

I_o = Intensity Reference Standard, 10^{-12} Watts per m^2

I_s = Intensity of Sound at Source (Newton-meters per m^2 or Joules per second or Watts per m^2)

k = Removal Rate Constant

K.E. = Kinetic Energy (Newton-meters or lb_f-ft)

m = Mass of the Medium (lb_m)

PPMv = Parts per Million by Volume

LIST OF SYMBOLS

(Continued)

R	=	Rate of Drying $\left(\frac{kg\ H_2O}{m^2, h} \text{ or } \frac{lb_m\ H_2O}{ft^2, h}\right)$
r	=	Amplitude (m or ft)
ρ	=	Density of the Medium (kg per m^3 or lb_m per ft^3)
t	=	Time (hour or minute or second)
v	=	Velocity the Sound Wave (m/s or ft/s)
W	=	Total of Weight of Solids (kg or lb_m)
W_s	=	Total Weight of Dry Solid (kg or lb_m)
X	=	Free Moisture Content (kg per kg or lb_m per lb_m)
x	=	Thickness of Air Layer (m or ft, Equation 2.13)
x	=	Distance from Sound Source (in or ft, Equation 2.16)
X_0	=	Initial Free Moisture Content (kg per kg or lb_m per lb_m)
X_1	=	Final Free Moisture Content (kg per kg or lb_m per lb_m)

CHAPTER 1

INTRODUCTION

1.1 Overview

Due to the increased usage of chemicals in the petroleum and chemical industries and in government facilities, significant amounts of hazardous wastes have been generated in the past decades. The lack of awareness of the potential of the hazardous wastes to impact negatively on human health and the environment led to mishandling and poor disposal practices.

Facing the need to stop further improper release of hazardous waste, a series of environmental laws were enacted. These laws include the Resource Conservation and Recovery Act (RCRA) of 1976, the Comprehensive Environmental Response Compensation and Liability Act (CERCLA) of 1980, and the Superfund Amendments and Reauthorization Act (SARA) of 1986.

The initiatives to clean up contaminated sites required by the laws and by using existing technologies exist. However, the amount of time and the cost required for clean up and the effectiveness of each technology varies. The current available technologies can be expensive and time consuming. Thus, the remedial method presented in this thesis targets the decontamination of hazardous wastes (volatile organic compounds) in soil, *in situ*.

A new patented technology called pneumatic fracturing was developed at the Hazardous Substance Management Research Center (HSMRC) at the New Jersey Institute of Technology (NJIT). The process involves the injection of high pressure

air into the soil to increase the permeability of a formation, allowing for a faster removal rate of the hazardous waste from the soil.

The feasibility of utilizing pneumatic based ultrasonic devices coupled with pneumatic fracturing in enhancing the removal of volatile organic compounds from soils was investigated previously (Fernandez, 1997). Laboratory bench scale studies of two selected sonic generators, a siren and a whistle, were used in his investigation. The research presented in this study is to further demonstrate the feasibility of the removal of VOC's from low permeability soil, utilizing sonic energy generated by a siren and also the effect of frequency.

1.2 Research Objective and Scope

Although remediation of contaminated soil using ultrasound energy is a relatively new technology its potential to achieve the clean up goal is promising. With many different types of pneumatic sound generators available, the study is complex.

The objective of this research is to study the effect of frequency from sonic energy for the removal of volatile organic compounds from low permeability soil. The pneumatic sound generator used in this study is a siren type generator designed and constructed at NJIT. Laboratory scale tests are to be performed using the siren at different frequencies to determine the degrees of enhancement achieved with each frequency. The result of the tests will then be compared to the results from the control runs where sonic energy is not applied.

CHAPTER 2

BACKGROUND OF STUDY

2.1 Overview of the Current *In Situ* Remediation Technologies

There are many remediation technologies available today for the treatment of contaminated soils. The two categories include *in situ* and *ex situ* treatment technologies. *In situ* treatment technologies are techniques that treat contaminants right on the site without excavating or moving the soil. *Ex situ* treatment technologies unlike the *in situ* treatment, require the removal of the contaminated soils from the subsurface and transport to a treatment facility on or off site for treatment.

Since *in situ* remediation treats the contaminants in place, there's no extra cost associated with the transport of the contaminated soils. Some of the current *in situ* technologies available for the treatment of volatile organic compounds include soil flushing, solidification, stabilization, degradation, soil vapor extraction, volatilization and chemical and biological treatment.

2.2 *In Situ* Remediation Enhancement Technologies

One of the most often used enhancement associated technologies that is currently used in the remediation of tight soil is soil fracturing. Soil fracturing is performed by administering a fluid, which is at a higher pressure than the consolidation pressure of the geologic formation to open up a fracture radially or vertically with respect to the

formation. This process is followed by injection of a granular material to keep the fracture open. There are currently three types of fracturing in use for *in situ* remediation and these are hydraulic fracturing, explosive fracturing, and pneumatic fracturing (Marks 1994).

Soil fracturing is used to enhance the removal of the VOC's from impacted soil. A fracture is a void in a tightly packed geologic formation. Where it does not exist naturally, fracturing the formation pneumatically can create this void space. When air is injected into the fractured formation, it travels through the open void space, the path of least resistance. Any moisture on the top of the fracture will evaporate into the air stream as the air injected into the formation passes through and leaves the soil. As the fractured soil is being dried by the air, this process lends itself to the analysis by the classical drying theory.

2.3 Basic Drying Theory

2.3.1 Typical Drying Curves

The drying process discussed in this section is concerned with the removal of the VOC's from the sand in the experimental tank. Drying, in general, is usually referred as the removal of relatively small amounts of liquid from the material, and evaporation means removal of large amounts of liquid from the material.

The removal of liquids from a solid material can be divided into four regions, according to the classical drying theory (Geankopolis, 1993). Figure 2.1 shows the four regions of a plot of the free moisture content versus time and the rate of drying versus free moisture content. The first region of the drying process, as shown in

Figure 2.1 (a), from point A to B, is very short. At time zero, the initial temperature of the solid is normally colder than its ultimate temperature, and the evaporation rate increases as the temperature rises and the process reaches the second region. If the initial temperature of the solid is high, then the process may start at point A′. As the process reaches point B of the curve, the surface temperature rises to its equilibrium temperature.

The second region, also referred to as the *constant-rate-of-drying* region, is the straight line labeled from point B to C. During this time, the process of drying is at a constant rate, the surface of the solid is initially very wet and a film of water is continuously seen on the surface. The water is simply removed from this surface film and the water acts as if no solid is present. The slope and hence, the rate during point B to C are constant as shown in Figure 2.1(a) as a straight line. The drying rate starts to decrease as the process reaches point C, the critical free moisture content, on the curve. At this time, the surface of the solid is no longer wet since there is insufficient amount of water to maintain a continuous film of water on the surface of the solid. During this period, the entire surface is not completely wet, and the wetted area progressively decreases. The drying process continues until it reaches point D. In this first falling-rate region, the rate of drying is often linear as a function of moisture content until it reaches point D. This CD line is called the *falling-rate* period as shown in Figure 2.1(a).

The last segment of the Drying-Rate Curve is another rapid fall in the rate of drying starting from point D when the surface is completely dry until it reaches point

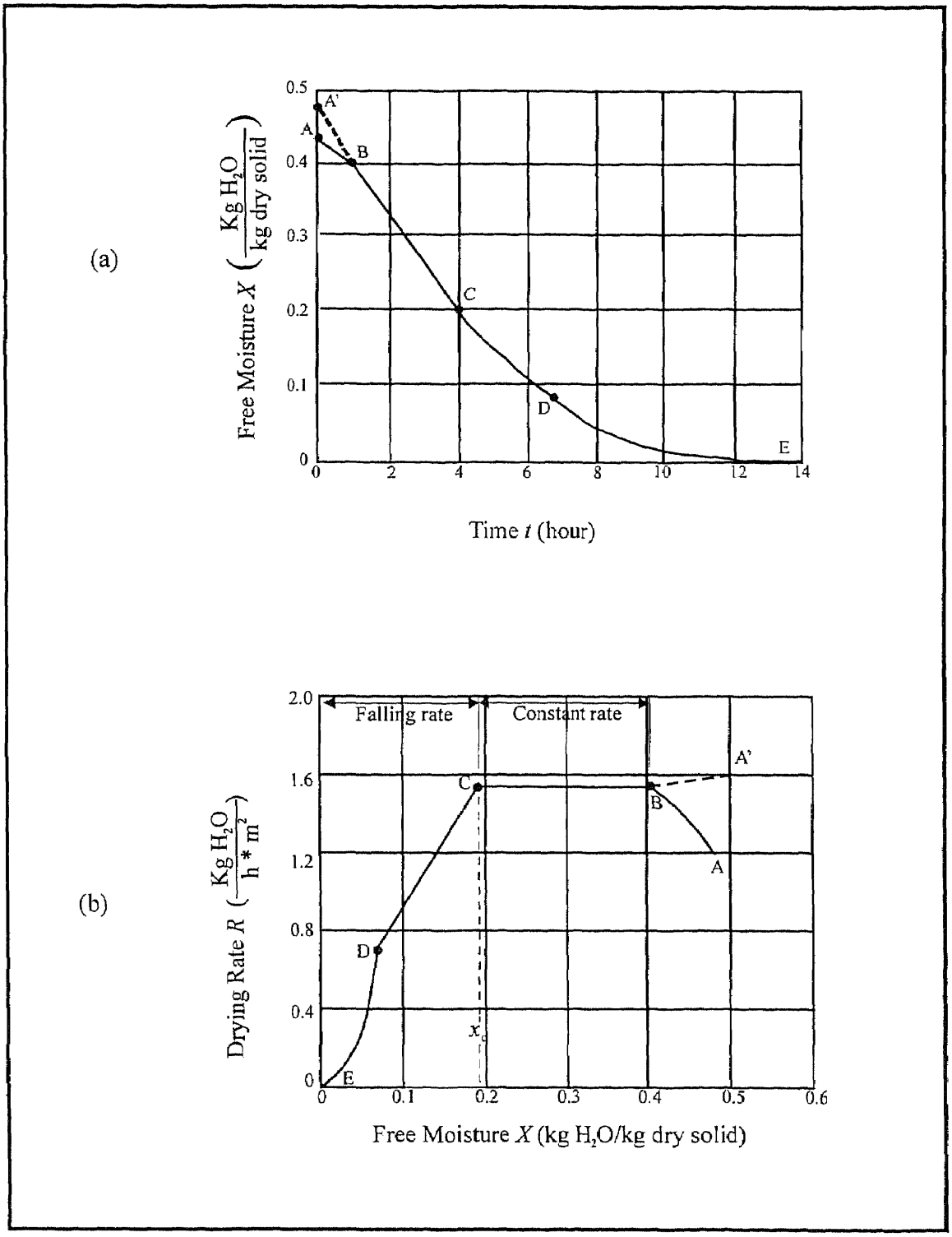

Figure 2.1 Typical Drying-Rate Curve from Geankoplis (1993). (a) Plot of Data as Free Moisture Versus Time (b) Rate of Drying Curve as Rate Versus Free Moisture Content

E, where the equilibrium moisture content is reached. In this region, the plane of evaporation gradually recedes away from the surface. The heat necessary for evaporation is now transferred through the solid to the plane of evaporation. The vaporized water must move through the solid to the solid surface and be removed by the airflow. In some cases, depending on the material being dried, the falling-rate period (line CD) may be missing completely or it may constitute all of the falling-rate period. In the case of the missing of point D, there will be only one line from C to E, omitting point D completely, forming the falling rate period.

2.3.2 Drying Theory

As described by the Typical Drying Rate Theory (Geankoplis 1993), normally the data from drying processes are collected from the laboratory experiments where the solids to be dried are mixed with a known amount of liquid and the weight is monitored as it dries. The free moisture content is defined as the fraction of the weight of the moisture remaining in the solids divided by the weight of the dry solid as expressed in the following equation:

$$X = \frac{W - W_s}{W_s} \tag{2.1}$$

Using this variable, the rate of removal is given by:

$$R = -\frac{W_s}{A}\frac{dX}{dt} \tag{2.2}$$

where R is the removal rate, W_s and A are constants. For the constant drying period,

Equation 2.2 becomes,

$$\int_{x_0}^{x_1} dX = -\frac{RA}{W_s}\int_0^t dt \tag{2.3}$$

and

$$X_1 - X_0 = -\frac{RA}{W_s}t \tag{2.4}$$

showing the free moisture content to be linear with time in the Constant Rate Period. For the Falling Rate region, it can be assumed that the rate is a linear function of the moisture content. Hence,

$$R = a\,X \tag{2.5}$$

Substituting Equation 2.5 into Equation 2.2 gives,

$$R = aX = -\frac{W_s}{A}\frac{dX}{dt} \tag{2.6}$$

or

$$\int_{x_0}^{x_1}\frac{dX}{X} = -\frac{aA}{W_s}\int_0^t dt \tag{2.7}$$

Hence,

$$\ln\frac{X_1}{X_0} = -\frac{aA}{W_s}t \tag{2.8}$$

or

$$X_1 = X_0 e^{-\frac{aA}{W_s}t} \tag{2.9}$$

The constant $\frac{aA}{W_s}$ can be represented by k, the removal rate constant as shown in the following equation,

$$X_1 = X_0 e^{-kt} \tag{2.10}$$

Equation 2.10 predicts a semi logarithmic correlation for the Falling Rate Region.

2.4 Overview of the Sonic Generator Selected and the Effect of Frequencies

Extensive studies of the principals and structural designs of different sonic generators have been discussed (Fernandez, 1997). This section will give a very general overview of sonic generators and the effect of frequency on the rate of drying.

Many types of sound generators are available today. According to the physical properties that allow the radiation of ultrasound, the transducers are divided into 5 main categories including electrostatic, electrodynamic, magnetostrictive, piezoelectric, and pneumatic transducers (Manthey and Kroemer, 1992).

For the purpose of this investigation, the selected sonic generator is in the category of pneumatic transducers. Pneumatic transducers are further divided into static and dynamic generators and these transducers produce sound waves of air. The siren, the sonic generator used in this research, is a dynamic generator. The basic principle governing this type of generator is that when a jet of air is periodically interrupted by a rotating device, resulting puffs of air set up condensations (regimes of high pressure) and rarefactions (regimes of low pressure) in the air stream. The result is the generation of sound waves with frequencies which are proportional to the

number of interruptions that the jet air is subjected to in a period of one second. Thus, the frequency is the number of the revolutions per second times the number of perforations per row on both the rotator and the stator, which are perfectly aligned (Allen 1947 and Wood 1937). These aligned perforations per row give the number of interruptions per revolution. Each interruption represents a cycle of rarefaction and condensation. The intensity of the sound generated by this type of generator depends on the amount of gas that is "blocked off" when the jet of air is interrupted and, hence, depends on the space between the rotator and the stator (Allen, 1959).

The intensity of a sound is defined as the rate of transfer of the vibrational energy per unit of area of the wave (Hausman and Slack, 1939). Intensity depends on both the amplitude which is the maximum displacement of the vibration from its mid position, and the frequency of the wave, or the number of vibrations per second. Consider a layer of air of thickness, x, and of unit cross sectional area. If v, is the velocity of wave propagation, then the kinetic energy is,

$$\text{K.E.} = \frac{1}{2}\frac{mv^2}{g_c} \tag{2.11}$$

The mass of material is the density of the medium, ρ, times the volume which is (x)(1). Furthermore, the velocity of the propagating wave is,

$$v = 2\pi rf \tag{2.12}$$

Therefore, the kinetic energy, in Newton-meters, becomes,

$$K.E. = \frac{1}{2}\frac{mv^2}{g_c} = \frac{\rho(x)(1)}{2g_c}(2\pi rf)^2 \tag{2.13}$$

The total energy or the energy density of the wave, in Newton-meters per m^3 or

Joules per m^3 is,

$$\frac{K.E.}{(x)(1)} = 2\pi^2 r^2 f^2 \rho \tag{2.14}$$

If the wave is traveling at a velocity of v, m/s, then the rate of transfer of vibrational energy is

$$\text{Intensity}, I = v \cdot \left(\frac{K \cdot E}{x \cdot 1} \right) = 2\pi^2 r^2 f^2 \rho v \tag{2.15}$$

in Newton-meters per m^2 per second or Joules per m^2 per second, or Watts per m^2. Hence, the intensity is proportional to the square of both the frequency and the amplitude.

In reality, the energy density of wave varies inversely as the square of the distance from its source. Since the energy density is proportional to the square of the amplitude, r, it follows that the amplitude of the wave will vary inversely as the distance from the source and, therefore, the intensity in a given medium at a given velocity of propagation and given frequency will decline with distance, x, from the source. A measure of this decay in sound energy is the attenuation coefficient. The intensity of sound at a distance from the source is given by,

$$I = I_s \exp(-\alpha x) \tag{2.16}$$

The sound intensity level is normally measured in decibels. Hence,

$$B = 10 \log_{10} I / I_0 \tag{2.17}$$

where the constant, I_0, is the reference standard and is the threshold of human hearing, 10^{-12} watts per m^2 (Sears, Zemansky and Young, 1987) and is the faintest intensity that can be heard by human ears.

CHAPTER 3

EXPERIMENTAL APPROACH

The objective of this research is to determine the effect of frequency on the removal of volatile organic compounds from soil using the siren coupled with pneumatic fracturing. The tests were conducted in the laboratory with both the siren and the soil testing cell constructed at NJIT.

The approach was to pack a known amount of sand in the test cell (see Figure 3.2) containing an artificial fracture made out of geotextile material aligned where the holes of the siren were located. Two PVC pipes with ¾ inch diameter were inserted into the tank to serve as extraction pipes to remove the effluent gas containing contaminants from the tank. The monitoring of the loss of moisture by weight over time was recorded by an electronic scale system and the concentration of the contaminant (a mixture of Ethyl alcohol and water) was analyzed by a gas chromatograph using a flame ionization detector (FID). Based on the measured data and the drying theory described in Chapter 2, conclusions were made on the effectiveness of the siren and the change of frequency.

3.1 Setup of Experimental Apparatus

Most of the experimental equipment and the apparatus set up used in this research are adopted from those used by Fernandez in his studies on a siren unit (Fernandez 1997). Some minor modifications were made to the apparatus and they will be discussed in the following sections of this chapter. Figure 3.1 will serve as a guide

for an overview of the process of the experiment. The measured data collected were the weight of the test cell and the concentration (parts per million by volume, PPMv) of ethanol in the exiting stream.

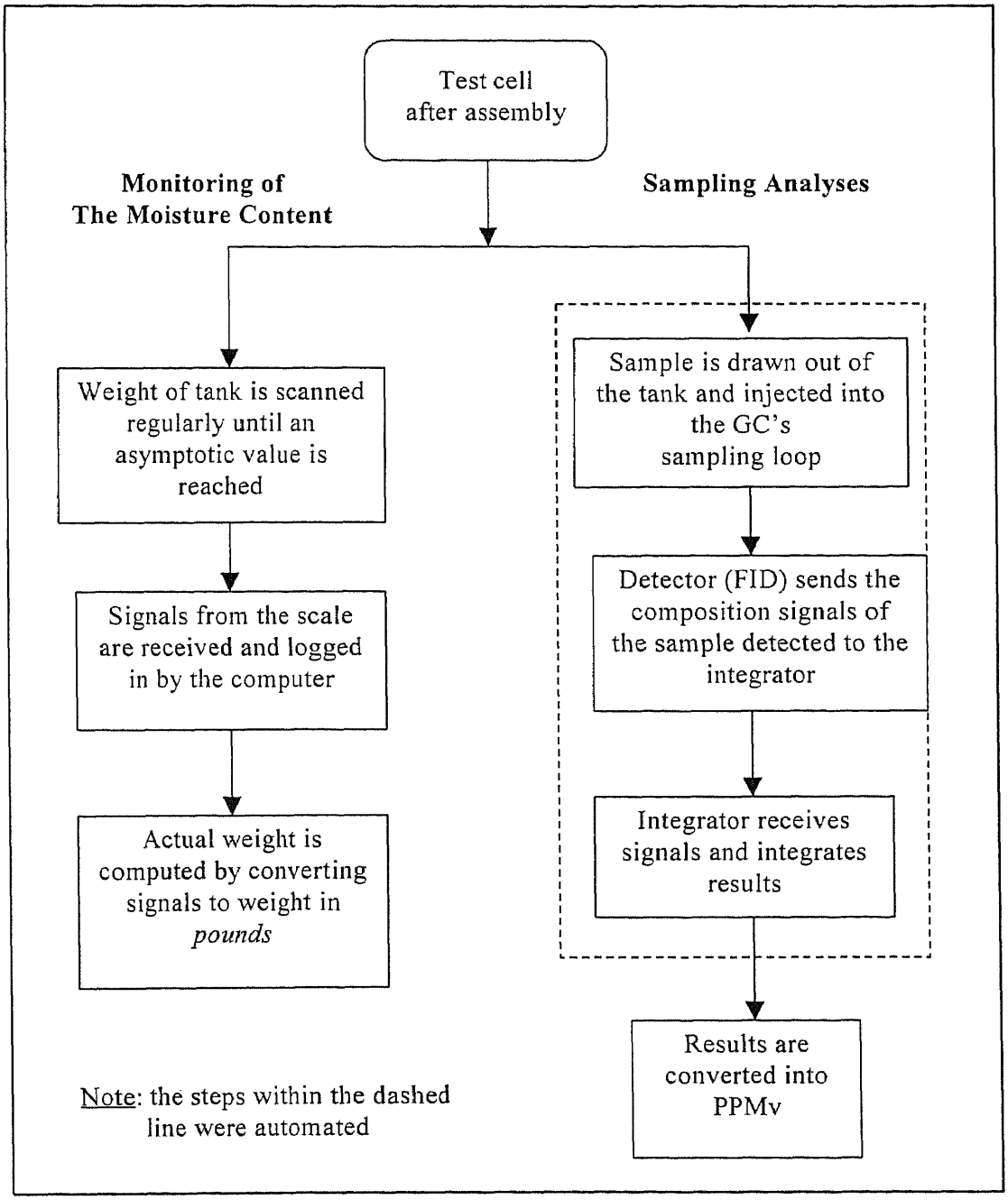

Figure 3.1 Overview of the Experimental Process

3.1.1 Setup of Experimental Tank

The tank (test cell) used for the experiment was made out of acrylic Plexiglass constructed at NJIT as used by Fernandez (1997). The shape of the tank is rectangular, 12 ½ inches square by 23 ¾ inches in height with a base attached to the tank made out of an 18 inch square by ¾ inch thick piece of acrylic plexiglass.

The cover of the tank was constructed with 2 square pieces of plexiglass, one is 11 inches square and the other one is 12 ½ inches square and ¾ inch thick. Both tank cover pieces have a center hole of 3 inches in diameter and other smaller holes for the extraction pipes. These Plexiglass covers were then bonded together by using Rez-N-Bond acrylic bonding compound. The edges of the tank were secured by placing angle iron to keep the tank safe under pressure (See Figures 3.2 and 3.3). During each experimental run, after the tank was packed, the tank cover was sealed by using Silicone II sealant for window and doors.

After the assembly of the tank, chlorinated polyvinyl chloride (CPVC) pipes were attached to the extraction pipes coming out of the tank. The pipes allow effluent gas to exit the tank and go into the gas chromatograph for analysis and in-house treatment (See Figure 3.2).

3.1.2 Setup of Electronic Scale System

The electronic scale system was used to monitor the measurements of the weight of the moisture in the experimental tank. The scale system was built by using 2 square pieces of aluminum plates sandwiching three electronic load cells (See Figure 3.4).

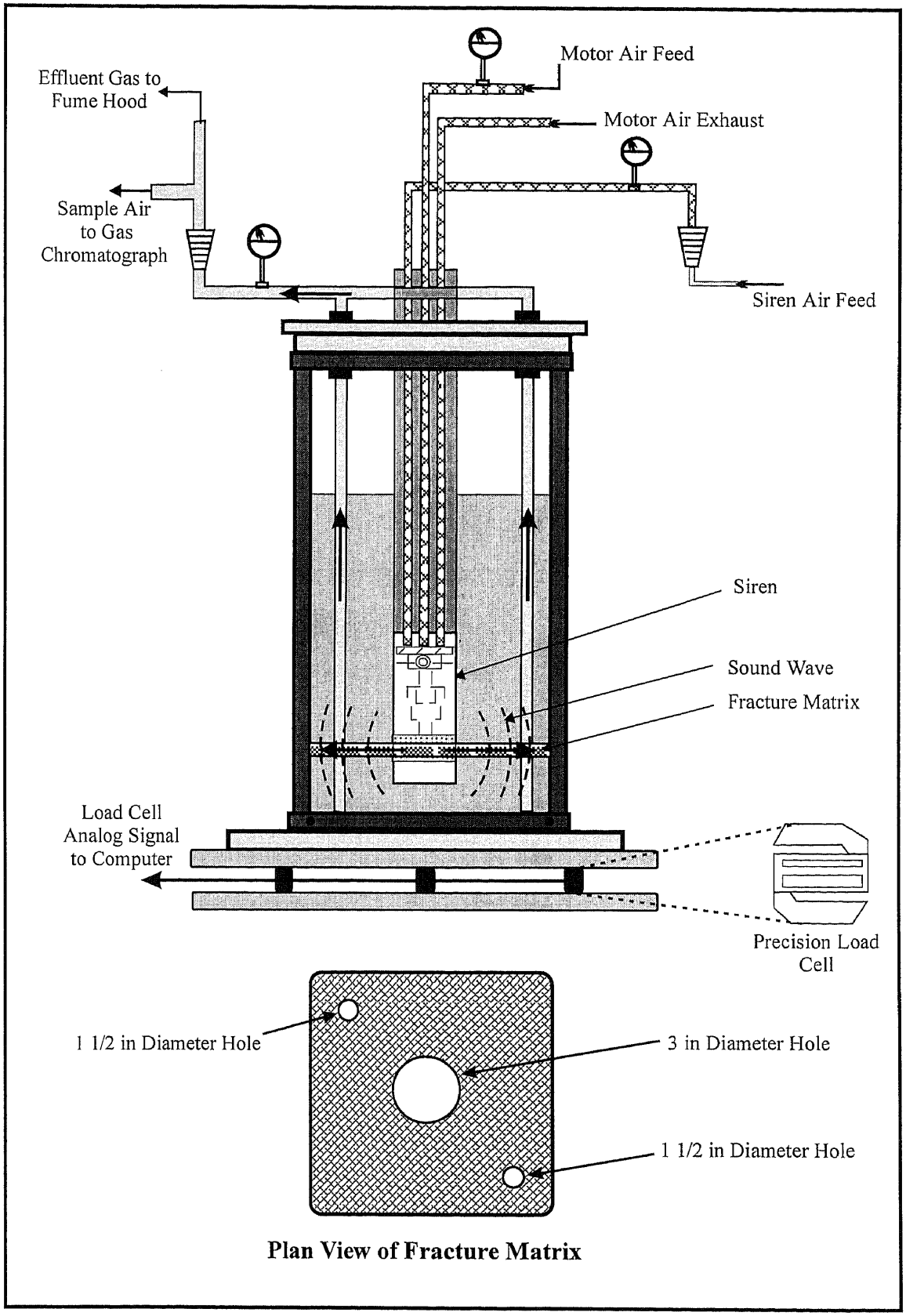

Figure 3.2 Apparatus Design

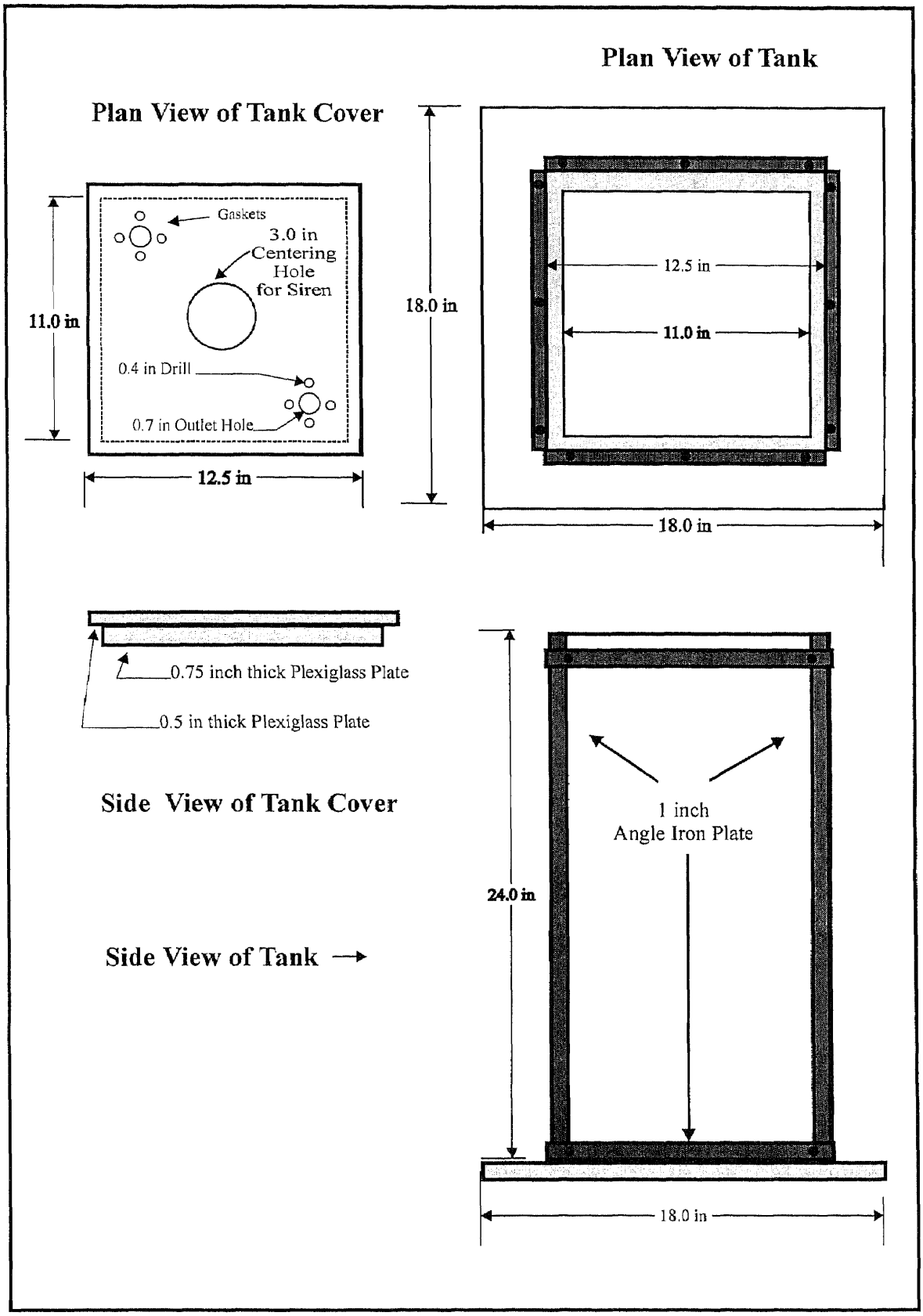

Figure 3.3 Experimental Tank Design

The electronic signals were then sent to a computer terminal and the data collected from the computer were converted into units of pounds.

The square aluminum plates were 20 inches square by ½ inch thick, purchased from Roncocas Metal Corporation in Roncocas, New Jersey. The electronic load cells were GSE model number 5353 (See Figure 3.5). The GSE Precision Load Cells were placed in a triangular arrangement between the aluminum plates. A Radio Shack DC regulated power supply of 13.8 volts was used to excite the load cells. A built in Wheatstone bridge inside each of the load cells provided a resistance to the voltage, which varied with weight. Each of the voltages generated by the load cells was transferred separately to a terminal block, Model Number 707 (DT707). The signals were then sent to a data translation system, the XL-System, purchased from Elexor Associates located in Booton, NJ. The signals were translated into a series of numbers, which were then converted into readings in the unit of *pounds*. The weight of the tank was monitored throughout the experiment with readings taken regularly.

3.1.3 Sample Analysis

The monitoring of the concentration of the volatile organic compounds (VOCs) in the tank throughout the experiment was important. For the purpose of this study, a gas chromatograph (GC) was used by attaching it to the extraction line coming out of the tank as shown on Figure 3.2.

Many steps were involved in the process of sample analysis (shown within the dash boundaries in Figure 3.1) and samples were drawn out of the exiting stream frequently (Tables B.4 to B.8). Therefore, the process of analyzing the concentration

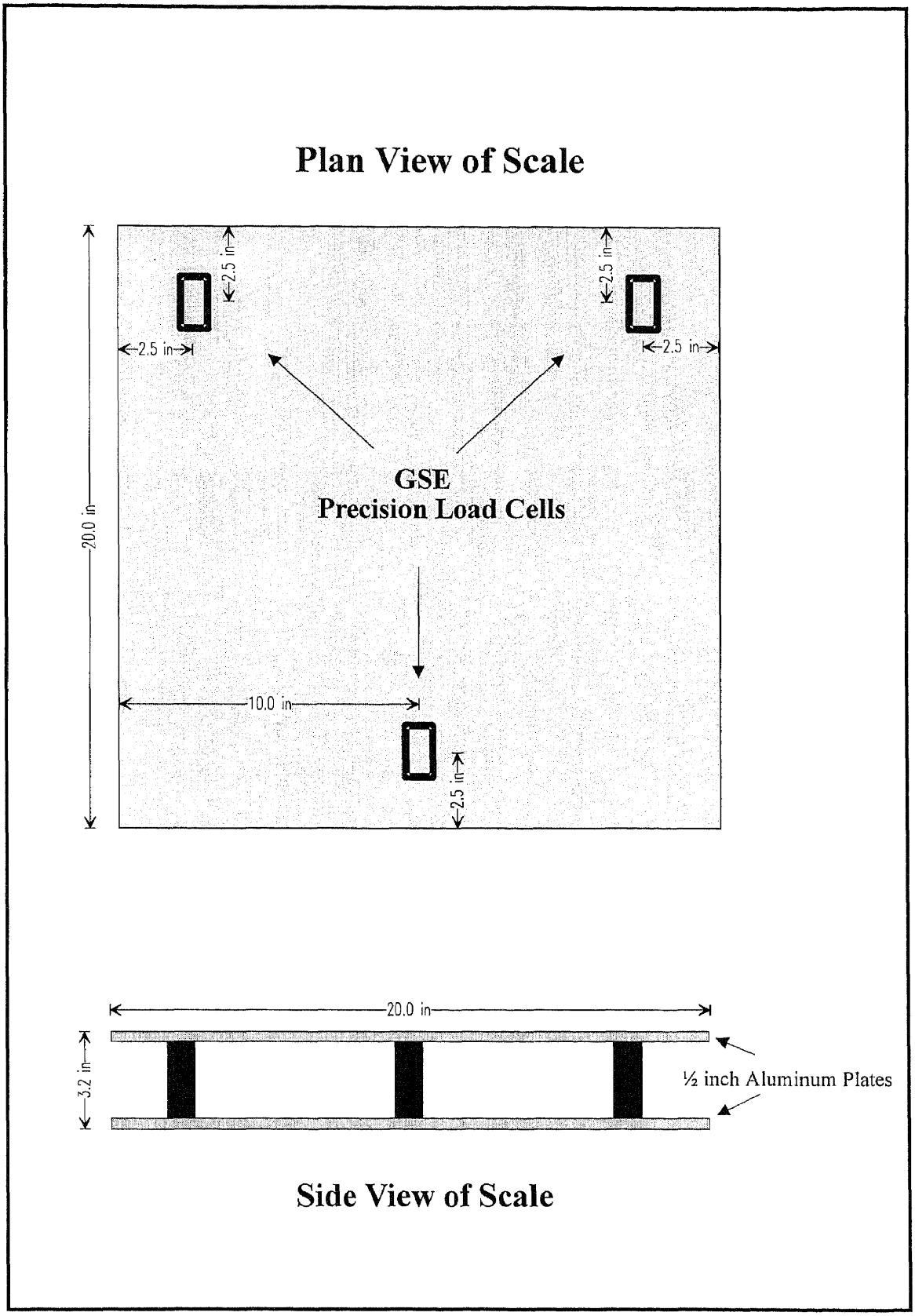

Figure 3.4 Electronic Scale System

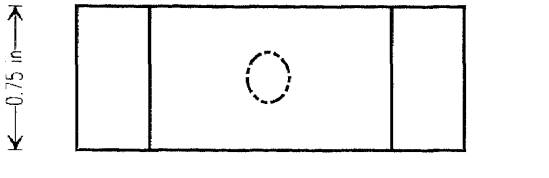

Plan View of Cell

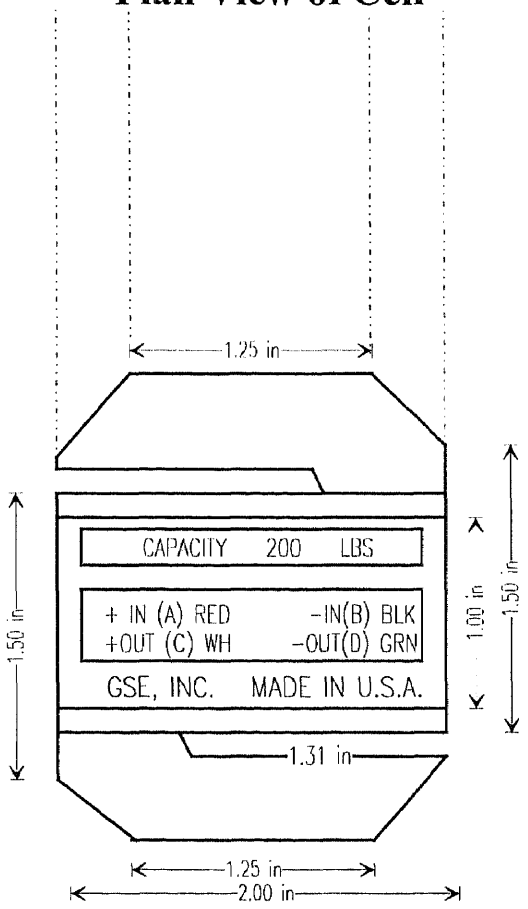

Side View of Cell

Figure 3.5 Precision Load Cell

of the VOCs was automated by using a Digital Valve Sequence Programmer (DVSP) by Valco Instruments (See Appendix D).

Chromatography, one of the most important techniques in environmental analysis, is a method used for separating very small quantities of complex mixtures. The amount of each component in the sample is measured as it leaves the column, by passing the effluent through a detector and integrating the detector signal over time. For quantification, the detector signal is fed into an integrator, producing a typical plot of signal versus time, as a series of peaks. The peak areas produced by the integrator relate to the quantity and the identity of each compound in the sample.

For the purpose of this research, attached to the GC is a Flame Ionization Detector (FID) which is sensitive to organic compounds and shows good sensitivity. To obtain the reading of the concentration of the outlet air exiting from the tank over time, an integrator was connected to the GC and produced a series of signals. These signals form a series of chromatographs with the area under the peaks listed. To determine the concentration of the samples, the areas under the peaks obtained from the integrator were converted into concentration readings in units of Parts Per Million by volume (PPMv) by using the equation obtained from the calibration of the GC. See Figure 3.6 for the GC calibration Curve and Appendix B for sample calculations.

The GC model used for this research was a Varian 3700 and Matheson Gas Product Particle Filter model number 6120 with a 0.2 micron efficiency connected to the extraction line of the outlet of the experimental tank. The sample gas stream was fed into a 3 milliliter sampling loop. The six-way valve system, which includes the sampling loop, feeds the contents of the loop into the GC's column for analysis.

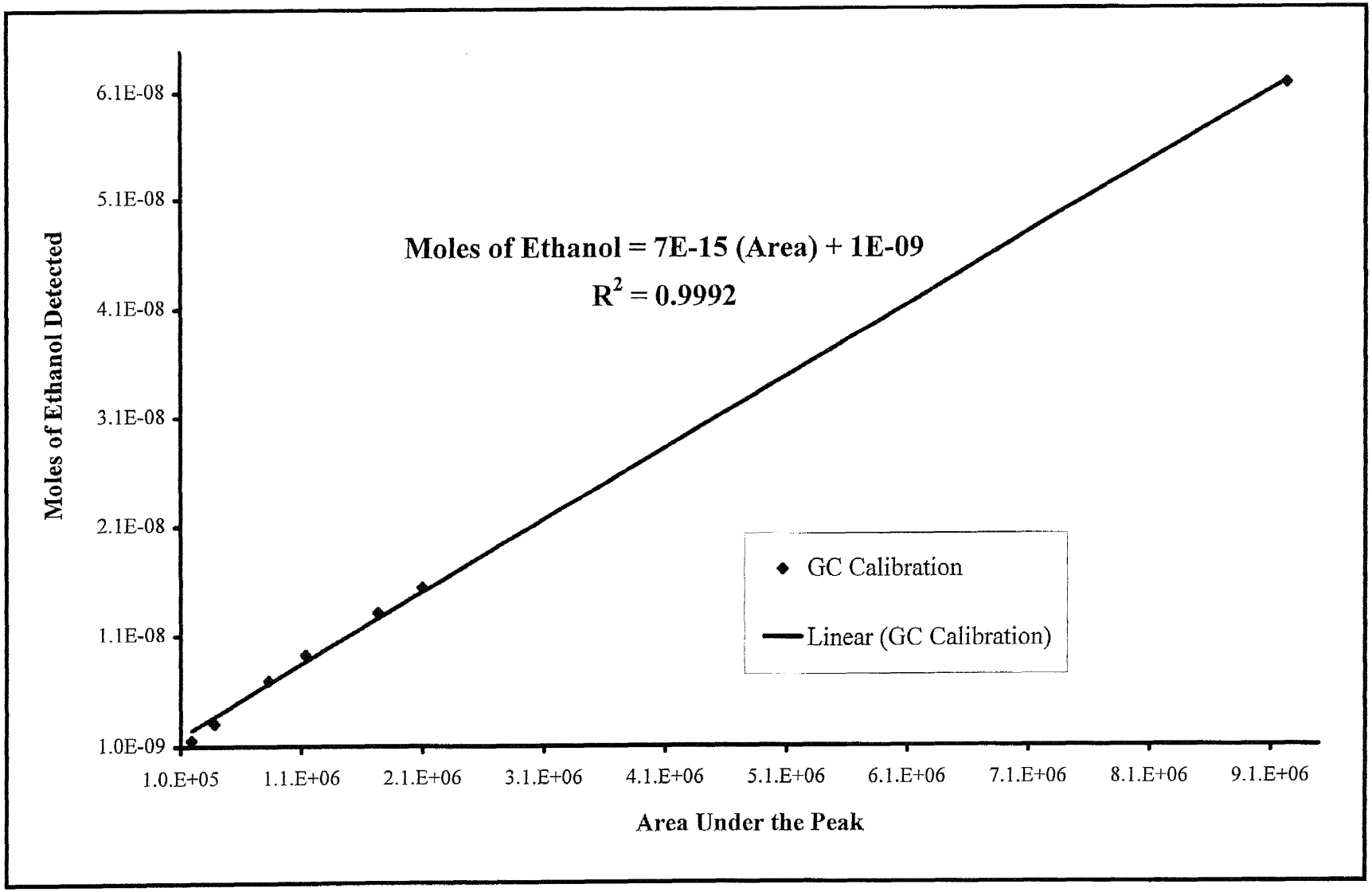

Figure 3.6 Calibration of the Gas Chromatograph

When loaded, the contents of the loop are fed into the column by the carrier gas, which is Nitrogen gas at 30 milliliters per minute. The GC's column is made of Carbopack with a length of 10 feet and a diameter of $^1/_8$ inch. The flow rate of the air and the hydrogen gas used for the FID were set at 330 milliliter per minute and 30 milliliter per minute, respectively. The temperature of the column was set at 70 degrees Centigrade and remained constant, and this temperature successfully separated the water vapor and ethyl alcohol from the gas sample to be analyzed. The sample in the loop along with the carrier gas was fed to a flame ionization detector (FID). The FID burned the hydrocarbons and generated signals that were sent to the integrator. The integrator, HP model 3396A, integrated the signals received from the detector into a series of peaks along with the areas integrated under the peaks. These areas correspond to the concentration of the ethanol solution in the effluent gas fed into the sampling loop. By using the calibration equation, the concentrations were calculated (See Figure 3.6).

3.1.4 Siren Design

The siren used for this research was constructed at NJIT, is the same device as used in the research studies done by Fernandez (1997). It is based on the concept of Allen and Rudnick (1947), stating that when a jet of air is periodically interrupted by a rotating device, the result is a sound wave whose frequency in Hertz is given by the product of the number of revolutions per second of the rotating device and the number of interruptions per revolution.

The siren was built by using a pneumatic motor with a rotator attached to it (see Figure 3.7). The motor with the attached rotator is then encased in a hollow cylinder, 3 inches in diameter, which is open at one end. Both the casing and the rotator contain 56 radial perforations per row in 6 rows which can be perfectly aligned. These holes each have a diameter of 2.1 millimeters and are equally spaced. Air is fed from the top of the cylinder casing through a ¼ inch Swagelock opening. After the siren was assembled, it was calibrated with a Digital Stroboscope Model Number 1965 by setting a known inlet air pressure and measuring the number of revolutions per minute generated by the motor. A linear equation was obtained for the calibration of the siren (See Figure 3.8, from Fernandez, 1997). From Figure 3.8, the speed of the siren at given air pressures fed into the motor can be determined and the frequency (Hertz) of the sound wave can be calculated.

When the pneumatic motor is in operation, the rotator rotates at a number of revolutions per minute (calculated by using the equation in Figure 3.8). The number of holes in each row of the stator and the rotator are sequentially aligned and non-aligned. Thus, when the holes are aligned, the air passes through freely creating a rarefaction (regime of low pressure) in the air stream. When the holes are not aligned, the air does not pass through freely creating a condensation (regime of high pressure). This combination of a condensation and a rarefaction constitutes a cycle of high and low pressure creating the sonic wave. With 56 holes per row, there are thus 56 cycles in each revolution and if this number is multiplied by the revolutions per second, the result is the frequency of the sound wave in Hertz.

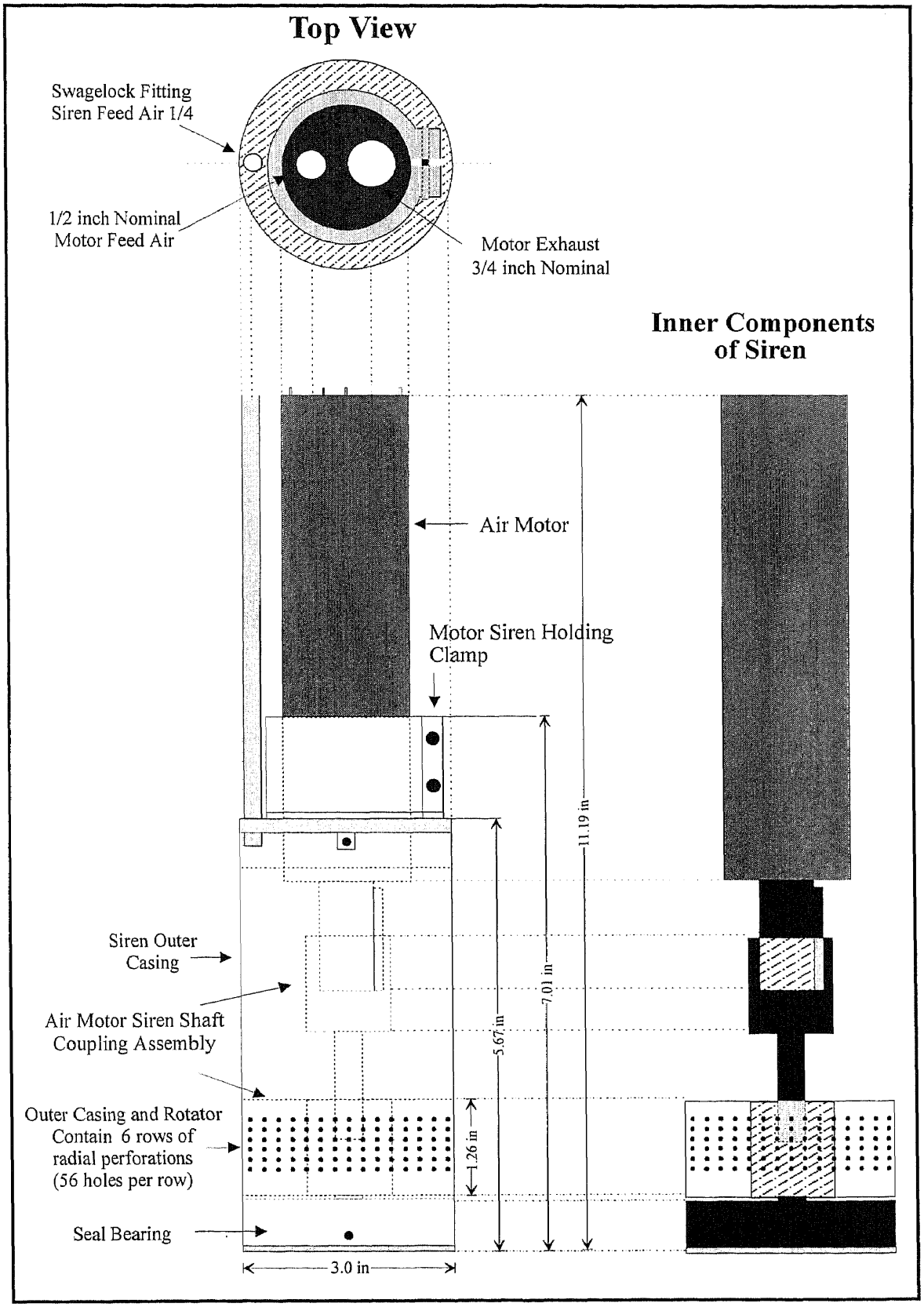

Figure 3.7 NJIT Siren Design from Fernadez (1997)

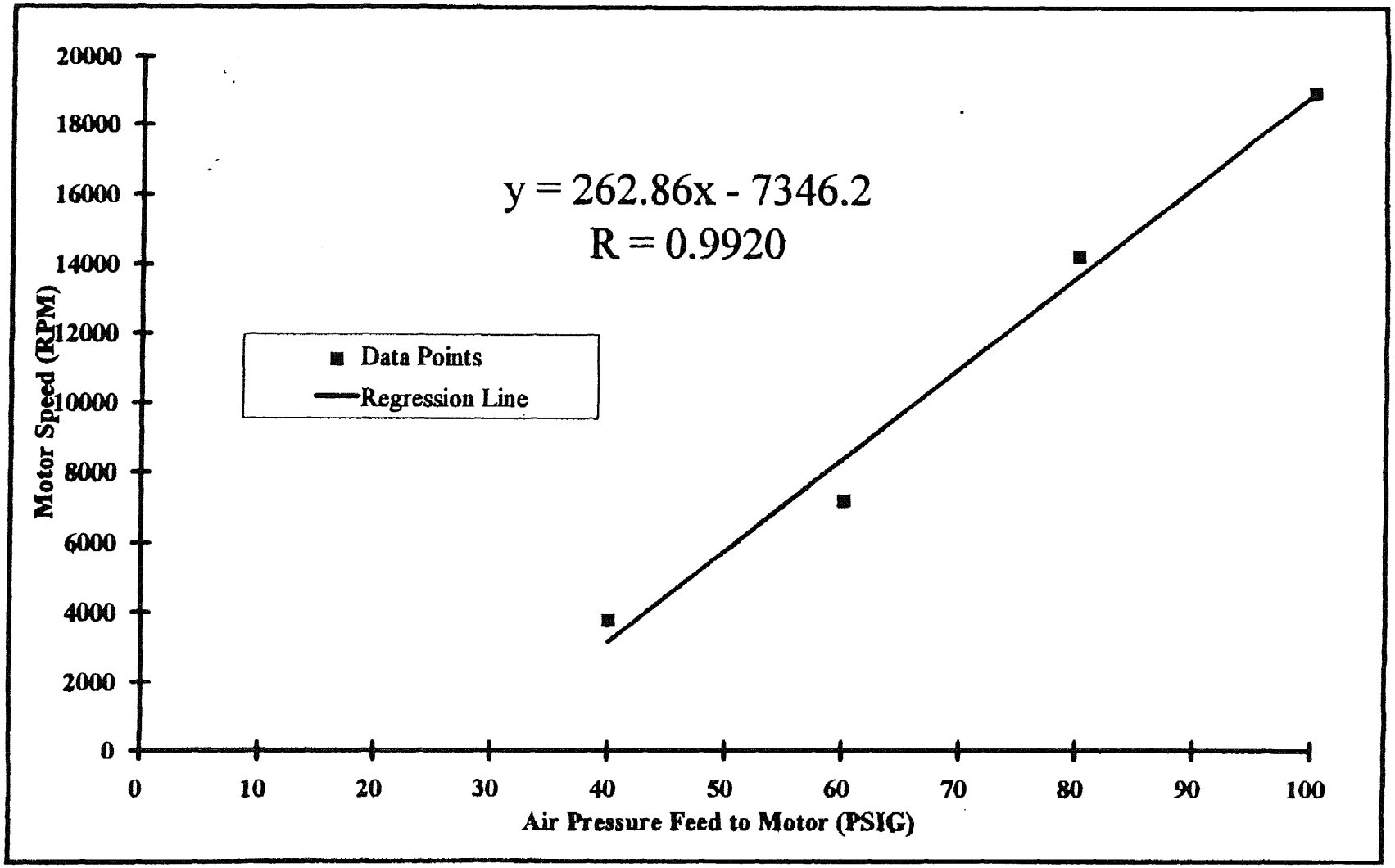

Figure 3.8 Siren Air Motor Calibration Line from Fernandez (1997)

The siren is located at the center of the tank at a height of 3 inches from the bottom with the perforations aligned with the geotextile fracture. To operate the siren, high pressure air at 40 psig to 85 psig (setting the frequency of the siren at 2,957 to 13,997 Hertz) was fed to the motor. Table 3.1 lists the important characteristics of the NJIT Siren.

Table 3.1 NJIT Siren Performance Characteristics

Siren Characteristics		Operational Parameters		
Outer Diameter (Inches)	**Number of Holes per Row**	**Inlet Motor Air Pressure (PSIG)**	**Motor Speed (RPM)**	**Frequency (Hertz)**
3.0	56	40	3,168	2,957
3.0	56	55	7,111	6,637
3.0	56	70	11,054	10,317
3.0	56	85	14,997	13,997
3.0	56	100	18,940	17,677

3.2 Experimental Procedure

The experiment was designed to start with 5 pounds of liquid moisture content and 95 pounds of 00-grade dry sand. The five pounds of liquid solution were composed of 4.5 pounds of water and 0.5 pounds of sample solution with the following components, 5% methanol, 90% ethanol, and 5% isopropyl alcohol by volume.

Before assembling the experimental unit, the water and the sample solution were mixed then poured into the dry sand and mixed carefully to ensure uniformity. To start the process of packing the tank, first the electronic scale was set up then the tank was placed on top of the scale. With the contaminated sand packed tightly to the 3 inch mark, the sandwiched layer of geotextile material was placed on top of the

sand. The extraction pipes and the sonic equipment were then placed in the end and the center of the tank respectively. Then the rest of the sand was placed in the tank, covering the pipes and the siren device. To ensure uniform packing density of each run, the sand was packed tightly and the height of the total packing extended to approximately 16 inches from the base of the tank. After packing the sand into the tank, it was sealed with silicon sealant and left undisturbed for 24 hours, allowing the sealant to dry out and the excess liquid to migrate to the bottom of the tank near the artificial fracture.

The experiment was then initiated by setting the inlet airflow rate at 7.0 standard cubic feet per minute (SCFM) and the pressure of the air feeding the siren at various settings. The sonic experiments were run under different frequencies, ranging from approximately 2,957 Hertz to 13,997 Hertz (air feed pressure ranging from 40 to 85 psig). Equipment limitations prevented higher frequency tests. During the experiment, the concentration of the outlet airflow and the weight of the tank were monitored. The sample analysis data were measured for approximately 30 to 50 hours and the moisture content weight was collected for approximately 60 hours (at intervals of every 60 seconds), depending on the amount of time required for the removal of the contaminants from each test run.

Following the siren runs at various frequencies, two baseline test runs were conducted. This was accomplished by using a 3 inch diameter PVC pipe with a similar perforation pattern as the siren, placed in the middle of the tank instead of the siren.

The siren motor was run at various speeds ranging from 3168 to 18940 revolutions per minute (2,957 to 13,997 Hertz). The inlet air fed into the siren was set at 7 standard cubic feet per minute at pressures ranging from 45 to 50 psig and the outlet flow rate of the air was measured to be 80 inches of water. The extraction pipes at the opposite corners of the tank allowed the air and vapors and the liquids in the soil to leave the tank by the pressure gradient (See Figure 3.2). The concentration of the contaminants and the weight of the free moisture were monitored as discussed in Sections 3.1.2 and 3.1.3.

The 00-sand used for 13,997 Hertz run was different in size from the rest of the test runs. The Grain Size Analyses using a standard method (ASTM D 1140-54) of the two different sands were compared as shown on Figure 3.9. The original sand was used for all of the experimental runs except for the run performed at a frequency of 13,997 Hertz.

Figure 3.9 compares the original and the new sand. The percent of sand passing through each sieve is plotted on the graph versus the particle size diameter. The results show that there isn't a significant difference in the particle size of the two different sands. The new sand, which was used only for the siren test run at 13,997 Hertz, appears to be only slightly coarser than the original sand. See Appendix E for the equipment and standard U.S. sieve sizes used and other details involving the particle size analysis of the sands.

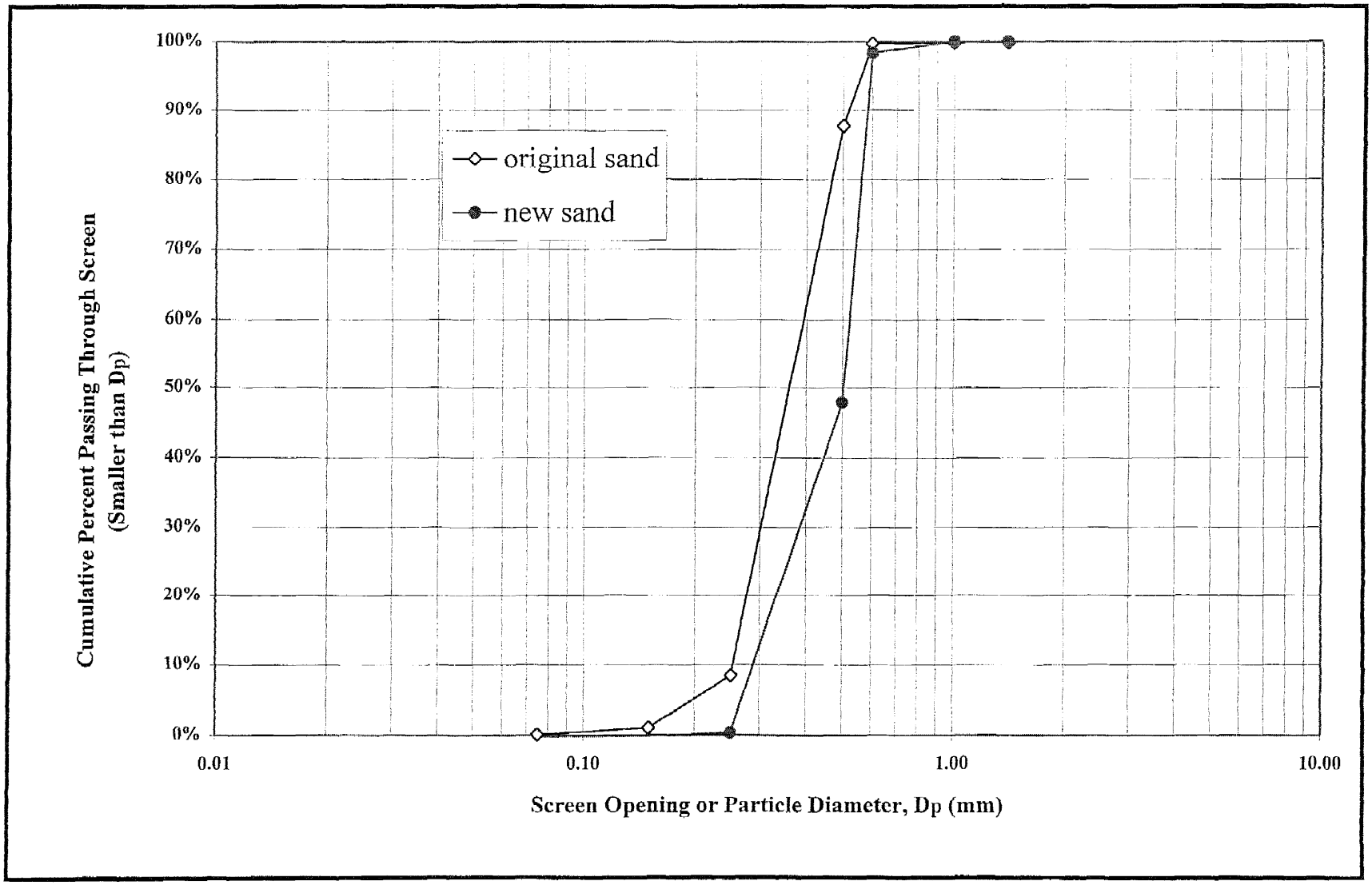

Figure 3.9 Grain Size Comparison of the Two Sands

CHAPTER 4

EXPERIMENTAL RESULTS AND DISCUSSION

Experimental test runs were conducted using the NJIT siren as well as baseline test runs (where the siren was not used). The frequency of the experimental test runs ranged from zero for the baseline test runs and approximately 2,957 to 13,997 Hertz for the siren test runs. For each run, the loss of the free moisture content in the test cell was recorded over time and the concentration of the soil contaminant in parts per million by volume (PPMv) in the effluent stream was also monitored frequently.

4.1 Data Analysis Method

4.1.1 Moisture Loss Over Time

The contaminants (moisture) in the sample were a mixture of water and ethyl alcohol and for each experimental test run, the weight of the free moisture content in the test cell was monitored. The weight of the test cell was recorded by the signals sent from the electronic scale system (as discussed in Section 3.1.2) to the computer, where the data were logged into a file. The reading of the weight of the tank was recorded at every 60 seconds for a period of 30 to 60 hours depending on the test run. The signals gathered by the computer were then converted into units of pounds. Knowing the weight of the moisture in the tank over time, the rate of the loss of the free moisture content is shown by plotting the free moisture content in the tank (Pounds of Contaminant per Pounds of Dry Sand) versus time (Hours), as predicted by the Drying-Rate Curve discussed in Chapter 2. The raw data, which were collected at 60 seconds intervals were then reduced

by taking a five minute average. The averaged data were then plotted versus time. Equation 10 as derived in Chapter 2 was used to correlate the data by plotting the averaged data over time on semi logarithmic coordinates and the corresponding slopes, intercepts, and coefficients are displayed on each graph. Sample calculations for the free moisture content and the correlations are shown in the Appendix (Figures A.1 to A.24).

4.1.2 Concentration of Ethanol Over Time

As discussed in Section 3.1.3, the monitoring of the concentration of the contaminants in the effluent stream was performed by using a gas chromatograph attached to the outlet of the test cell. The effluent stream of the test cell carries the contaminants (mixture of ethanol and water) in gas form as they exit the tank. As the signals from the detector which was connected to the GC were sent to the integrator, the integrator plotted out a series of numbers representing the areas under the peaks. The areas given by the integrator each represents a concentration of a contaminant, as detected by the detector (the Flame Ionization Detector was the choice of detector for its ability to detect volatile organic compounds).

The sampling of the outlet gas was monitored and recorded frequently, especially during the Constant Rate of Drying Period. Therefore, for the first few hours of each experiment, the Digital Valve Sequence Programmer (DVSP) was set to take readings of the concentration of the gas stream exiting the test cell at every 15 minutes. During the Falling Rate Period, the samples were analyzed less frequently until the concentration of the outlet gas reached asymptotic level, which is approximately 30 to 40 hours from the initial time of the start of the experiment (see Tables B.4 to B.8).

The data (areas under the peaks) collected from the integrator were then converted into units of parts per million by volume (PPMv) by using the linear equation obtained from the GC calibration curve. Then the concentrations of the contaminants in PPMv were plotted versus time. The behavior of the data showed a trend that called for the breaking of the curve into 2 separate regions, as discussed in Chapter 2 by the theory behind a typical drying process. Thus, the curve is divided into a constant rate and a falling rate region. In the constant rate region where the concentration is dropping, the time range is about 0 to approximately 1 to 3 hour. The data were plotted on linear coordinates versus time with corresponding coefficients displayed on each graph. The remaining data fall in the *falling rate* region where the slope is constant. In this region, the concentration of ethanol is plotted versus time in semi logarithmic form. Sample calculations, tables and plots of the results and the correlations for the concentration of the contaminant are found in Appendix B.

4.2 Discussion of Results

In this section, the results will be discussed and correlated to determine the effect of the frequency of the siren on the removal rate of the contaminant, the time required to reach asymptotic value and the estimated penetration depth in the drying process. Each aspect of the study is discussed in greater detail in the following sections.

4.2.1 Effect of Frequency

The operating range of the siren in this study was set at approximately 2,957 to 13,997 Hertz because of equipment limitations. The purpose of this study is to find the effect of

the change in frequency with respect to the behavior of the moisture contaminant and its removal rate over time. The weight loss and the concentration of ethanol are the variables used for monitoring the effect of frequency. Experimental test runs using the siren were performed with four different frequencies in the range of 2,957 to 13,997 Hertz and one in the baseline *mode*.

4.2.1.1 Weight Loss of the Moisture: Figures A.1 to A.24 found in Appendix A are the results of the free moisture content versus time plots in four different frequencies (2957, 6637, 10317, 13997, and baseline test runs). Figures A.1 to A.8 represent graphs of the measured free moisture content data plotted versus time. Free moisture content is the fraction of moisture remaining in the test cell at a given time. All of the graphs show the same trend as discussed in the Basic Drying Theory in Chapter 2. In the beginning of the test run, the moisture removal rate is very rapid and as it reaches the falling rate region, the removal rate slows down and eventually reaches asymptotic value.

The measured free moisture content data were further reduced by taking the average at every 5 minutes and plotted versus time as shown in Figures A.9 to A.16. To obtain a correlation, the averaged free moisture content data were plotted versus time on a semi logarithmic plot using an exponential curve fit and setting the known appropriate initial values as the y-intercept. The appropriate corresponding coefficients, as shown on Figures A.17 to A.24, are displayed on each graph. The graphs are in the form of Equation 2.10,

$$X_1 = X_0 e^{-kt}$$

where k is the removal rate constant (hr^{-1}), t is time (hour), X_0 is the initial free moisture content , and finally X_1 is the free moisture content at time t. Table 4.1 shows the summary of the removal rate constant coefficients obtained from the correlations of the averaged free moisture content data versus time as shown in Figures A.17 to A.24. The correlation coefficients for these measurements were excellent.

Table 4.1 Removal Rate Constants of Free Moisture Content versus Time

Siren Frequency (Hertz)	Removal Rate Constant k, hr^{-1}	Correlation Coefficient, R^2
Baseline (Run 1)	0.0324	0.9378
Baseline (Run 2)	0.0388	0.8767
2,957 (Run 1)	0.0418	0.9847
2,957 (Run 2)	0.0562	0.9357
6,637 (Run 1)	0.0443	0.8952
6,637 (Run 2)	0.0468	0.9610
10,317	0.0390	0.9678
13,997	0.0784	0.9278

Figure 4.1 is a correlation of the removal rate constants of free moisture constants versus time obtained from this study in comparison to the results of the studies performed by Fernandez (1997) using the NJIT Siren and the Whistle. The correlation for the whistle with a slope of $9x10^{-6}$ showed a greater removal rate than that demonstrated by the results of the siren, which yielded $2x10^{-6}$ for both Fernandez and this study.

However, the siren, operated at a total frequency range of 0 to 14,946 Hertz, showed no great significant difference between the results obtained by Fernandez (0 to 14,946 Hertz) and this study (0 to 13,997 Hertz). Both of the siren data were further

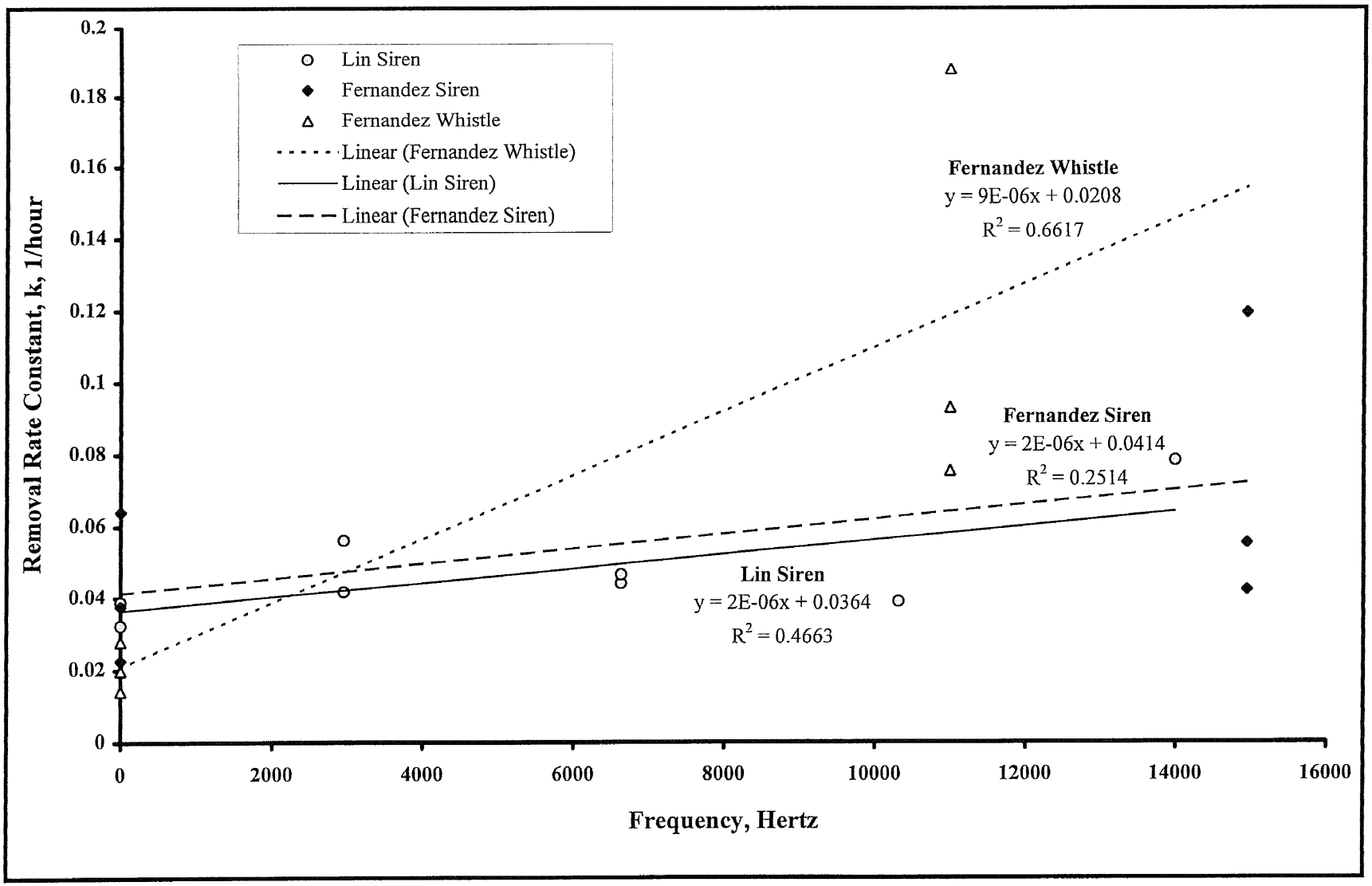

Figure 4.1 Comparison of All Removal Rate Constants versus Frequency

correlated in Figure 4.2, yielded a slope of $2x10^{-6}$. Hence, there appears to be only a very small increase in the removal rate constant as frequency rises and the correlation coefficients are poor (R^2 is 0.3112 and $R^2 = 0.4663$).

4.2.1.2 Concentration of Ethanol Versus Time: Figures B.1 to Figures B.15 found in Appendix B are different graphs of concentration of ethanol versus time using the data collected from the gas analyses for the siren and baseline test runs. By following the Constant Rate of Drying Theory as discussed in Chapter 2, the data were divided into two regions, the constant rate and falling rate regions.

Figures B.1 to B.5 represent the measured concentration of ethanol in parts per million volume (PPMv) versus time. Figures B.6 to B.10 represent the plot of the concentration of ethanol versus time in the constant rate region on linear arithmetic coordinates for all the test runs performed. The plots were then correlated with a linear curve fit and the coefficients are displayed on each graph. Figures B.10 to B.15 were the plot of concentration of ethanol versus time in the falling rate region for all the test runs. The graphs were plotted on semi logarithmic coordinates and correlated with exponential curve fit with the coefficients displayed on each graph. Table 4.2 is a summary of the removal rate coefficients obtained from the correlation of the plots of the concentration of ethanol versus time for both the constant rate and the falling rate regions (Figures B.6 to B.15). Due to poor measurement difficulties, some data as shown in Table 4.2, were not available. The removal rate constants were not available for experimental runs conducted at 13,997 Hertz. And frequencies of 2,957 and 6,637 Hertz, the results for the duplicate

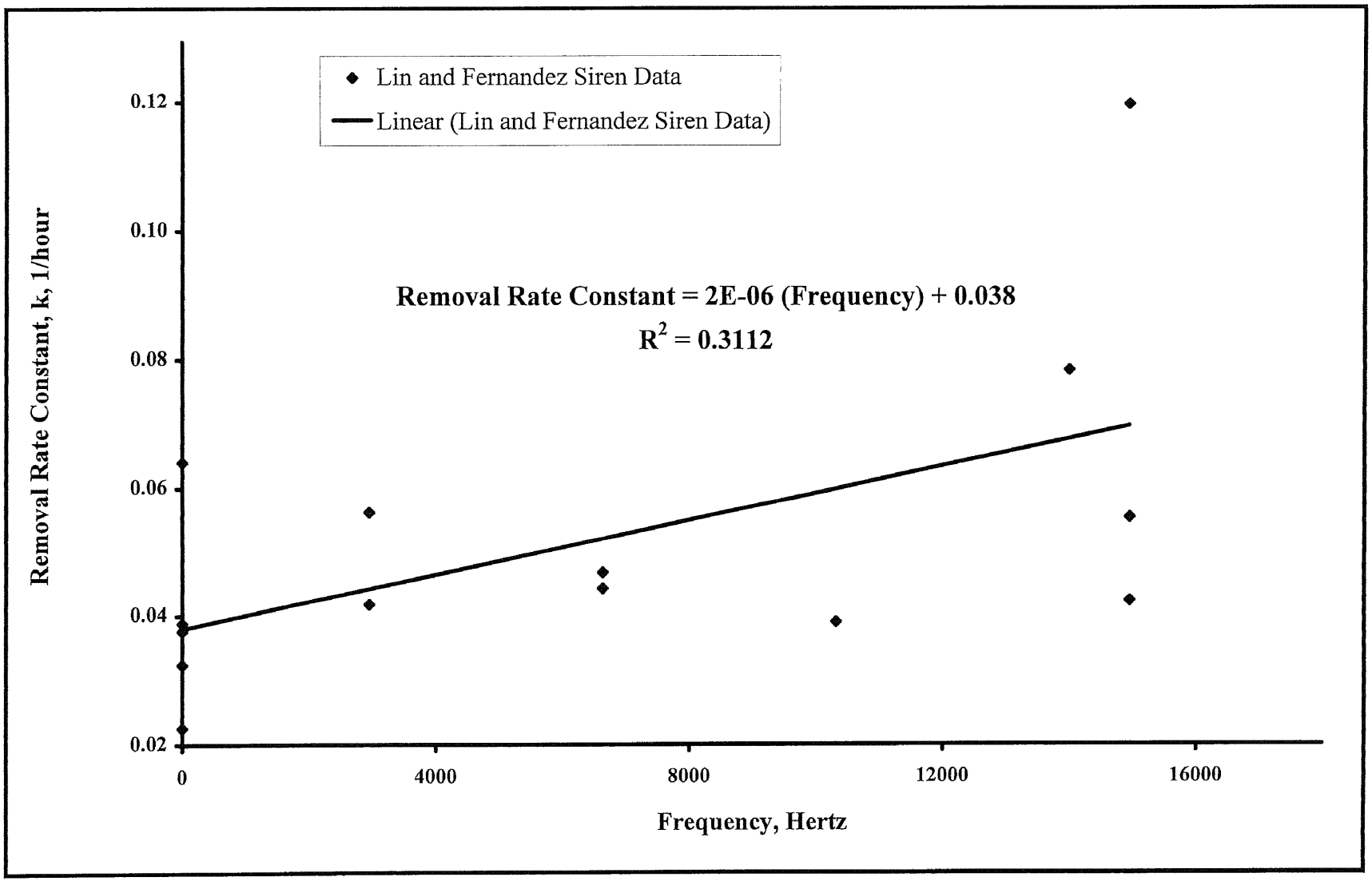

Figure 4.2 Comparison of Removal Rate Constants Versus Frequency for the Siren

runs were also not available. The reason for the missing data is that the gas chromatograph did not perform consistently throughout the experiments. Many problems were associated with the GC giving scattered results. Since some of the data were very scattered, the GC was calibrated twice with 2 different sets of conditions. The original conditions used for the calibration of the GC were used for both the baseline test runs ($Moles\ of\ Ethanol = 1x10^{-15}\ (area) + 2x10^{-9}$).

The equation given in Figure 3.6, which is the calibration equation

$$Moles\ of\ Ethanol = 7x10^{-15}\ (area) + 1x10^{-9}$$

was used for all of the experimental test runs performed with the siren at the frequency range of 2,957 to 13,997 Hertz. The concentrations measured at 6,637 Hertz appear to be very high. There is no apparent reason for this measurement. Appendix B lists the details of the conditions used including the automation of the processes involved in the analyses of the gas samples.

Table 4.2 Removal Rate Constants of the Concentration of Ethanol Versus Time

Siren Frequency (Hertz)	***k*, hr^{-1} Constant Rate Region**	***k*, hr^{-1} Falling Rate Region**
Baseline (Run 1)	302.84	0.055
Baseline (Run 2)	554.47	0.0909
2,957 (Run 1)	168.98	0.0687
2,957 (Run 2)	*	*
6,637 (Run 1)	*	*
6,637 (Run 2)	2056.4	0.1721
10,317	50.707	0.0652
13,997	*	*

* Data not available

4.2.2 Effect of Frequency on Time to Reach Asymptotic Value

The asymptote is the point in time where the moisture content reaches a constant value. As shown on the free moisture content versus time plots (Figures A.1 to Figures A.16), the trend of the plots started off with a high moisture content and dropped very rapidly in a short period of time. As it reached the falling rate region, the moisture content decreased in a diminishing rate and eventually reached an asymptotic value where the moisture content remained the same for infinite time. The estimated time to reach asymptotic state is summarized in Table 4.3. The estimated values were taken from Figures A.9 to A.16, where the averaged measured data were used.

The estimated time to reach asymptotic value is between 35 to 50 hours as summarized in Table 4.3. This information is also graphically presented in Figure 4.3, which shows only a slight decrease in the time to reach asymptotic value as the frequency rises. Figure 4.3 shows that the change in frequency does not significantly affect the time required to reach asymptotic value. Fernandez (1997), however, showed that the asymptotic values are lower and are reached much sooner with the whistle.

Table 4.3 Summary of Estimated Time to Reach Asymptotic Value

Siren Frequency (Hertz)	Estimated Time to Reach Asymptotic State (Hour)
Baseline (Run 1)	50
Baseline (Run 2)	40
2,957 (Run 1)	45
2,957 (Run 2)	35
6,637 (Run 1)	35
6,637 (Run 2)	50
10,317	45
13,997	35

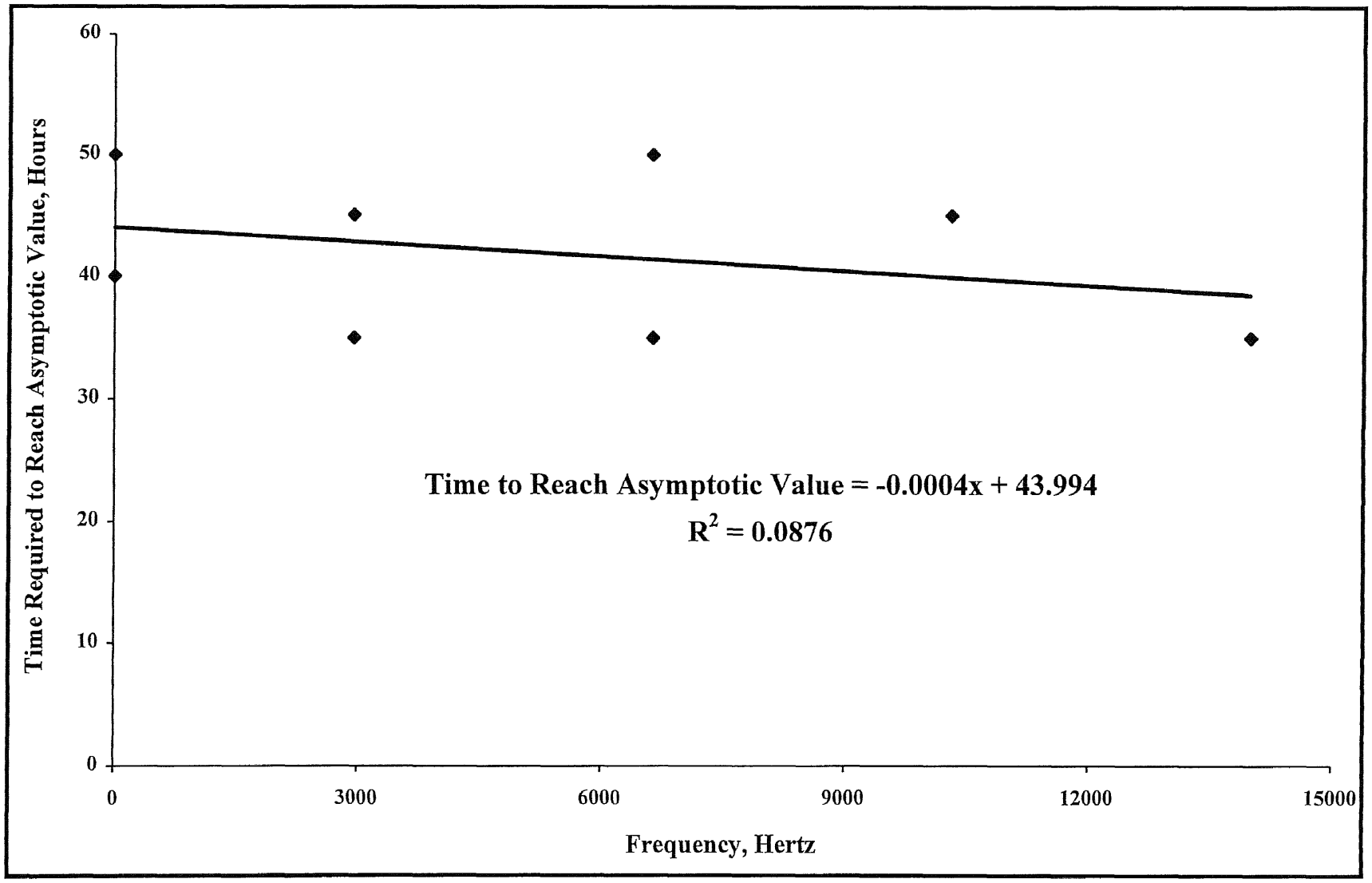

Figure 4.3 Required Time To Reach Asymptotic Value Versus Frequency

4.2.3 Estimated Penetration Depth in Drying with Frequency

The estimated equivalent bed depth of the penetration of the drying process for each frequency can be estimated. Using the method of taking the ratio of the free moisture content weight at time zero and the initial soil height to the asymptotic value of the free moisture content, the equivalent bed depth of the penetration of the drying process is estimated. This information can be useful when deciding on the location and the depth of the siren in a field project. Table 4.4 is a summary of the bed depth of the penetration in the drying process as well as the free moisture content that remained in the test cell at asymptotic value. See Appendix C for a sample calculation of the equivalent bed depth of the penetration of the drying process.

Table 4.4 Estimated Bed Depth of the Penetration of the Drying Process with Frequency

Siren Frequency (Hertz)	**Free Moisture Remaining in the Test Cell at Asymptotic Value (lbs contaminant per lbs dry sand)**	**Equivalent Bed Depth of the Penetration of The Drying Process (inches)**
Baseline (Run 1)	0.009	9.011
Baseline (Run 2)	0.01	8.778
2,957 (Run 1)	0.008	9.270
2,957 (Run 2)	0.0075	9.426
6,637 (Run 1)	0.0075	9.458
6,637 (Run 2)	0.005	10.103
10,317	0.008	9.334
13,997	0.002	10.890

The bed depth above the siren was 13 inches. From the summary of the free moisture remaining in the test cell at asymptotic value listed in Table 4.4, the results show that the siren did not effectively remove all of the free moisture content in the

test cell. The free moisture content level remained in the test cell at an asymptotic value, which is in the range of 0.002 to 0.01 pounds of contaminant per pounds of dry sand. The top 1 to 3 inches of the bed remained moist. Figure 4.4 is a plot of the equivalent bed depth of the penetration of the drying process versus frequency (Table 4.4). For the frequency ranges used in this study, the change in frequency shows a slight increase in the bed depth to which drying occurred. The correlation coefficient is however poor, as the data are scattered and the results are not significant. Fernandez (1997) showed that with the whistle, the entire bed was almost dried. Since the whistle used by Fernandez (1997) had a sound level of 160 decibels and the frequency was 11 kHz (in the same range as this study), it is believed that the sound level is and important factor in the improved drying. The siren sound levels were about 98 to 125 decibels. Using Equation 2.16, the intensity of the whistle and siren can be compared at 11 kHz. Table 4.5 shows a comparison of the frequency, sound level and intensity of the siren and the whistle.

Table 4.5 Comparison of Calculated Intensity for the Siren and the Whistle

	Siren	**Whistle**
Frequency, Hertz	14,946[1]	11,000[1]
Sound Level, dB	125[1]	160[1]
Intensity, W/m^2	3.1623	10,000

1 Fernandez (1997)

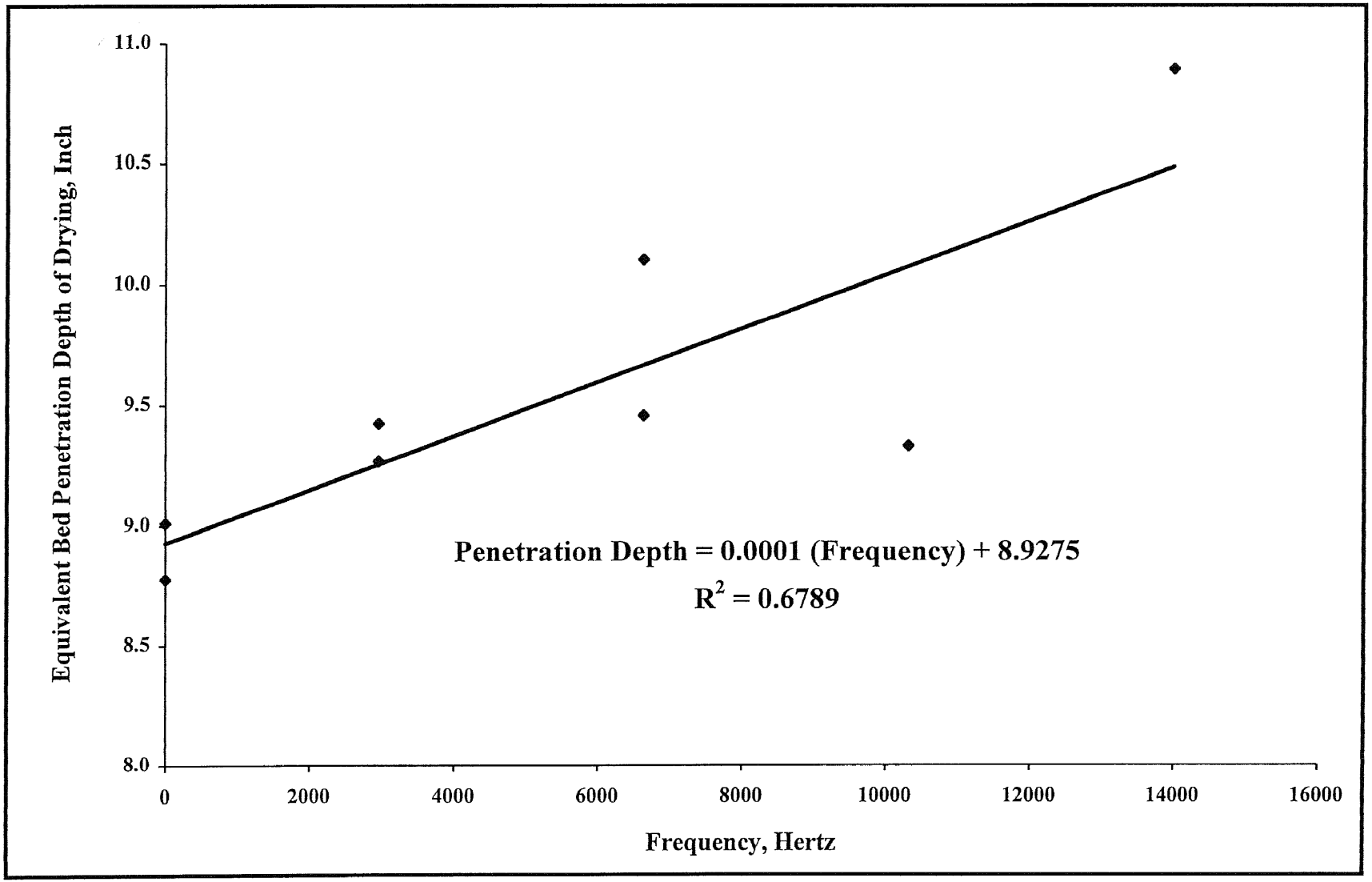

Figure 4.4 Equivalent Bed Depth of the Penetration of Drying Versus Frequency

Hence, the whistle is generating an intensity of about 3,162 times more than the siren. Equation 2.15 shows that for the same frequency and air density, the factors giving rise to higher intensity are amplitude and velocity of the wave. The velocity of the wave is given by

$$v = f\lambda \qquad (4.1)$$

"The wave velocity, v, is determined completely by the properties of the transmitting medium and does not depend on either the frequency of the source or the wavelength. It follows that whenever f changes there must be a corresponding change in λ" (Hausman and Slack, 1939). Therefore, the principle factor for the comparative change in intensity is the amplitude. The greater amplitude of the whistle is thus resulting in greater bed depth of the penetration of the drying process and the whistle practically dried the entire bed (Fernandez, 1997) but the siren did not.

Boucher (1958) states that sonic drying is best achieved at sound frequencies between 7 kHz and 20 kHz and sound intensities greater than 145 dB. One would therefore conclude that a sound source generator should be designed to operate at the threshold of ultrasonic frequencies (15 to 20 kHz) and at as high an intensity possible. Penetration in any field study will be affected by the attenuation coefficient as the amplitude of the wave declines with distance.

CHAPTER 5

CONCLUSIONS AND RECOMMENDATIONS

The conclusions of the study are:

1. The improvement in the contaminant removal rate as frequency rises for the range of frequencies used in this study (2,957 Hertz to 13,997 Hertz) is not significant.
2. A comparison of the siren data with the whistle data in Fernandez (1997) would lead one to believe that sound level or intensity is a very important factor in enhancing the removal rate of the contaminants.
3. A comparison of the siren and the whistle cannot be made because of the large difference in sound intensity.

The recommendations of the study are:

1. Studies should be made to determine the attenuation coefficient for the sound intensity to determine the extent of penetration of the sound wave in the bed.
2. An attempt should be made to redesign the siren to operate at a frequency of 20 kHz and at an intensity of greater than 145 dB.
3. An attempt should be made to redesign the whistle to operate at a frequency of 20 kHz and an intensity of greater than 145 dB.

APPENDIX A

SAMPLE CALCULATIONS, TABLES, AND FIGURES FOR FREE MOISTURE CONTENT VERSUS TIME TESTS

In this section of the appendix, the results of the free moisture content tests for the siren performed at frequencies of 2957, 6637, 10317, and 13997 Hertz and the baseline tests are presented. First, the experimental condition is given in Table A.1, followed by a sample calculation on how to obtain the packing height of the tank. Then, a sample calculation is demonstrated on the method used to determine the free moisture content of the data collected. Following the sample calculations, Tables A.2 to A.6 are presented, where the calculated free moisture content and the elapsed time are listed for all the test runs performed. Finally, Figures A.1 to A.24 are presented, where the calculated free moisture content is plotted versus time.

A.1 Experimental Conditions for Both the Siren and Baseline Tests

As mentioned earlier in Chapter 3, all of the test runs were performed under the same experimental conditions to avoid introducing extra variables or unknowns. Since this research focuses on the study of the effect of the change in frequency by the siren, the only condition changed during the experimental runs was the settings of the frequencies. The applied frequencies ranged between 3,957 to 13,997 Hertz and the baseline test runs were the runs where the siren was not used. Table A.1 is a summary of the experimental conditions used for both the siren and the baseline test runs (see Table 3.1 for the NJIT Siren Operating Characteristics).

Table A.1 Experimental Conditions

Parameter	Siren and Baseline Tests
Inlet Air Volumetric Flow	40 PSIG
Outlet Air Volumetric Flow	7 SCFM at 80 Inches of Water
Fracture Material and Approximate Area	Geotextile ½ inch thick 0.767 square ft.
Packing Density	95 lb per cubic foot
Liquid Content in Soil	5 % by weight
Contaminant Content	10 % ethanol 90 % water

A.2 Experimental Packing Height Calculations

For each run, the tank was packed to a packing density of 95 pounds per cubic foot and 5 % moisture content. This was accomplished by first weighing 95 pounds of the 00-grade dry sand followed by calculating the total mass of the bed with the moisture content. The total mass of the bed is determined by the following equation:

$$\text{Total Mass of Bed} = \frac{\text{Dry Sand}}{\text{Fraction of Dry Sand}} = \frac{95\,\text{lbs}}{0.95} = 100\,\text{lbs} \qquad \text{(A.1)}$$

From Equation A.1, 95 pounds of dry sand are used and the amount of moisture is 5 pounds. This moisture content is further divided into 10 % ethanol and 90 % of water by weight.

To determine the total bed volume of sand, the total weight of the bed was divided by the target density, which was 95 pounds per cubic foot.

$$\text{Total Bed Volume} = \frac{100\,\text{lb of total bed}}{95\,\text{lbs of total bed} / \text{ft}^3} = 1.053\,\text{ft}^3 \qquad \text{(A.2)}$$

To calculate the total volume of the tank, all the parts found in the tank had to be considered. The following parts were found in the tank, the siren, the ½ inch geotextile fracture and the two extraction pipes. The sum of these parts is the total volume of the bed. The volume of the siren is 0.065 ft^3, the total volume of the 2 extraction pipes is 0.00920 ft^3 and the volume of fracture is 0.03196 ft^3.

Therefore, Total Volume of Bed

$= 0.065\ ft^3 + 0.00920\ ft^3 + 0.03196\ ft^3 + 1.053\ ft^3 = 1.1592\ ft^3$ (A.3)

In order to determine the height of the bed, the total volume of the bed, as obtained from Equation A.3, is divided by the cross sectional area of the bed, as demonstrated in Equation A.4:

$$\frac{\text{Total Volume of Bed}}{\text{Cross Sectional Area}} = \frac{1.1592\ ft^3}{1.03066\ ft^2} \quad \text{(A.4)}$$

$$= 1.1247\ ft = 13.5\ inch = \text{Calculated Bed Height}$$

The measured height of the bed was approximately 15 inches.

A.3 Sample Calculations and Tables of Free Moisture Content in the Tank versus Time

Tables A.2 to A.6 present the results of the siren in various frequencies and baseline tests runs. The frequencies applied to the tests range from approximately 2,957 Hertz to 13,997 Hertz.

The level of the moisture content in the test cell was monitored throughout the experiment. The electronic scale system was programmed to scan and record the weight of the test cell at every 60 seconds and as discussed in Section 3.2, the

computer connected to the load cells of the scale system logged the data in a file. Tables A.2 to A.6 represent the results of the various test runs performed.

The first column of each table shows the elapsed time which is the averaged time in a two hour interval. For example, at time zero the elapsed time is zero. At Hour 1, the shown elapsed time is the average taken from time 1 minute to 120 minute. For Hour 3, the shown elapsed time is from 101 minute to 240 minute, etc. The next column is the weight of the moisture in the tank in pounds and the last column shows the free moisture (moisture in the tank per pound of dry sand). For frequencies where a duplicate run was made, the table extends to 2 additional columns with the results of the data listed in columns 4 and 5 of the table. A total of 8 runs were performed, 2 were baseline tests and the rest were siren tests in 4 different frequencies (2957, 6637, 10317 and 13997 Hertz).

The following is a sample calculation of how the free moisture content was determined. Take Table A.2 as an example. At time zero, the weight of the moisture in the tank is 5.10 pounds and the weight of the sand is 94.03 pounds. To determine the free moisture content,

$$\text{Free Moisture Content} = \frac{\text{weight of moisture in test cell}}{\text{total weight of dry sand}} \tag{A.5}$$

$$= \frac{5.10}{94.03} = 0.05424 \quad \frac{\text{lb of moisture}}{\text{lb of dry sand}}$$

Table A.2 Free Moisture Content Results for Baseline Tests

	Baseline Test (Run 1)		**Baseline Test (Run 2)**	
Elapsed Time (Hour)	Weight of Moisture in Tank (lb)	Free Moisture (lb of moisture per lb dry sand)	Weight of Moisture in Tank (lb)	Free Moisture (lb of moisture per lb dry sand)
0	5.100	0.05424	5.148	0.05507
1	4.753	0.05055	4.653	0.04977
3	4.367	0.04644	4.190	0.04482
5	3.920	0.04169	3.797	0.04061
7	3.632	0.03863	3.435	0.03675
9	3.503	0.03725	3.205	0.03429
11	3.307	0.03517	2.893	0.03095
13	3.140	0.03339	2.595	0.02776
15	2.979	0.03169	2.363	0.02528
17	2.772	0.02948	2.142	0.02291
19	2.318	0.02466	2.034	0.02176
21	2.066	0.02197	1.937	0.02072
23	1.987	0.02113	1.859	0.01989
25	1.854	0.01971	1.747	0.01868
27	1.673	0.01779	1.677	0.01794
29	1.663	0.01769	1.548	0.01655
31	1.645	0.01749	1.449	0.01550
33	1.583	0.01684	1.381	0.01477
35	1.537	0.01634	1.285	0.01375
37	1.441	0.01532	1.232	0.01317
39	1.328	0.01412	1.237	0.01323
41	1.175	0.01250	1.173	0.01254
43	1.138	0.01211	1.122	0.01200
45	1.061	0.01129	1.026	0.01097
47	0.975	0.01037	0.996	0.01065
49	1.380	0.01468	0.967	0.01035
51	0.888	0.00944	0.946	0.01012
53	1.029	0.01094	0.984	0.01053
55	1.031	0.01097	0.873	0.00934
57	1.019	0.01084	0.867	0.00927
59	0.936	0.00996	-	-
61	0.935	0.00994	-	-
63	0.761	0.00809	-	-
65	0.628	0.00668	-	-

Table A.3 Free Moisture Content Results for a Frequency of 2,957 Hertz

	2,957 Hertz (Run 1)		**2,957 Hertz (Run 2)**	
Elapsed Time (Hour)	Weight of Moisture in Tank (lb)	Free Moisture (lb of moisture per lb dry sand)	Weight of Moisture in Tank (lb)	Free Moisture (lb of moisture per lb dry sand)
0	4.9140	0.05378	5.0100	0.05423
1	4.4804	0.04904	4.3864	0.04748
3	4.4198	0.04838	3.8187	0.04134
5	4.1112	0.04500	3.3075	0.03580
7	3.7318	0.04084	2.8987	0.03138
9	3.4452	0.03771	2.6142	0.02830
11	3.1935	0.03495	2.3517	0.02546
13	2.8375	0.03106	2.2580	0.02444
15	2.6052	0.02852	2.1565	0.02334
17	2.3812	0.02606	1.9992	0.02164
19	2.1892	0.02396	1.9065	0.02064
21	2.0117	0.02202	1.4545	0.01574
23	1.8095	0.01981	1.2170	0.01317
25	1.6970	0.01857	1.2370	0.01339
27	1.6347	0.01789	1.1307	0.01224
29	1.4942	0.01635	1.0072	0.01090
31	1.4765	0.01616	0.9617	0.01041
33	1.3005	0.01423	0.8575	0.00928
35	1.1108	0.01216	0.7712	0.00835
37	1.0435	0.01142	0.8197	0.00887
39	0.9562	0.01047	0.7595	0.00822
41	0.8740	0.00957	0.8207	0.00888
43	0.7825	0.00856	0.7797	0.00844
45	0.6880	0.00753	0.7185	0.00778
47	-	-	0.7030	0.00761

Table A.4 Free Moisture Content Results for a Frequency of 6,637 Hertz

	6,637 Hertz (Run 1)		6,637 Hertz (Run 2)	
Elapsed Time (Hour)	Weight of Moisture in Tank (lb)	Free Moisture (lb of moisture per lb dry sand)	Weight of Moisture in Tank (lb)	Free Moisture (lb of moisture per lb dry sand)
0	5.0000	0.05508	5.0000	0.05514
1	4.9672	0.05472	4.7346	0.05221
3	4.5405	0.05002	4.2992	0.04741
5	4.2962	0.04733	3.8307	0.04224
7	4.0657	0.04479	3.4810	0.03839
9	3.8360	0.04226	3.1627	0.03488
11	3.6542	0.04026	2.8142	0.03103
13	3.3687	0.03711	2.4362	0.02687
15	3.1487	0.03469	2.2517	0.02483
17	2.8497	0.03140	2.0045	0.02211
19	2.5427	0.02801	1.7987	0.01984
21	2.1610	0.02381	1.6627	0.01834
23	1.6812	0.01852	1.5567	0.01717
25	1.4082	0.01551	1.4615	0.01612
27	1.2275	0.01352	1.3915	0.01535
29	1.1170	0.01231	1.3285	0.01465
31	0.8967	0.00988	1.2887	0.01421
33	0.8585	0.00946	1.2197	0.01345
35	0.8902	0.00981	1.1282	0.01244
37	0.8557	0.00943	0.9542	0.01052
39	0.8222	0.00906	0.8645	0.00953
41	0.7757	0.00855	0.7507	0.00828
43	0.7602	0.00838	0.6672	0.00736
45	0.6097	0.00672	0.6322	0.00697
47	0.5490	0.00605	0.4815	0.00531
49	-	-	0.4022	0.00444
51	-	-	0.4677	0.00516
53	-	-	0.4817	0.00531
55	-	-	0.3937	0.00434
57	-	-	0.3340	0.00368
59	-	-	0.3247	0.00358

Table A.5 Free Moisture Content Results for a Frequency of 10,317 Hertz

Elapsed Time (Hour)	Weight of Moisture in Tank (lb)	Free Moisture (lb of moisture per lb dry sand)
0	5.1880	0.05540
1	4.9000	0.05200
3	4.4790	0.04800
5	4.1090	0.04400
7	3.7220	0.04000
9	3.3860	0.03600
11	3.1160	0.00300
13	2.8700	0.03100
15	2.7130	0.02900
17	2.6660	0.02800
19	2.2370	0.02400
21	2.0520	0.02200
23	2.0020	0.02100
25	1.9030	0.02000
27	1.7790	0.01900
29	1.6920	0.01800
31	1.5920	0.01700
33	1.4890	0.01600
35	1.3960	0.01500
37	1.3450	0.01400
39	1.2460	0.01300
41	1.1440	0.01200
43	1.1720	0.01300
45	1.1530	0.01200
47	1.1560	0.01200
49	1.125	0.012
51	1.064	0.011
53	1.009	0.011
55	0.972	0.01
57	0.918	0.01
59	0.855	0.009
61	0.824	0.009
63	0.831	0.009

Table A.6 Free Moisture Content Results for a Frequency of 13,997 Hertz

Elapsed Time (Hour)	Weight of Moisture in Tank (lb)	Free Moisture (lb of moisture per lb dry sand)
0	4.6800	0.04923
1	4.1266	0.04341
3	3.5737	0.03759
5	3.0963	0.03257
7	2.6375	0.02774
9	2.2208	0.02336
11	1.9575	0.02059
13	1.7305	0.01820
15	1.5320	0.01612
17	1.2690	0.01335
19	1.1865	0.01248
21	1.1215	0.01180
23	1.0083	0.01061
25	0.7735	0.00814
27	0.6400	0.00673
29	0.4977	0.00524
31	0.3982	0.00419
33	0.3467	0.00365
35	0.2987	0.00314
37	0.2262	0.00238
39	0.1995	0.00210
41	0.2232	0.00235
43	0.2355	0.00248
45	0.2322	0.00244
47	0.1885	0.00198
49	0.2197	0.00231
51	0.1455	0.00153
53	0.0930	0.00098
55	0.1405	0.00148
57	0.1845	0.00194
59	0.1915	0.00201

A.4 Figures for Free Moisture Content versus Time

The results of the siren and the baseline test runs at various frequencies for the free moisture content are presented. Figures A.1 to Figures A.24 are different graphs of free moisture content versus time plots in different frequencies and baseline test runs. As discussed in Section 4.2.1.1, the raw data for each run, were first plotted versus time then further reduced by taking the average at every 5 minutes and plotted versus time. Finally, the averaged data were plotted on semi logarithmic coordinates to obtain the corresponding coefficients.

Figures A.1 to A.8 represent graphs of the measured free moisture content data (raw data) plotted versus time. Free moisture content is the fraction of the moisture remaining in the test cell at a given time, as demonstrated in the sample calculations found in Section A.3 of this Appendix.

Figures A.9 to A.16 represent the averaged free moisture content data plotted versus time. To obtain a correlation of the free moisture content versus time for each test run, Figures A.9 to A.16 were plotted on semi logarithmic coordinates. Figures A.17 to A.24 represent the graphs for the averaged semi logarithmic curve fit of free moisture versus time plot with the correlation following the form of Equation 2.10,

$$X_1 = X_0 e^{-kt}$$

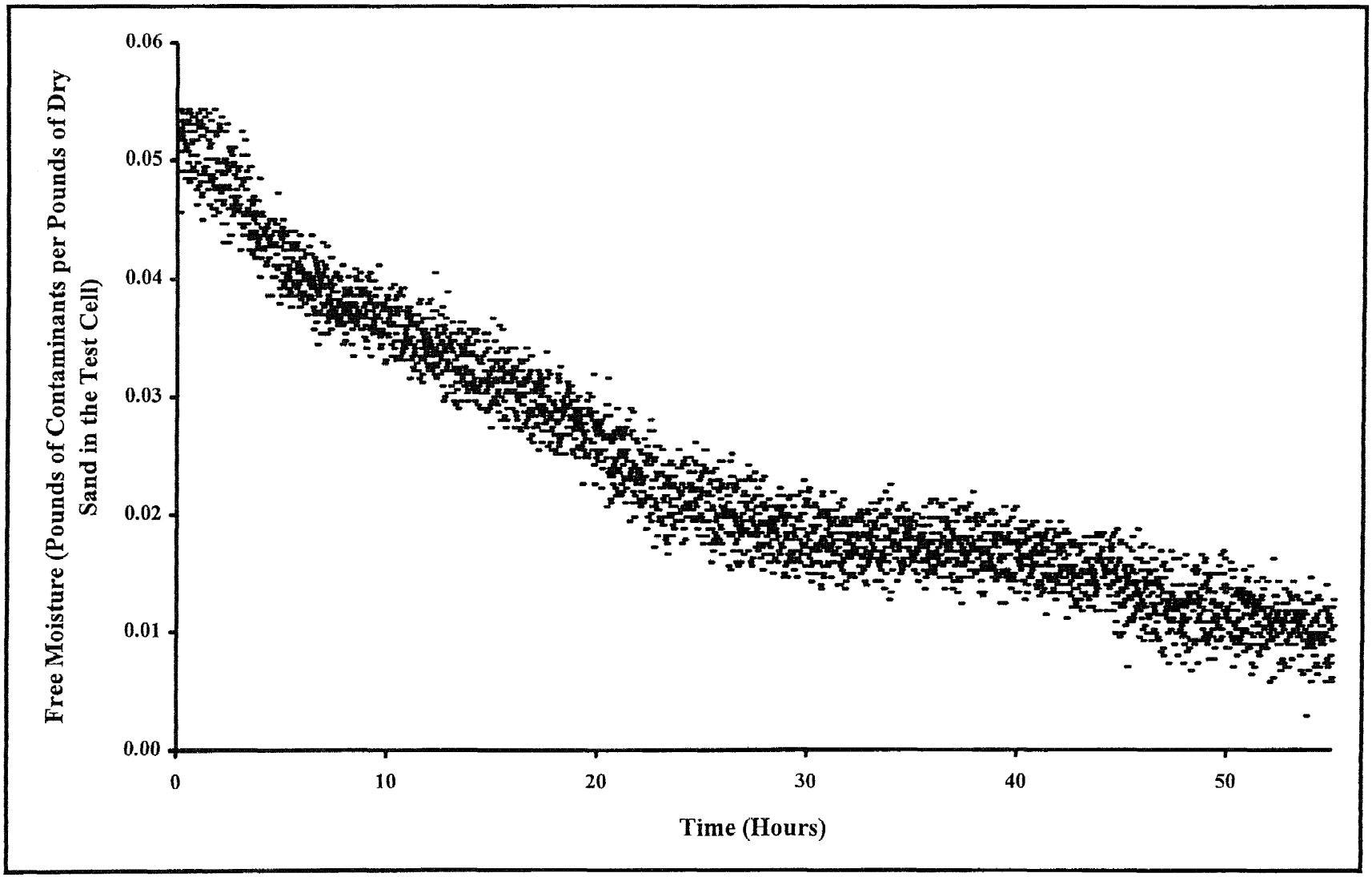

Figure A.1 Measured Data of Free Moisture Versus Time for Baseline Test (Run 1)

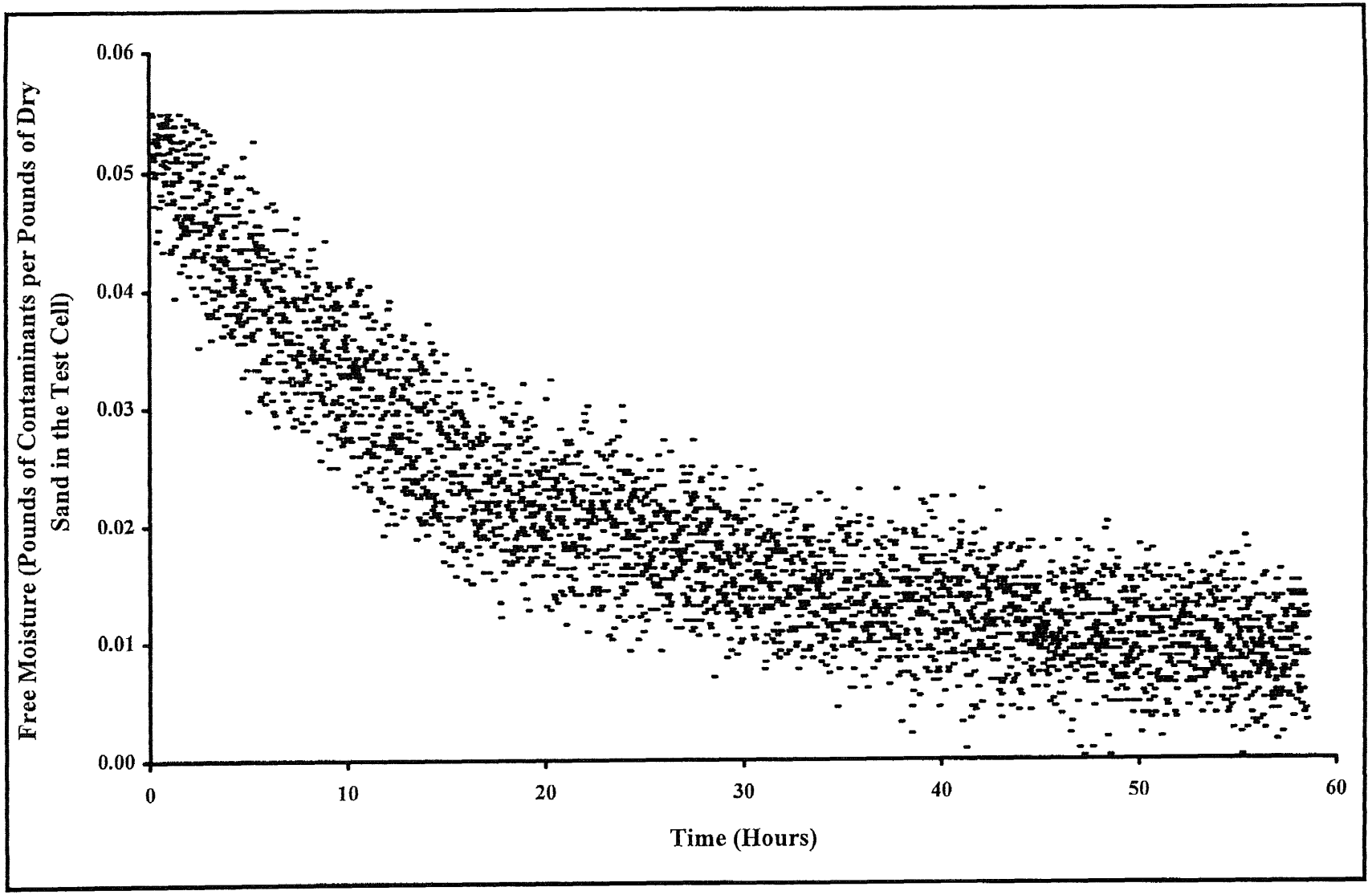

Figure A.2 Measured Data of Free Moisture Versus Time for Baseline Test (Run 2)

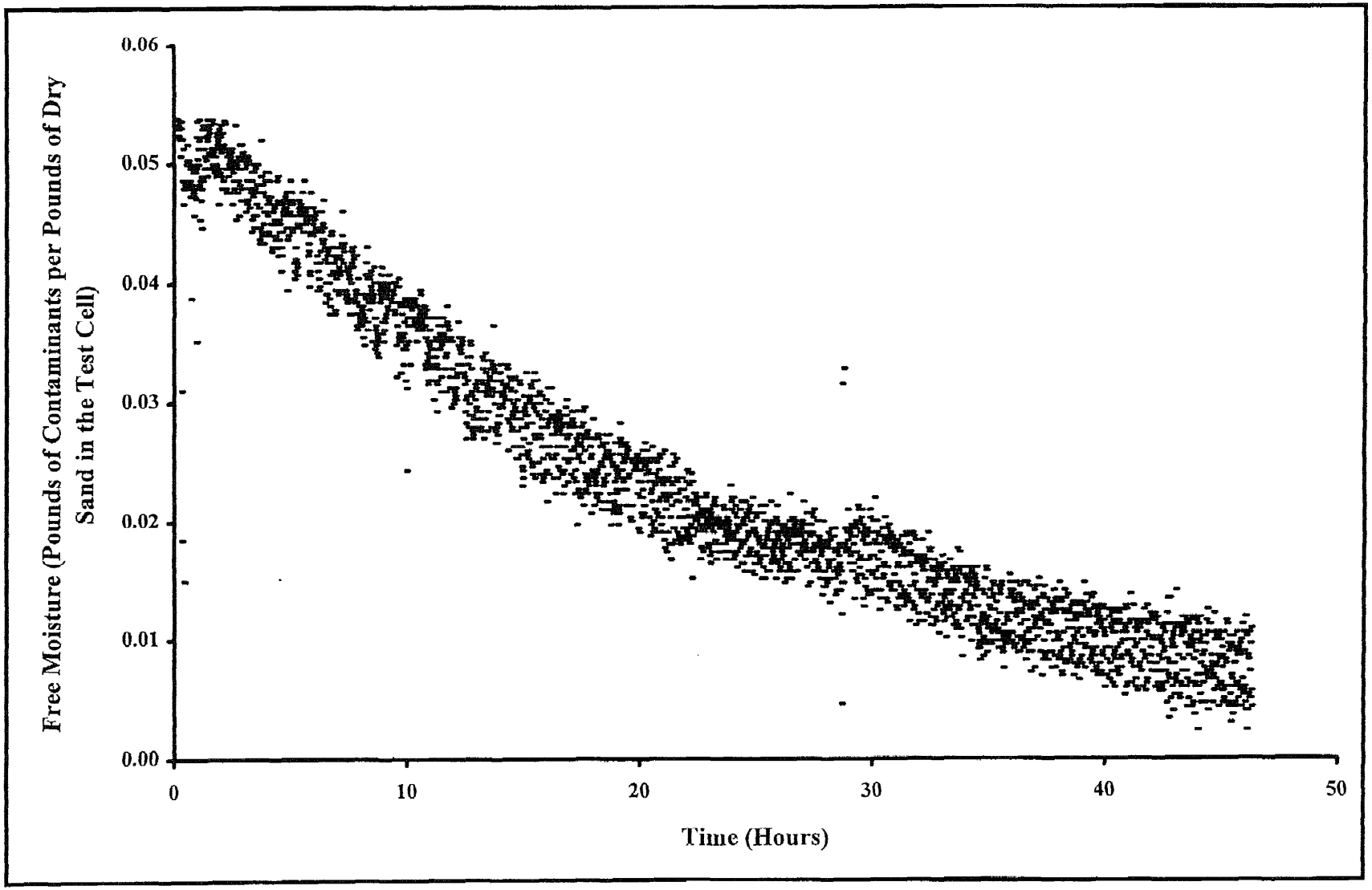

Figure A.3 Measured Data of Free Moisture Versus Time for a Frequency of 2,957 Hertz (Run 1)

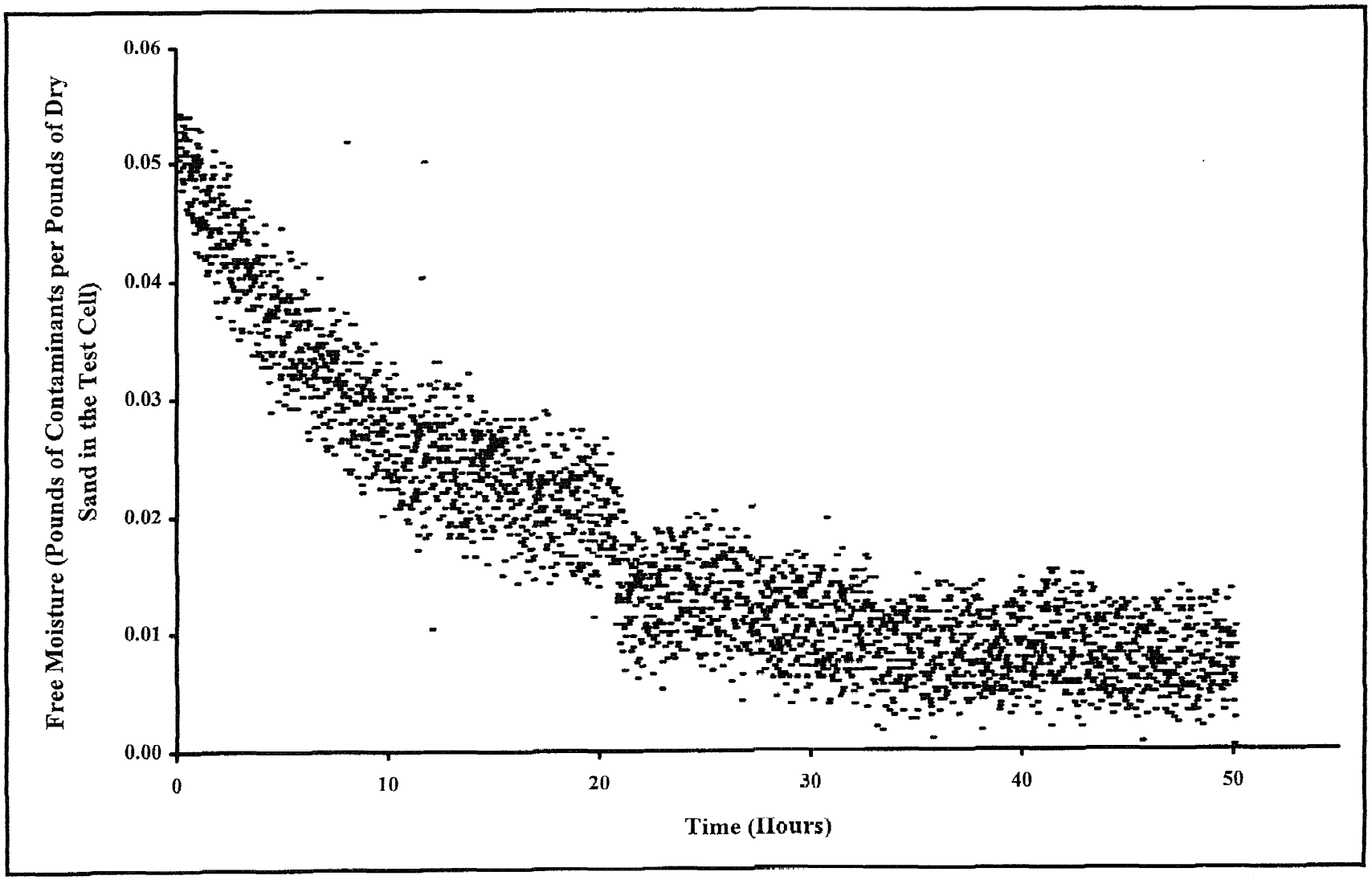

Figure A.4 Measured Data of Free Moisture Versus Time for a Frequency of 2,957 Hertz (Run 2)

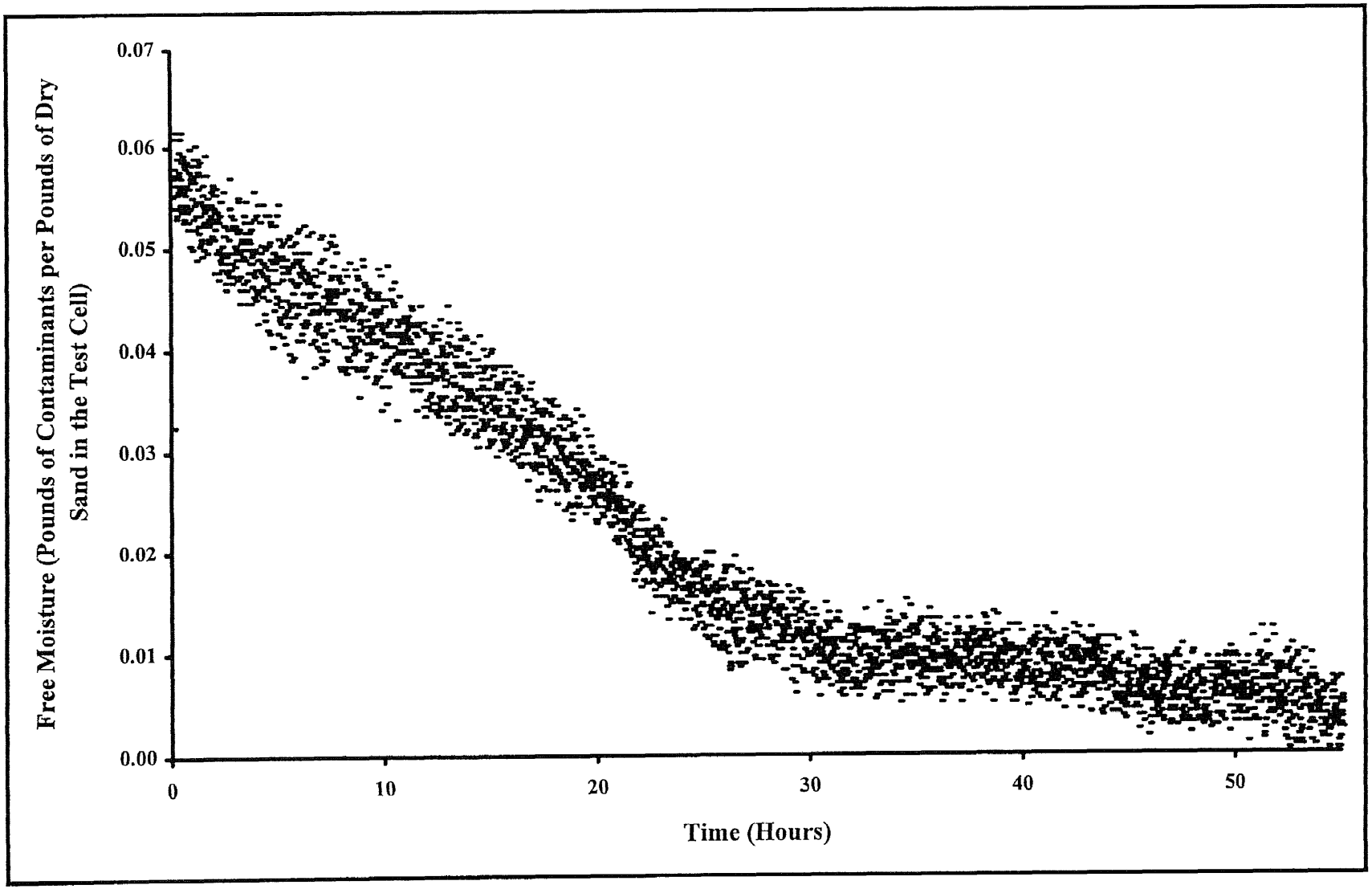

Figure A.5 Measured Data of Free Moisture Versus Time for a Frequency of 6,637 Hertz (Run 1)

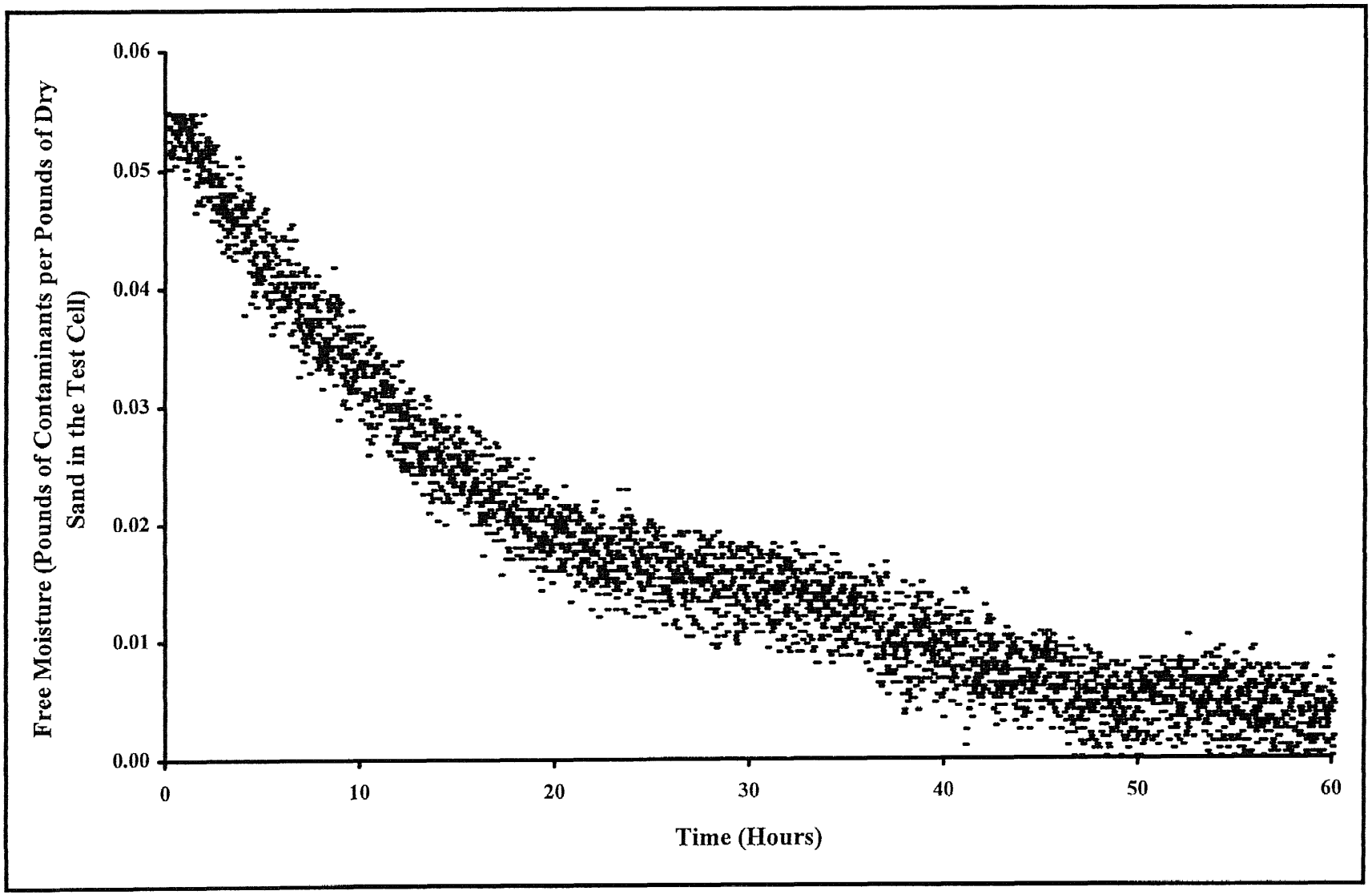

Figure A.6 Measured Data of Free Moisture Versus Time for a Frequency of 6,637 Hertz (Run 2)

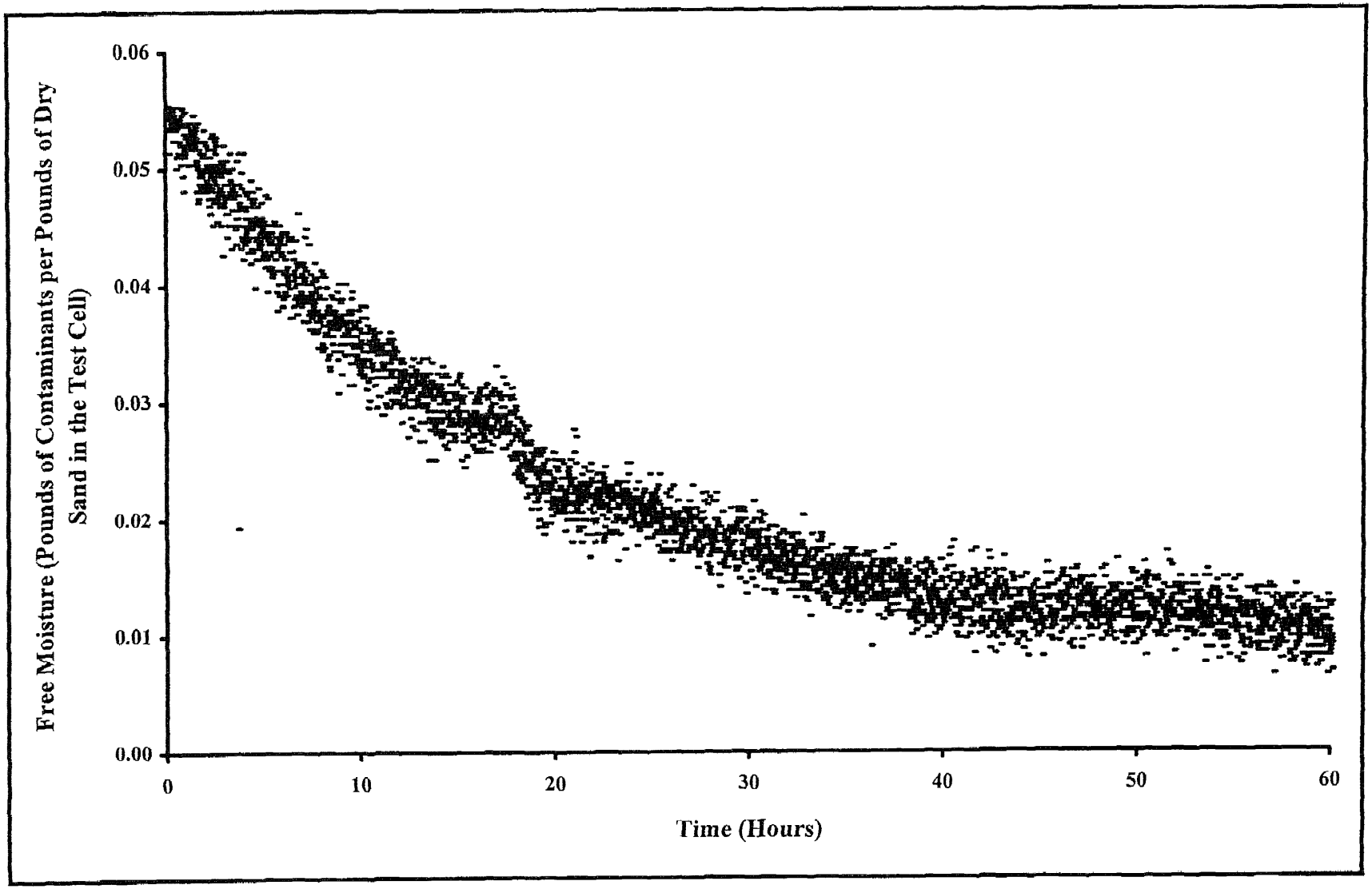

Figure A.7 Measured Data of Free Moisture Versus Time for a Frequency of 10,317 Hertz

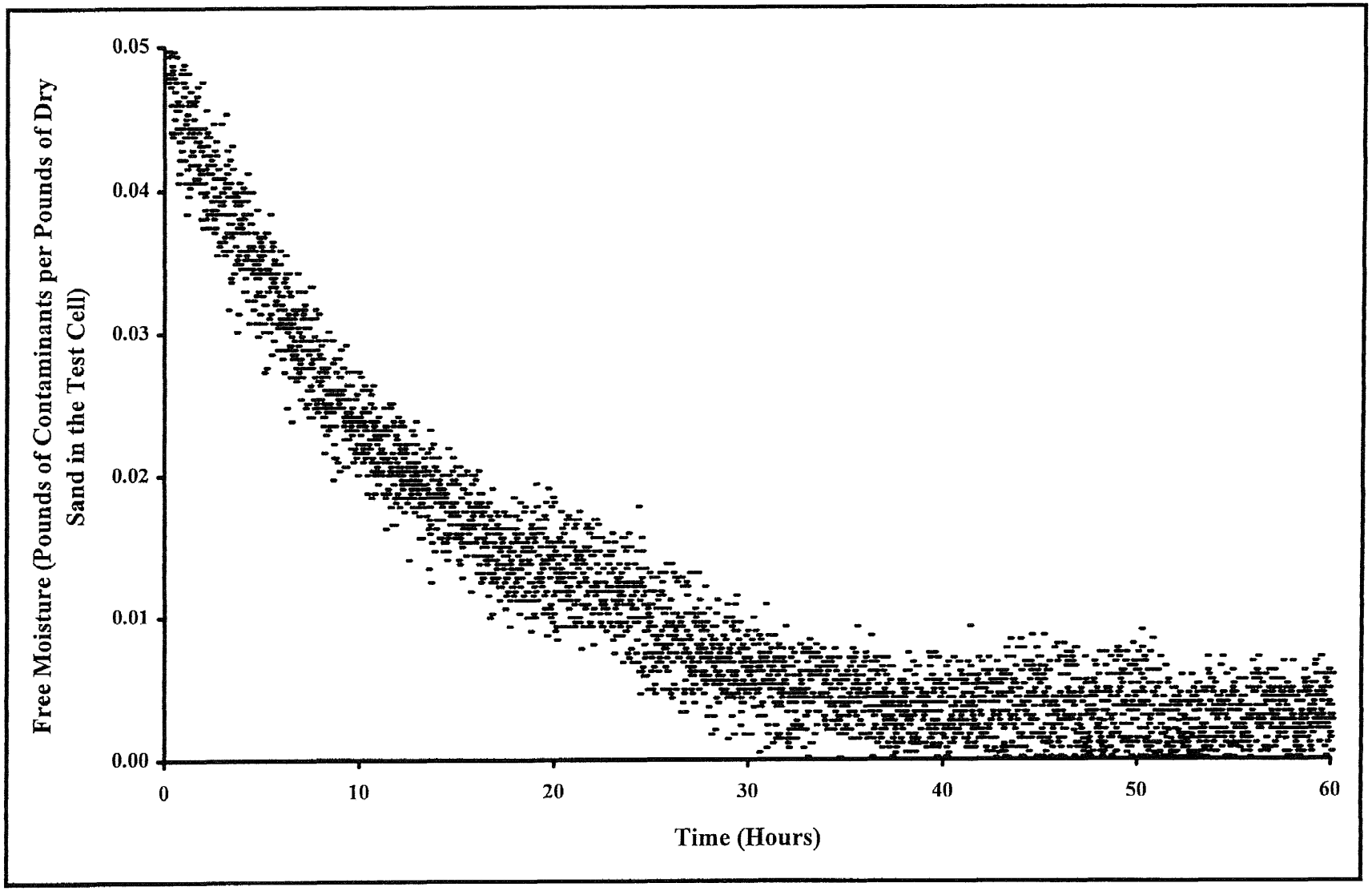

Figure A.8 Measured Data of Free Moisture Versus Time for a Frequency of 13,997 Hertz

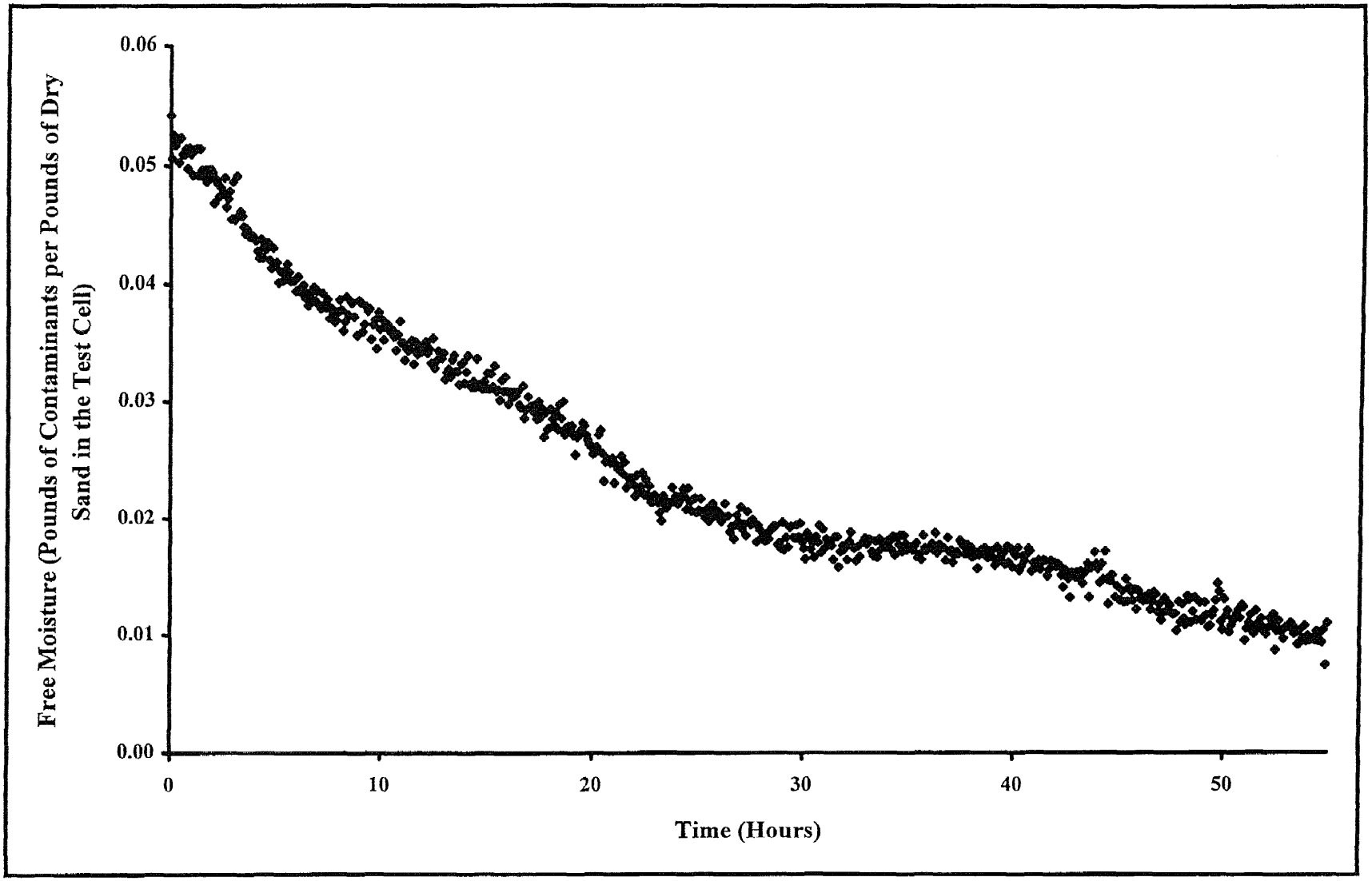

Figure A.9 Averaged Data of Free Moisture Versus Time for Baseline Test (Run 1)

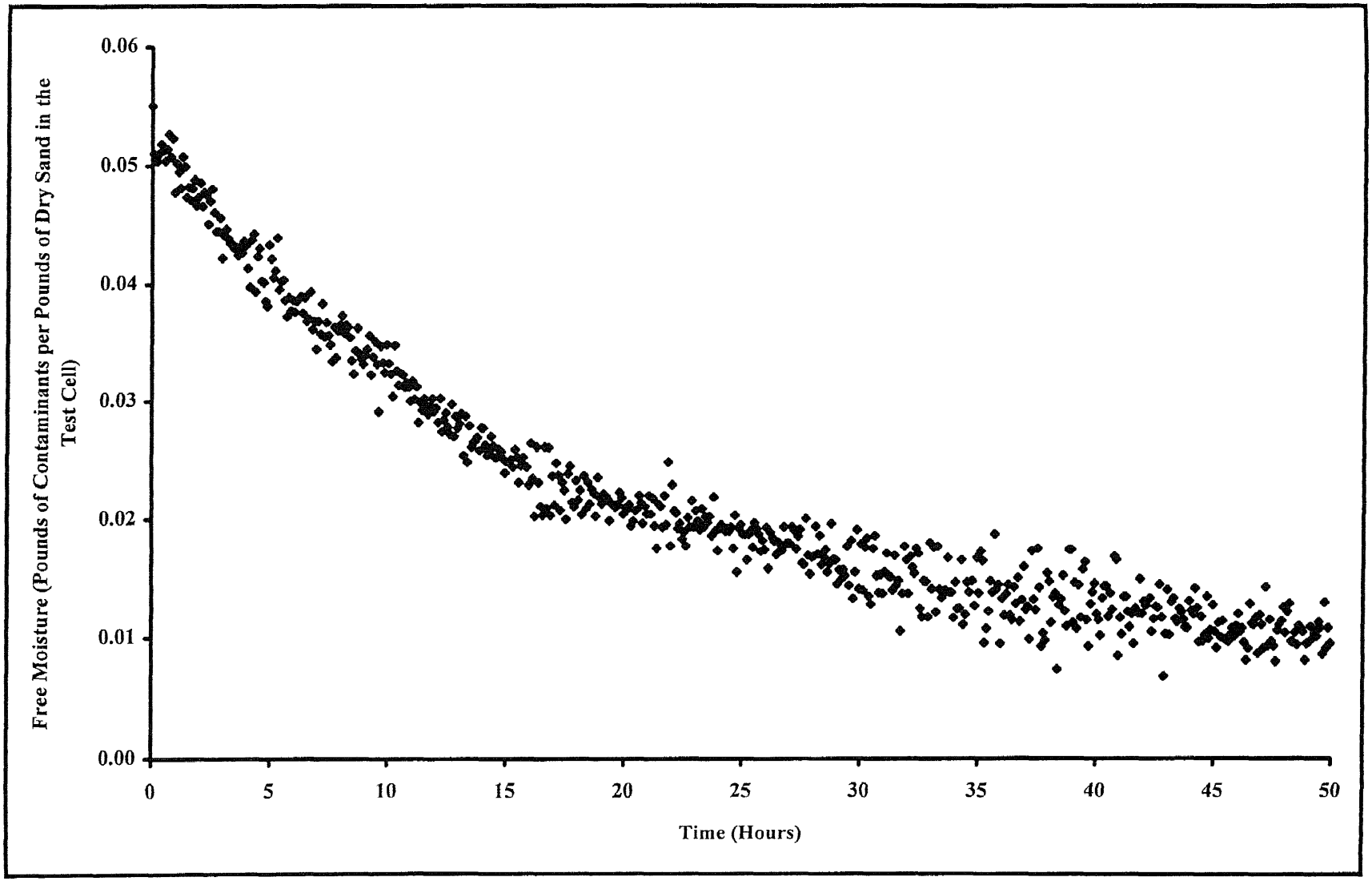

Figure A.10 Averaged Data of Free Moisture Versus Time for Baseline Test (Run 2)

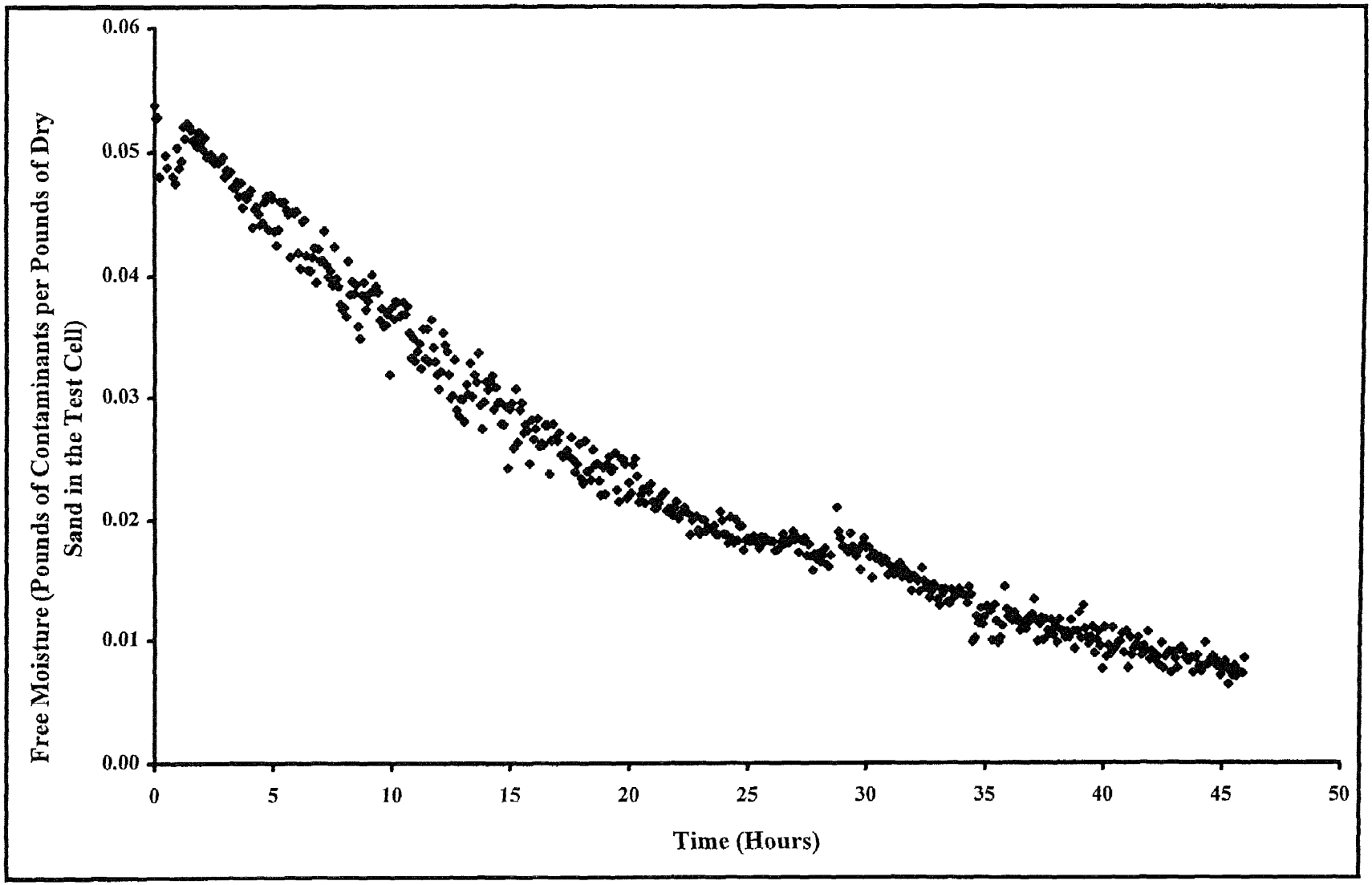

Figure A.11 Averaged Data of Free Moisture Versus Time for a Frequency of 2,957 Hertz (Run 1)

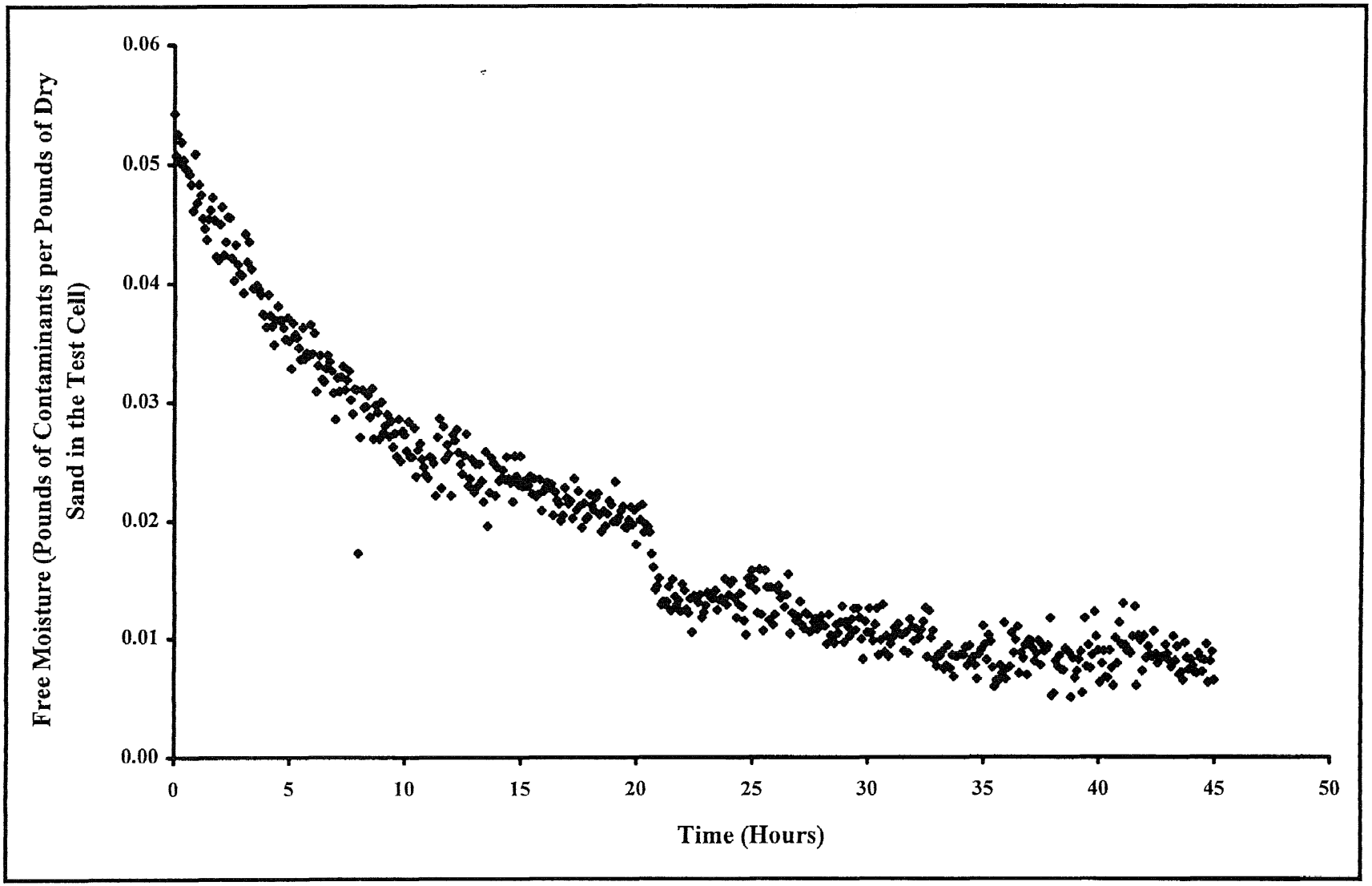

Figure A.12 Averaged Data of Free Moisture Versus Time for a Frequency of 2,957 Hertz (Run 2)

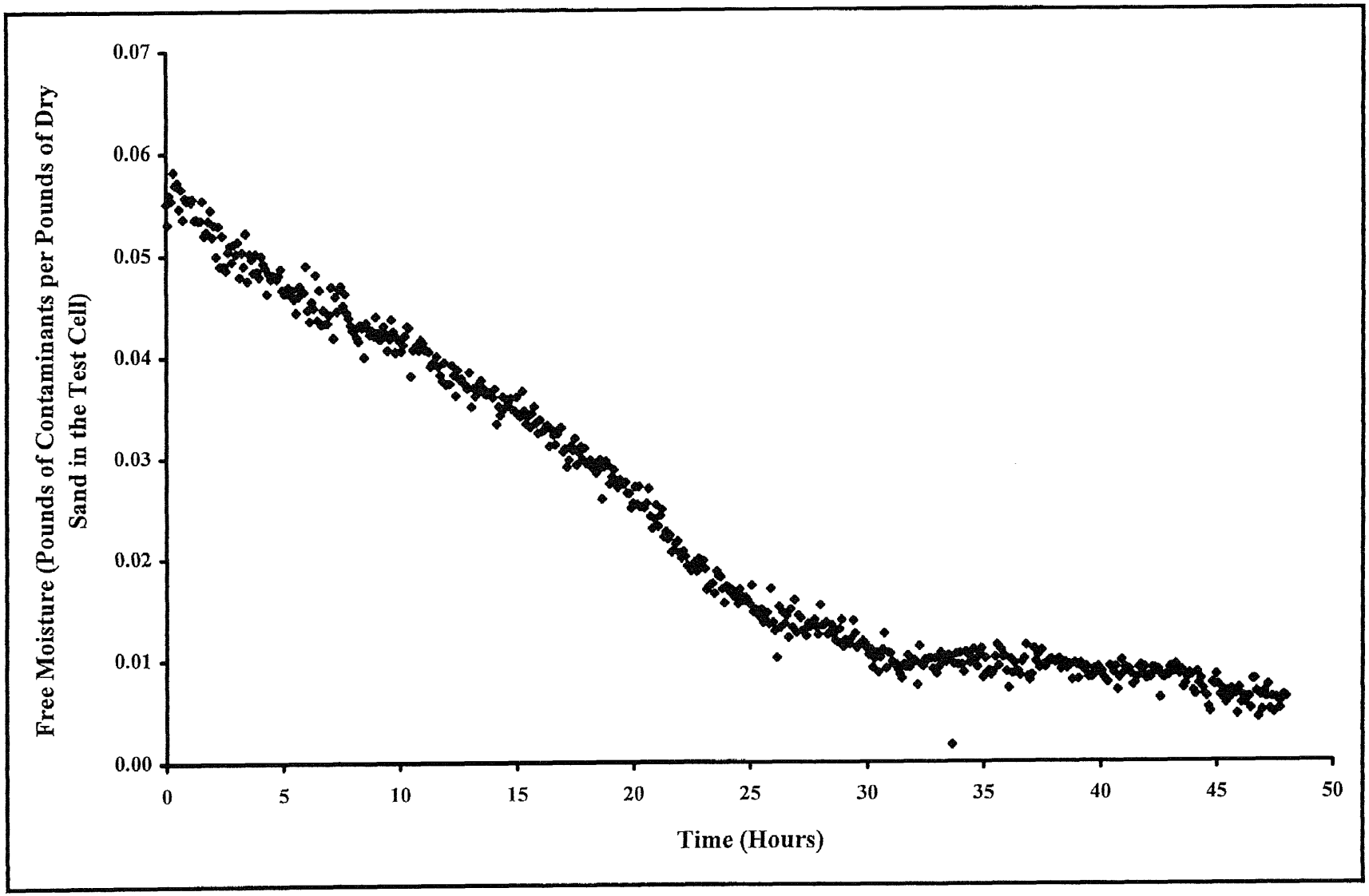

Figure A.13 Averaged Data of Free Moisture Versus Time for a Frequency of 6,637 Hertz (Run 1)

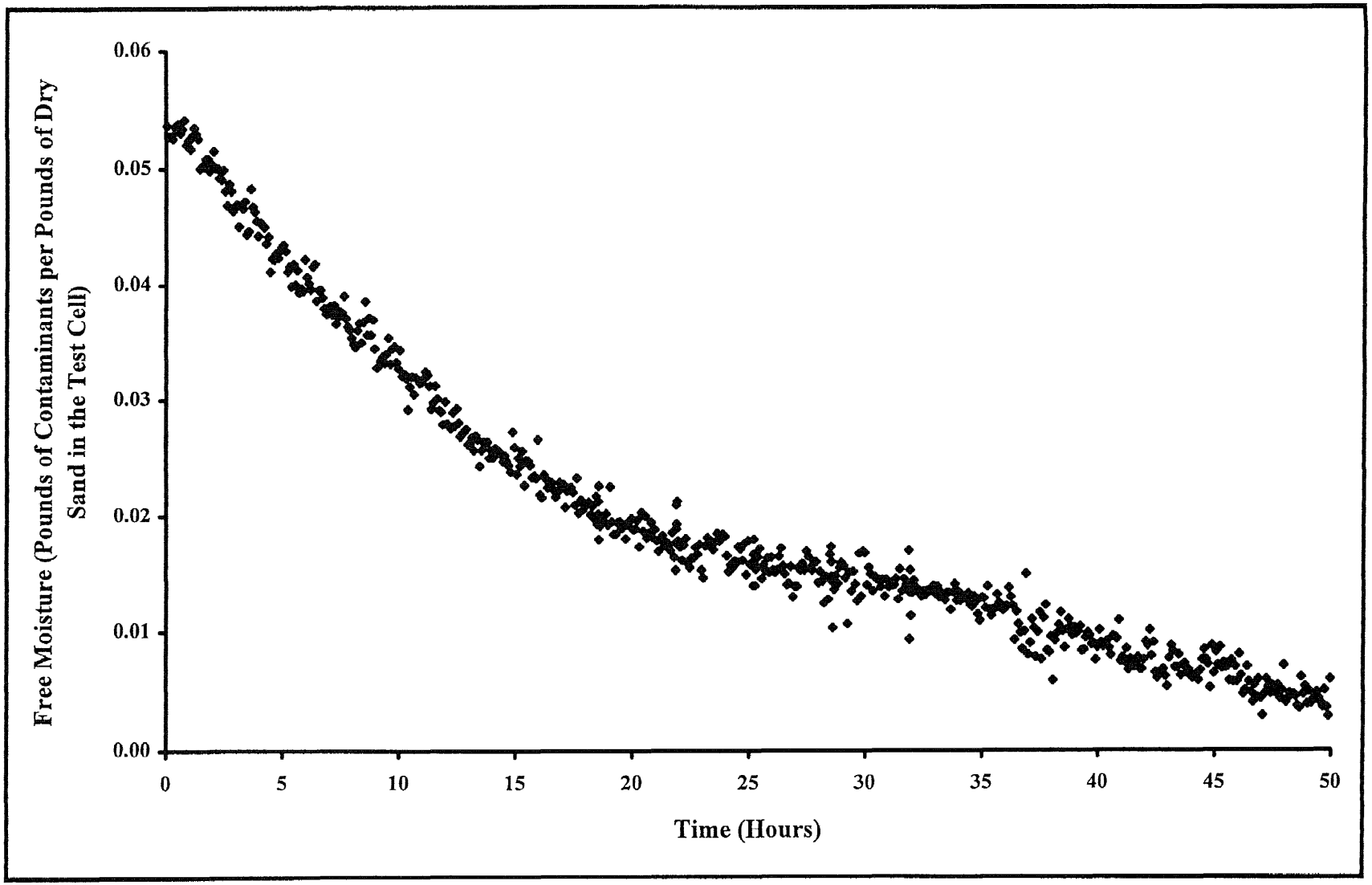

Figure A.14 Averaged Data of Free Moisture Versus Time for a Frequency of 6,637 Hertz (Run 2)

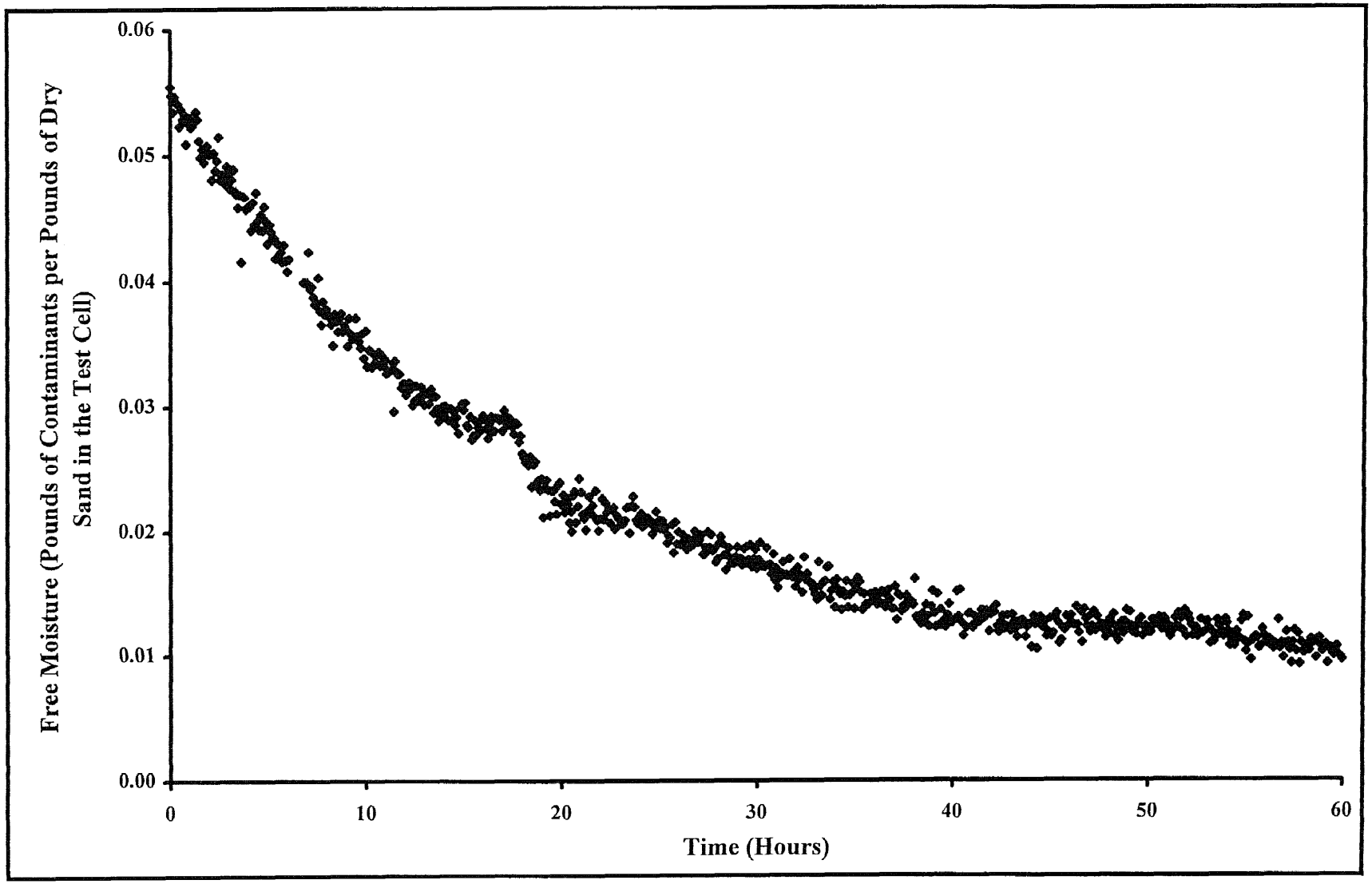

Figure A.15 Averaged Data of Free Moisture Versus Time for a Frequency of 10,317 Hertz

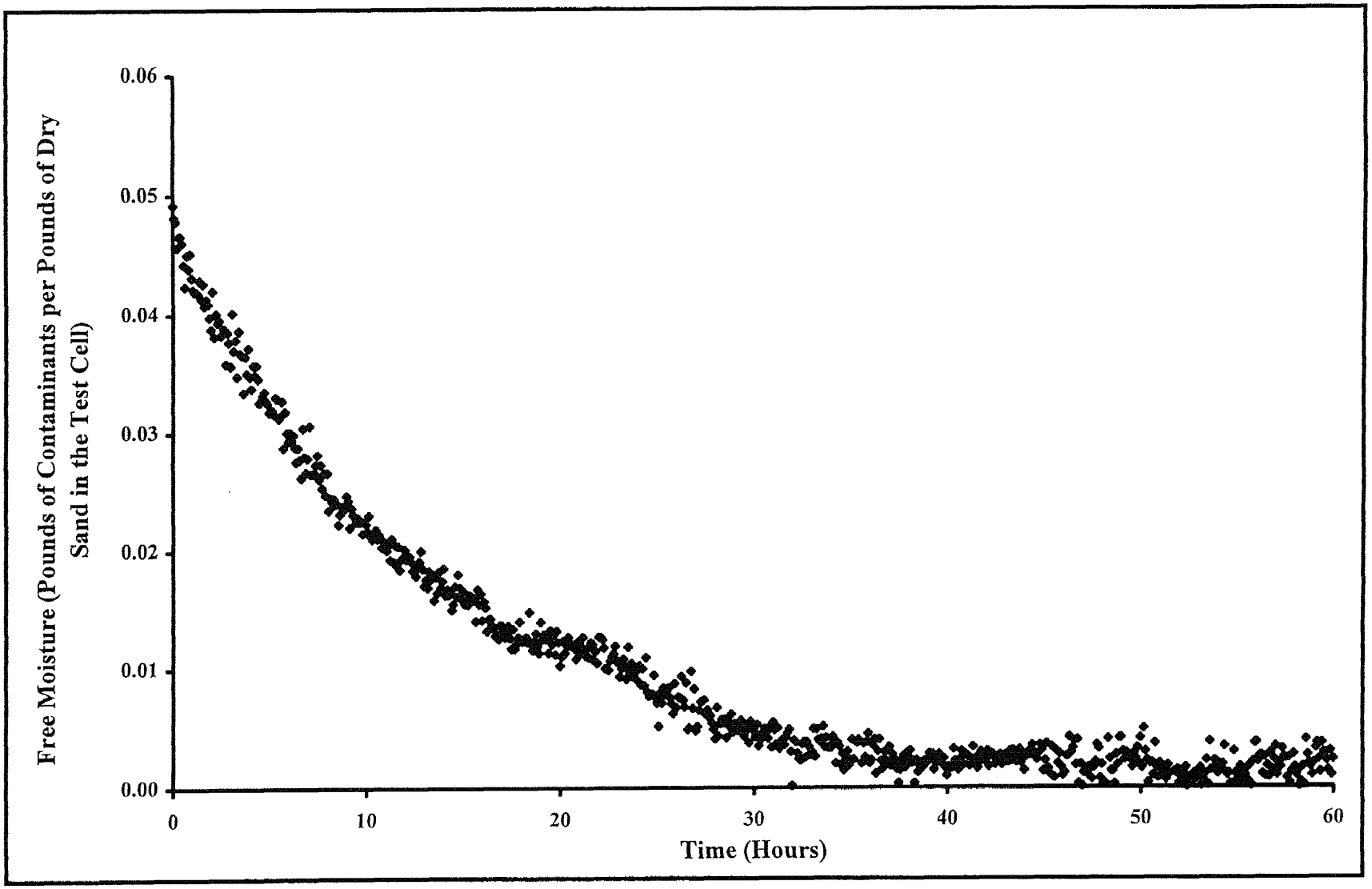

Figure A.16 Averaged Data of Free Moisture Versus Time for a Frequency of 13,997 Hertz

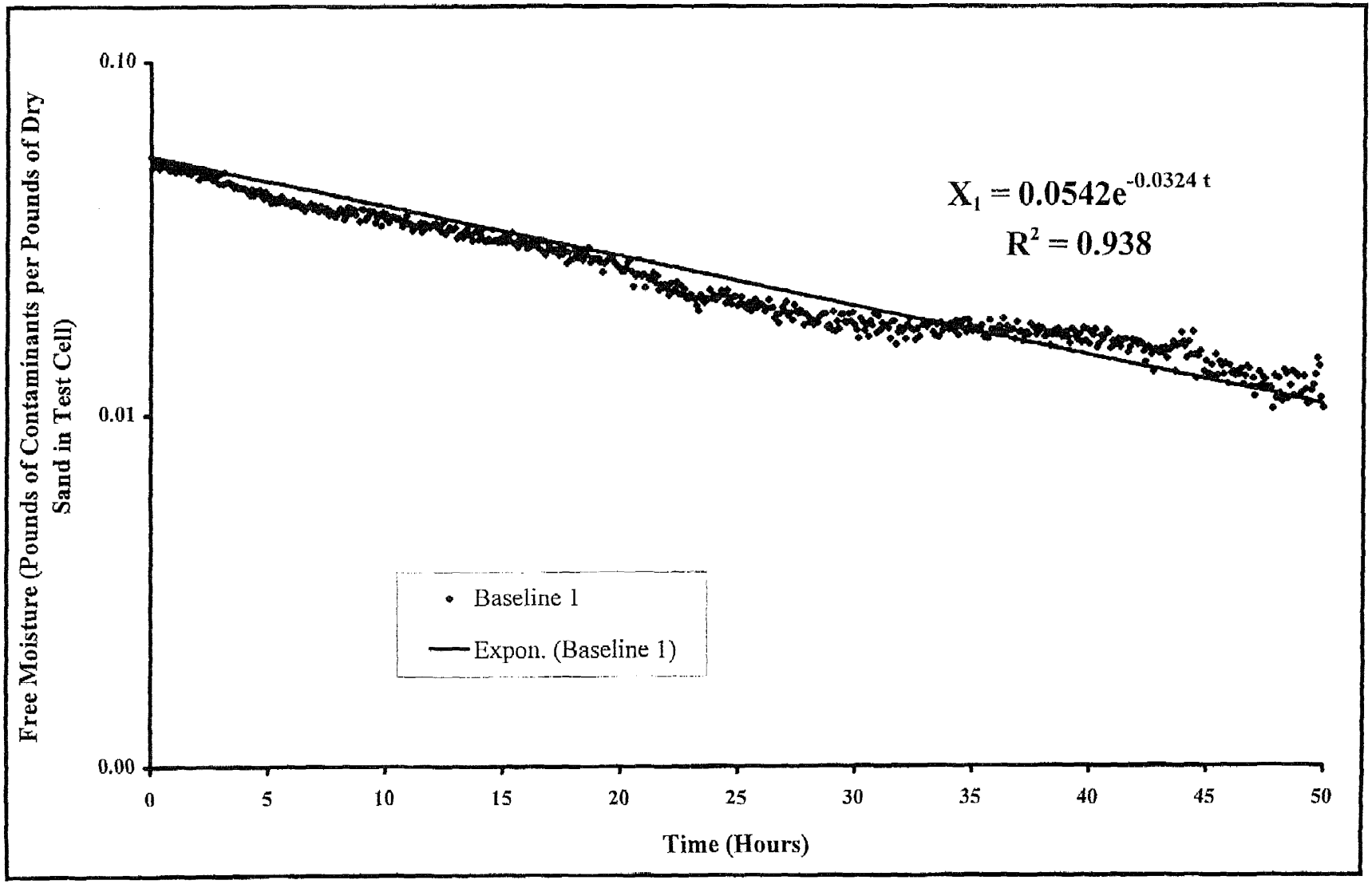

Figure A.17 Averaged Semi Logarithmic Curve Fit of Free Mositure Versus Time for Baseline Test (Run 1)

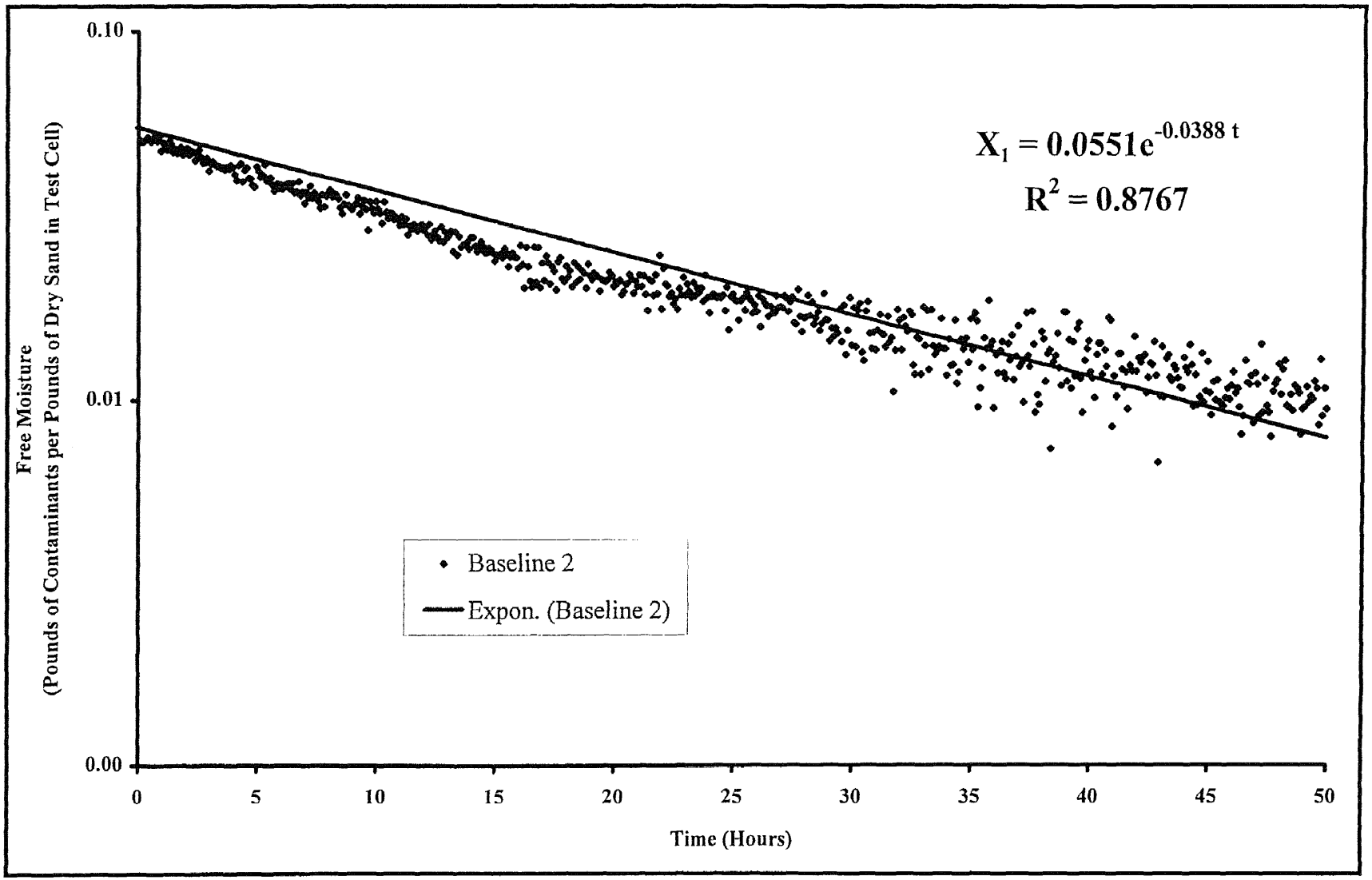

Figure A.18 Averaged Semi Logarithmic Curve Fit of Free Mositure Versus Time for Baseline Test (Run 2)

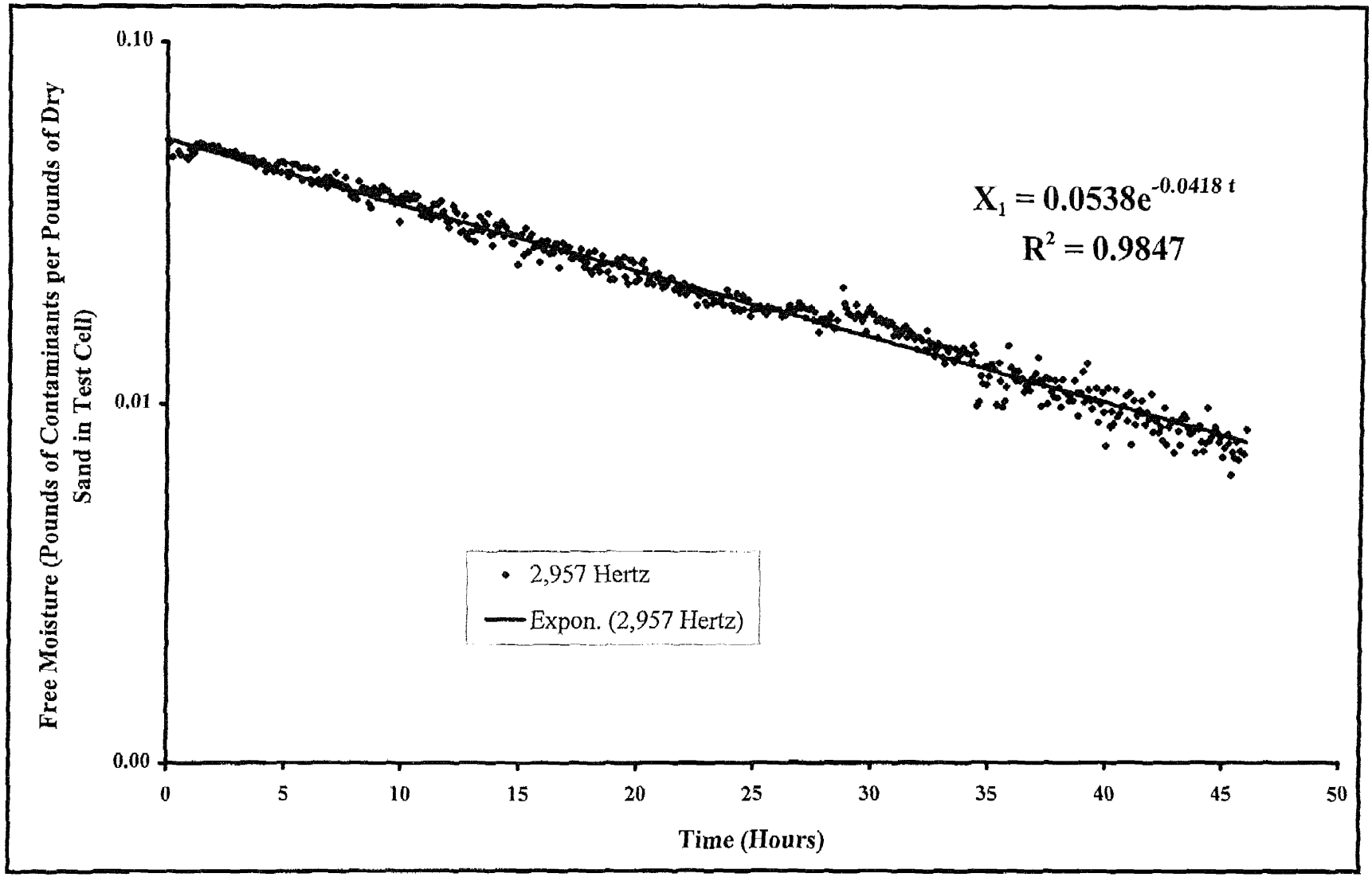

Figure A.19 Averaged Semi Logarithmic Curve Fit of Free Mositure Versus Time for a Frequency of 2,957 Hertz (Run 1)

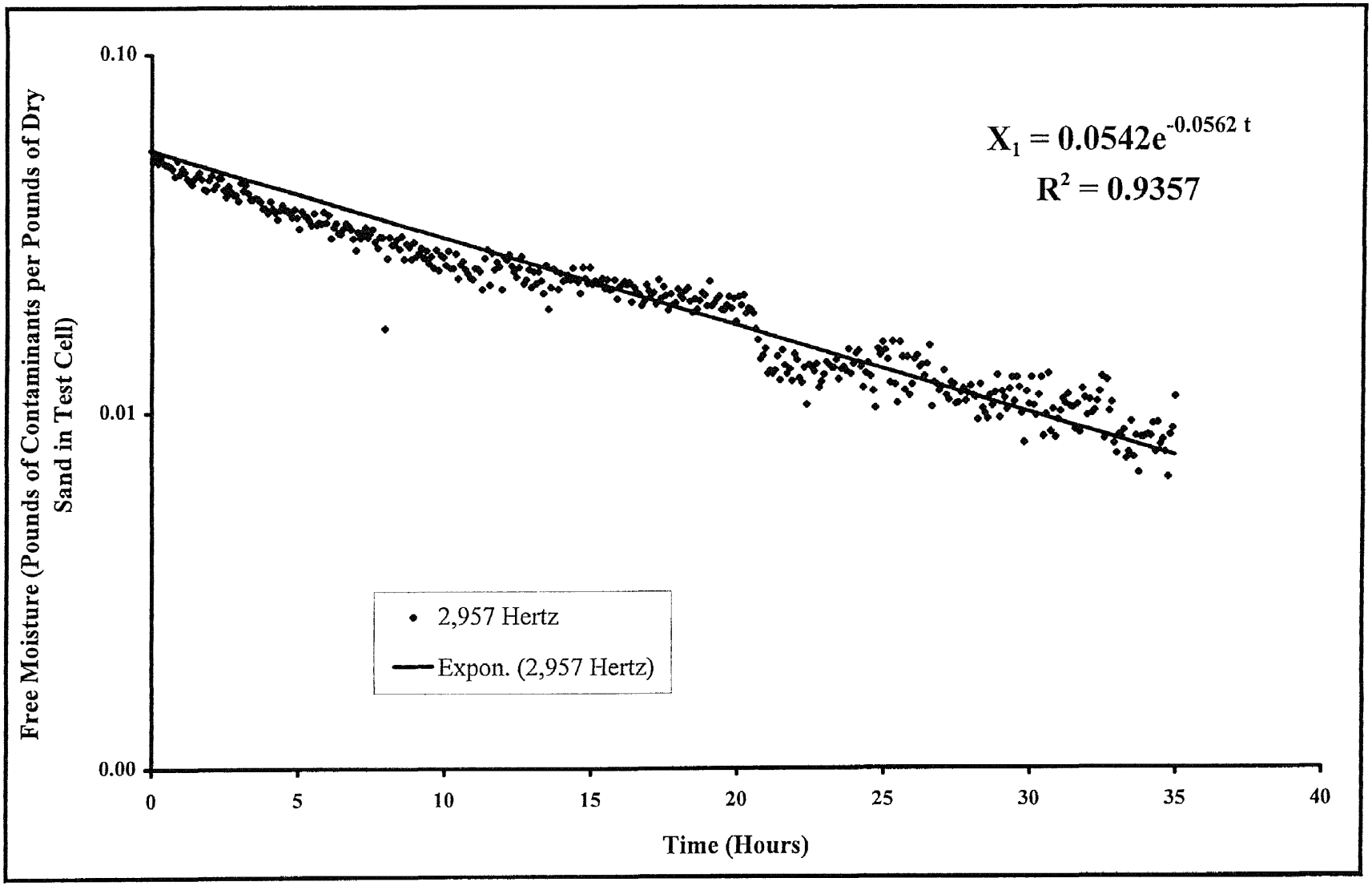

Figure A.20 Averaged Semi Logarithmic Curve Fit of Free Mositure Versus Time for at Frequency of 2,957 Hertz (Run 2)

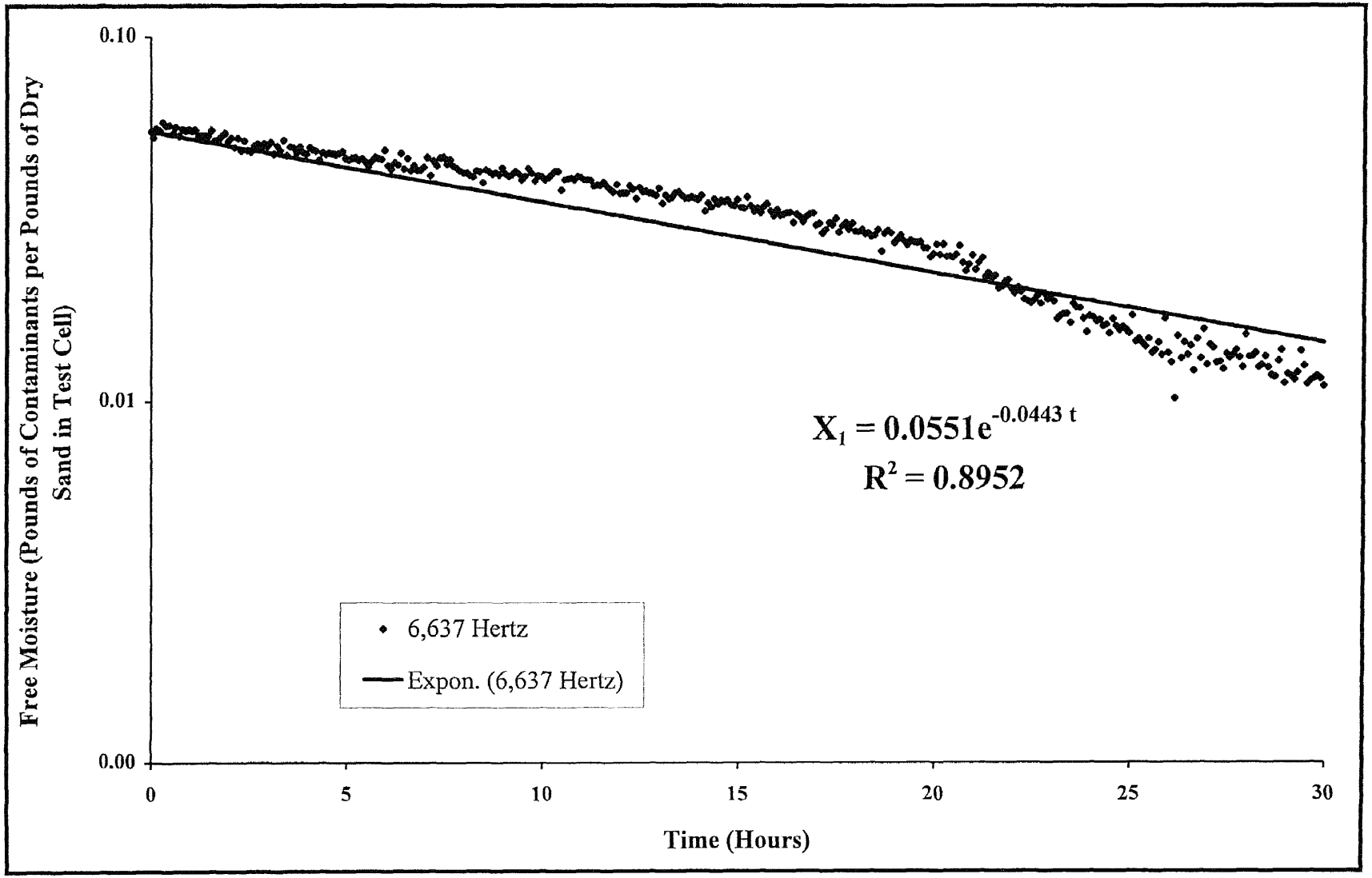

Figure A.21 Averaged Semi Logarithmic Curve Fit of Free Moisture Versus Time for a Frequency of 6,637 Hertz (Run 1)

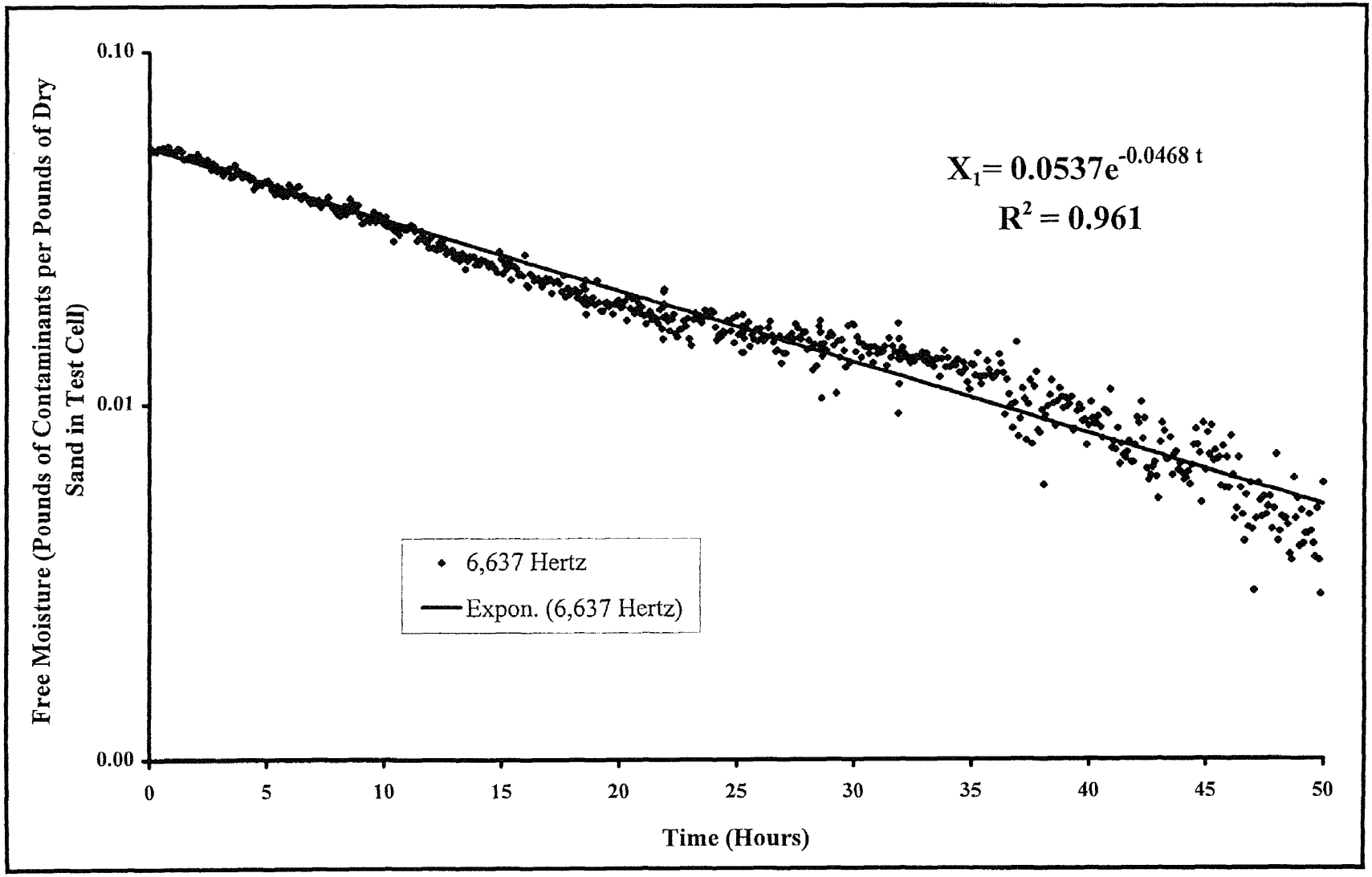

Figure A.22 Averaged Semi Logarithmic Curve Fit of Free Mositure Versus Time for a Frequency of 6,637 Hertz (Run 2)

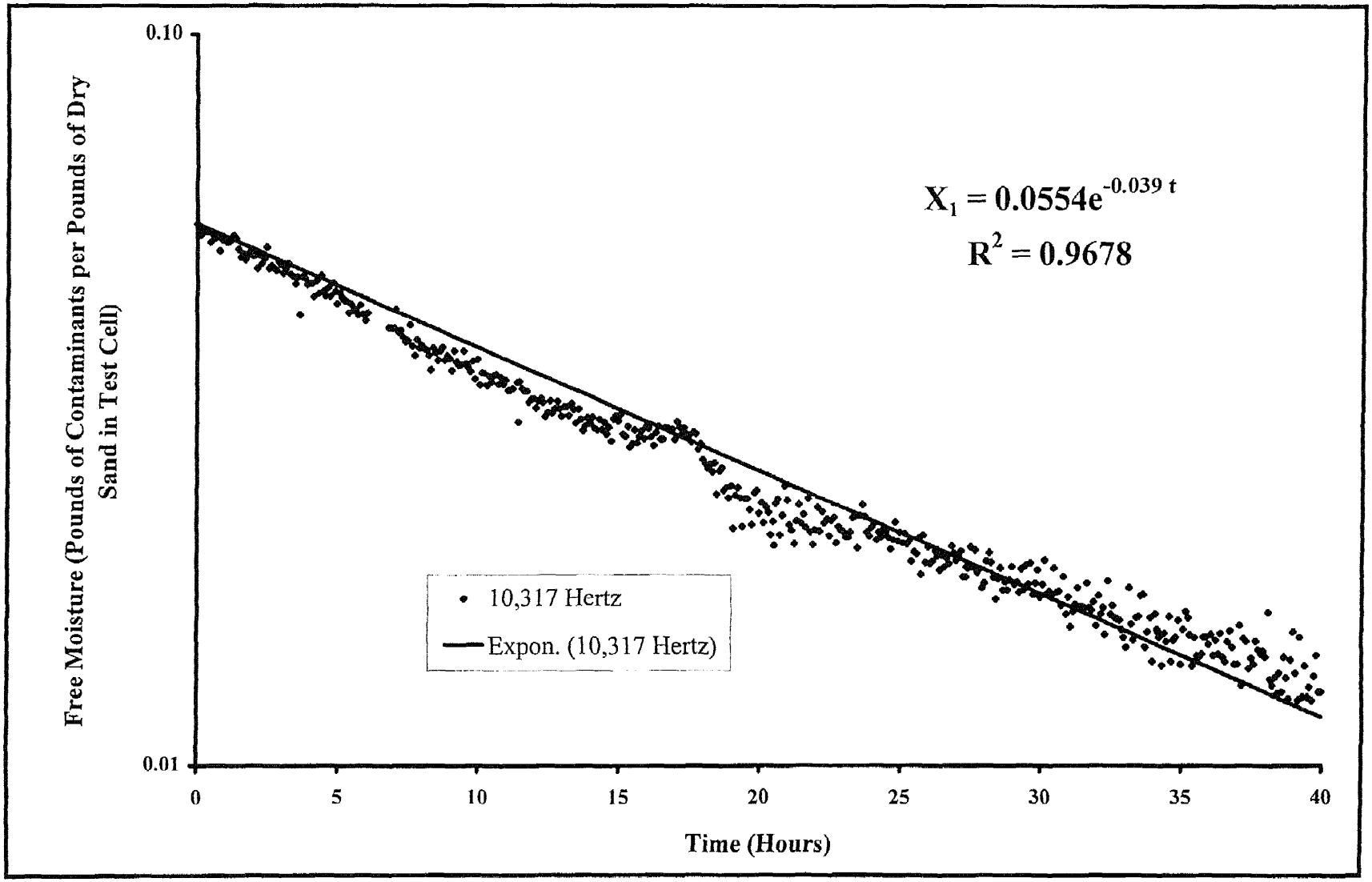

Figure A.23 Averaged Semi Logarithmic Curve Fit of Free Mositure Versus Time for a Frequency of 10,317 Hertz

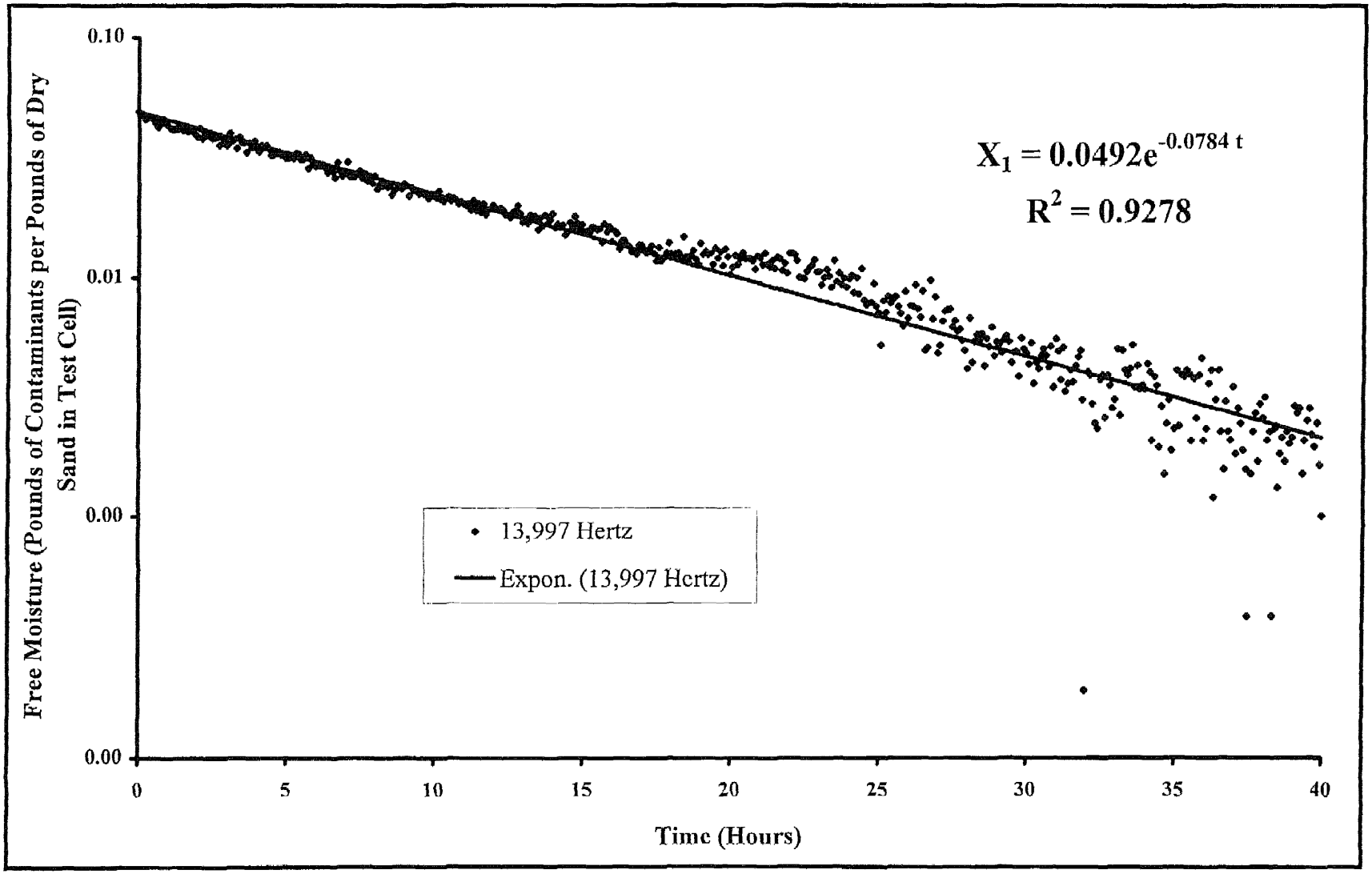

Figure A.24 Averaged Semi Logarithmic Curve Fit of Free Mositure Versus Time for a Frequency of 13,997 Hertz

APPENDIX B
ANALYSIS OF GAS SAMPLES AND CALCULATIONS

As discussed in Section 3.1.3, the monitoring of the concentration of the volatile organic compounds in the test cell throughout the experiment was important. For the purpose of this study, a GC was used by attaching to the extraction line coming out of the tank. Figure B.1 shows basic components included in a GC system. The heated areas of the system are shown by the broken lines.

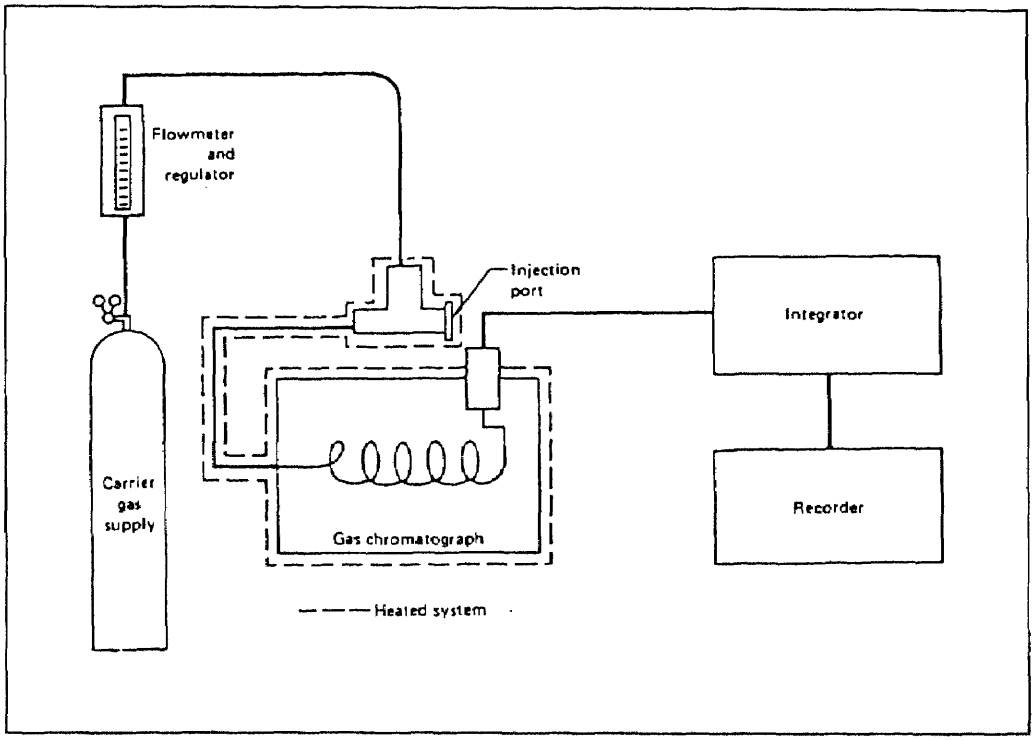

Figure B.1 Basic Components in a GC System from Walker (1977)

Seven sample solutions were made by mixing an ethyl alcohol composed of a 90% by volume ethanol solution with water. Table B.1 shows the composition and properties of the sample solution used in the calibration of the gas chromatograph

(GC) as well as for the experimental tests. Table B.2 shows the composition of the solutions prepared and used in the calibration of the GC, as well as the concentration in moles per liter, the area under the peak obtained from the integrator, and the number of moles injected into the GC for each sampling. Table B.3 provides information on the condition of the GC's setting. Finally, the results were plotted into a graph of Moles of Ethanol Detected versus Area Under the Peak. A linear regression line of *y=7E-15X+1E-09* (see Figure 3.6) and a correlation with an R^2 value of 0.9996 were obtained. (As explain in Section 4.2.1.1, another calibration curve applies to the baseline test runs 1 and 2)

Table B.1 Composition and Properties of The Ethyl Alcohol

Compound	Specific Gravity	% by Volume	Molecular Weight
Methanol	0.7914	5	32.04
Ethanol	0.7893	90	46.07
Isopropyl	0.7855	5	60.11

B.1 Calibration of the GC

The method for calibrating the GC involved simple steps. First, a series of sample solutions with different concentrations were prepared using ethyl alcohol with the composition listed in Table B.1 and distilled water. As shown in Table B.2, a total of seven solutions were prepared. Each solution was made with a different amount of ethyl alcohol as indicated in column 2 of the table. Then, these solutions were diluted with water up to 100 milliliters (except solution 7). After the solutions were

prepared, an amount of 1 micro liter (μl) for each solution was injected into the GC for analysis. The results were a series of peak areas obtained from the integrator. As discussed in Section 3.1.3, the integrator receives and integrates the signals sent by the detector. The detector will detect the amount of ethyl alcohol and hence the composition of the compound in the sampling loop. In Table B.2, column 3 shows the concentration of each sample, column 4 shows the detected areas obtained from the integrator, and the last column indicates the number of moles in the sample solution injected for each sampling.

Table B.2 Composition of the Samples Used and Data Obtained For the Calibration of the Gas Chromatography

Solution	Amount of Ethyl Alcohol	Concentration (moles/liter)	Area Under the Peak (Volts-Sec)	Number of Moles Injected
1	10 μl	1.54194E-03	189,779	1.54194E-09
2	20 μl	3.08387E-03	380,011	3.08387E-09
3	45 μl	6.93871E-03	828,296	6.93871E-09
4	60 μl	9.25162E-03	1,136,137	9.25162E-09
5	85 μl	1.31065E-02	1,735,192	1.31065E-08
6	100 μl	1.54194E-02	2,097,802	1.54194E-08
7	1 ml *	6.1677E-02	9,230,834	6.16775E-08

* Solution 7 was prepared with 1 ml of ethyl alcohol and diluted with water up to 250 ml.

B.2 Sample Calculation for Table B.2

Using solution 1 listed on Table B.2 as an example, 10 micro liters of 90% ethanol and 100 ml of water shows the concentration of ethanol in the sample solution is:

$$\left(\frac{10\ \mu l \text{ of } C_2H_5OH}{100\ ml \text{ of } H_2O}\right)\left(\frac{1x10^{-3}\ ml}{1\ \mu l}\right)\left(\frac{90\ \%}{100\ \%}\right)\left(\frac{0.7893\ g}{ml}\right)\left(\frac{1 mol}{46.07\ g}\right)\left(\frac{1000\ ml}{1\ liter}\right) \qquad \text{(B.1)}$$

and the result of equation B.1 is 1.54194 x 10^{-3}moles per liter of solution.

Each injection of the sample into the sampling loop was made consistently in the amount of 1 micro liter. Since the sample injection was 1 micro liter, the number of moles in the sample is,

$$(1.0\mu l)\left(\frac{1\,\text{liter}}{1x10^{6}\,\mu l}\right)\left(\frac{1.54194x10^{-3}\,moles}{liter}\right) = 1.54194 \text{ x } 10^{-9} \text{ moles} \qquad \text{(B.2)}$$

The GC is a very sensitive piece of equipment, therefore it is very important to keep the conditions consistent. The temperatures, flow rate of the gases and the sensitivity range were monitored closely throughout the experiments. A new calibration of the GC is required when any condition listed in Table B.3 is changed.

Table B.3 Gas Chromatogram Conditions

Temperature	Column: 70 °C Injector: 150 °C FID : 200 °C
Flow Rate	Nitrogen: 30 ml per min Air : 330 ml per min Hydrogen: 30 ml per min
Sensitivity Range	10 E-11 amps per MV

B.3 Sample Calculation for PPMv

Using Table B.6 as an example, at time 0.25 hour, the integrated area of ethanol is 2.21E+7. To calculate the concentration of the ethanol present in the sample in PPMv, follow the following steps,

1. Given the calibration curve obtained (Figure 3.6) and using the regression equation,

$$y = \text{number of moles} = 7\text{x}10^{-15} \cdot \text{integrated area} + 1\text{x}10^{-9} \qquad \text{(B.3)}$$

substituting the integrated area of 2.21 x 10^7 into equation B.3, gives

$$y = \text{number of moles} = \left(7\text{x}10^{-15}\right)\cdot\left(2.21\text{x}10^{7}\right) + 1\text{x}10^{-9}$$

$$= 1.557\text{x}10^{-7} \text{ moles of ethanol}$$

2. To determine the concentration of ethanol:

$$\text{Concentration of Ethanol in } \frac{\text{moles}}{\text{liter}} \text{ of gas} = \frac{\text{Number of Moles of Ethanol}}{\text{Volume of Sampling Loop}} \qquad \text{(B.4)}$$

Knowing that there are 1.557 x 10^{-7} moles of ethanol, the sampling loop is 0.003 liter, and equation B.4 becomes:

$$\text{Concentration of Ethanol in } \frac{\text{moles}}{\text{liter}} \text{ of gas} = \frac{1.557 \text{ x } 10^{-7} \text{ moles of gas}}{0.003 \text{ liter of gas}} \qquad \text{(B.5)}$$

$$\text{Concentration of Ethanol} = 5.19x10^{-5} \frac{\text{moles of ethanol}}{\text{liter of gas}}$$

3. To convert moles per liter to PPMV, equation B.5 is used,

$$\text{PPMv} = \left(\text{volumtric flow rate}\right)\left(\frac{\text{Concentration of Ethanol}}{\text{Total Molar Flow Rate}}\right)x10^{6} \qquad \text{(B.6)}$$

The volumetric Flow Rate is 7 standard cubic feet per minute (SCFM), as found on Table A.1. Since there are 28.32 liters per cubic feet, using simple conversion of units, 7 SCFM becomes 198.24 liters per minute. Total molar flow rate is calculated from the ideal gas law,

$$n = \frac{PV}{RT} = \frac{(1\ \text{atm})\left(198.24\ \frac{\text{liter of gas}}{\text{minute}}\right)}{(298\ \text{K})\left(0.082054\ \frac{\text{lit} \cdot \text{atm}}{\text{K} \cdot \text{mol}}\right)} \qquad \text{(B.7)}$$

$$= 8.107\ \frac{\text{moles of gas}}{\text{minute}}$$

Going back to equation B.6,

$$198.24 \frac{\text{liter of gas}}{\text{min}} \left[\frac{5.19\text{x}10^{-5} \frac{\text{moles of ethanol}}{\text{liter of gas}}}{8.107 \frac{\text{moles of gas}}{\text{min}}} \right] \text{x}10^{6} \qquad \text{(B.8)}$$

$$= 1269.108 \frac{\text{moles of ethanol}}{\text{moles of gas}}$$

Table B.4 Results of GC Analysis for Baseline Test (Run 1)

Actual Time (Hour)	Integrated Area of Ethanol (Volt*Sec)	Outlet Concentration of Ethanol (PPMv)
0.25	8.0E+07	664.53
0.75	6.3E+07	533.68
1.00	5.1E+07	434.33
1.25	4.2E+07	359.72
1.50	3.4E+07	294.82
2.50	1.8E+07	159.06
2.75	1.5E+07	137.33
3.00	1.3E+07	123.44
3.25	1.3E+07	118.73
3.50	1.1E+07	108.04
3.75	1.0E+07	99.49
4.00	9.9E+06	96.70
4.25	8.8E+06	87.80
4.50	8.7E+06	86.94
4.75	7.7E+06	79.16
5.00	7.5E+06	77.35
5.25	6.9E+06	72.60
5.50	6.9E+06	72.61
5.75	6.2E+06	66.46
6.00	5.9E+06	64.74
6.25	6.1E+06	66.14
6.50	5.6E+06	61.87
9.00	4.6E+06	53.40
9.25	4.4E+06	52.53
9.75	4.2E+06	50.34
10.25	4.1E+06	49.88
10.75	3.8E+06	47.58
11.25	3.7E+06	46.73
11.75	3.7E+06	46.28
12.25	3.5E+06	44.72
21.75	1.39E+06	27.65
22.75	1.33E+06	27.13
23.75	1.13E+06	25.52
24.77	9.21E+05	23.81
25.53	9.10E+05	23.72
27.62	7.12E+05	22.11
29.73	6.01E+05	21.20
29.98	5.92E+05	21.12
30.25	5.72E+05	20.96
30.52	5.61E+05	20.87
30.78	5.63E+05	20.89
41.33	5.10E+04	16.72

Table B.5 Results of GC Analysis for Baseline Test (Run 2)

Actual Time (Hour)	Integrated Area of Ethanol (Volt*Sec)	Outlet Concentration of Ethanol (PPMv)
0.50	9.04E+07	752.98
0.75	6.31E+07	530.76
1.00	4.75E+07	403.41
1.25	3.89E+07	333.37
1.75	3.12E+07	270.69
2.00	2.82E+07	245.86
2.25	2.02E+07	180.69
3.50	1.00E+07	97.81
3.75	7.75E+06	79.45
5.00	5.76E+06	63.22
7.75	2.96E+06	40.42
8.00	1.82E+06	31.11
12.00	1.35E+06	27.28
14.00	1.38E+06	27.59
14.75	1.24E+06	26.41
18.50	5.12E+05	20.48
20.25	2.73E+05	18.52
21.00	1.88E+05	17.84
21.50	7.80E+04	16.94
24.00	1.12E+04	16.39
24.25	5.95E+04	16.79
24.75	1.62E+05	17.62
25.25	2.08E+04	16.47
25.50	6.83E+04	16.86
28.50	1.36E+04	16.41
29.75	2.29E+04	16.49
30.50	4.99E+04	16.71

Table B.6 Results of GC Analysis for a Frequency of 2,957 Hertz (Run 1)

Actual Time (Hour)	Integrated Area of Ethanol (Volt*Sec)	Outlet Concentration of Ethanol (PPMv)	Actual Time (Hour)	Integrated Area of Ethanol (Volt*Sec)	Outlet Concentration of Ethanol (PPMv)
0.25	2.21E+07	1269.11	15.50	9.61E+06	556.45
0.50	2.11E+07	1212.26	17.00	9.11E+06	528.03
0.75	2.04E+07	1171.93	18.50	8.67E+06	502.95
1.00	1.99E+07	1141.40	20.00	8.17E+06	474.25
1.25	1.94E+07	1115.56	21.50	7.48E+06	435.08
1.50	1.90E+07	1092.76	23.00	6.94E+06	404.09
1.75	1.87E+07	1073.04	24.00	6.64E+06	387.13
2.00	1.83E+07	1053.02	26.00	5.25E+06	307.82
2.25	1.80E+07	1035.39	27.25	4.60E+06	270.55
2.50	1.77E+07	1019.38	28.92	3.95E+06	233.38
2.75	1.75E+07	1004.41	30.42	3.19E+06	190.44
3.00	1.72E+07	989.28	31.92	2.79E+06	167.29
3.50	1.67E+07	960.07	33.42	2.42E+06	146.37
3.75	1.65E+07	947.49	34.92	2.04E+06	124.44
4.25	1.60E+07	922.52	36.42	1.69E+06	104.80
4.75	1.56E+07	899.26	37.92	1.40E+06	87.78
5.00	1.53E+07	881.61	40.92	1.51E+06	94.22
5.50	1.50E+07	863.75	42.42	1.28E+06	81.11
5.75	1.47E+07	847.58	43.92	1.05E+06	67.86
6.00	1.45E+07	833.61	45.42	8.29E+05	55.47
6.50	1.40E+07	806.55	46.92	6.84E+05	47.16
8.00	1.29E+07	746.90	48.42	5.67E+05	40.50
9.50	1.23E+07	711.14	49.92	4.69E+05	34.90
11.00	1.16E+07	667.83	51.42	4.04E+05	31.18
12.50	1.08E+07	624.49	52.92	3.72E+05	29.38
14.00	1.02E+07	588.20	54.42	3.18E+05	26.29

Table B.7 Results of GC Analysis for a Frequency of 6,637 Hertz (Run 2)

Actual Time (Hour)	Integrated Area of Ethanol (Volt*Sec)	Outlet Concentration of Ethanol (PPMv)	Actual Time (Hour)	Integrated Area of Ethanol (Volt*Sec)	Outlet Concentration of Ethanol (PPMv)
0.00	7.12E+07	4069.20	11.00	7.88E+06	457.89
0.33	5.43E+07	3103.60	11.33	7.29E+06	424.10
0.67	4.71E+07	2698.24	11.67	6.76E+06	393.76
1.00	4.27E+07	2444.07	12.00	6.14E+06	358.57
1.33	3.94E+07	2258.87	12.33	5.85E+06	341.97
1.67	3.70E+07	2118.18	12.83	5.24E+06	307.23
2.00	3.50E+07	2005.15	13.33	4.67E+06	274.37
2.33	3.32E+07	1900.13	13.83	4.02E+06	237.36
2.67	3.15E+07	1805.55	14.33	3.77E+06	223.27
3.00	3.00E+07	1722.11	14.83	3.57E+06	211.85
3.33	2.87E+07	1645.30	15.33	3.32E+06	197.71
3.67	2.74E+07	1573.23	15.83	3.05E+06	182.17
4.00	2.62E+07	1503.75	16.33	2.73E+06	163.68
4.33	2.50E+07	1433.90	16.83	2.54E+06	152.94
4.67	2.39E+07	1373.33	17.33	2.33E+06	140.86
5.00	2.29E+07	1316.51	17.83	2.10E+06	128.10
5.33	2.19E+07	1260.37	18.33	1.87E+06	114.84
5.67	2.10E+07	1207.20	18.83	1.69E+06	104.74
6.00	2.00E+07	1151.86	19.83	1.35E+06	85.22
6.33	1.92E+07	1101.73	21.33	1.02E+06	66.56
6.67	1.82E+07	1046.68	22.83	7.86E+05	53.00
7.00	1.73E+07	995.65	24.33	6.27E+05	43.91
7.33	1.64E+07	943.36	25.83	4.99E+05	36.63
7.67	1.55E+07	893.46	27.33	4.26E+05	32.47
8.00	1.46E+07	842.55	28.83	4.48E+05	33.73
8.33	1.38E+07	793.85	65.17	2.76E+04	9.73
8.67	1.29E+07	744.81	65.67	2.45E+04	9.55
9.00	1.21E+07	699.65	66.17	2.15E+04	9.38
9.33	1.14E+07	655.95	66.67	1.77E+04	9.16
9.67	1.06E+07	614.03	67.17	1.53E+04	9.02
10.00	9.92E+06	573.95	67.67	1.44E+04	8.97
10.33	9.20E+06	532.86	68.17	1.24E+04	8.86
10.67	8.51E+06	493.44			

Table B.8 Results of GC Analysis for a Frequency of 10,317 Hertz

Actual Time (Hour)	Integrated Area of Ethanol (Volt*Sec)	Outlet Concentration of Ethanol (PPMv)	Actual Time (Hour)	Integrated Area of Ethanol (Volt*Sec)	Outlet Concentration of Ethanol (PPMv)
0.25	1.81E+07	163.71	9.00	3.02E+06	40.92
0.50	1.68E+07	153.20	9.25	2.91E+06	40.06
0.75	1.47E+07	136.13	9.50	2.88E+06	39.78
1.00	1.33E+07	124.96	9.75	2.72E+06	38.44
1.25	1.20E+07	114.45	10.00	2.60E+06	37.51
1.50	1.09E+07	105.31	10.25	2.54E+06	37.02
1.75	1.00E+07	97.89	10.50	2.39E+06	35.79
2.00	9.24E+06	91.60	10.75	2.33E+06	35.26
2.25	8.69E+06	87.11	11.00	2.25E+06	34.66
2.50	7.98E+06	81.37	11.25	2.18E+06	34.08
2.75	7.56E+06	77.89	11.50	2.05E+06	32.98
3.00	7.10E+06	74.18	11.75	1.98E+06	32.41
3.25	6.55E+06	69.72	12.00	1.92E+06	31.93
3.50	5.53E+06	61.40	12.25	1.89E+06	31.71
3.75	6.09E+06	65.90	12.50	1.79E+06	30.90
4.00	5.71E+06	62.84	12.75	1.72E+06	30.35
4.25	5.38E+06	60.19	13.00	1.67E+06	29.88
4.50	5.25E+06	59.09	13.25	1.34E+06	27.21
4.75	5.24E+06	59.04	13.50	1.51E+06	28.63
5.00	4.88E+06	56.11	13.75	1.45E+06	28.11
5.25	4.70E+06	54.59	14.00	1.39E+06	27.66
5.50	4.53E+06	53.25	16.75	7.57E+05	22.47
5.75	4.45E+06	52.54	20.25	2.69E+05	18.50
6.00	4.40E+06	52.20	20.75	3.50E+05	19.15
6.25	4.17E+06	50.31	21.00	2.61E+05	18.43
6.50	4.07E+06	49.49	21.75	2.47E+05	18.32
6.75	3.94E+06	48.43	22.25	2.22E+05	18.11
7.00	3.81E+06	47.33	22.75	1.94E+05	17.88
7.25	3.76E+06	46.98	23.25	1.68E+05	17.67
7.50	3.59E+06	45.59	26.25	5.62E+04	16.76
7.75	3.50E+06	44.83	26.75	6.82E+04	16.86
8.00	3.47E+06	44.58	27.25	5.54E+04	16.75
8.25	3.35E+06	43.64	28.25	2.80E+04	16.53
8.50	3.18E+06	42.24	29.25	1.96E+04	16.46
8.75	3.14E+06	41.88			

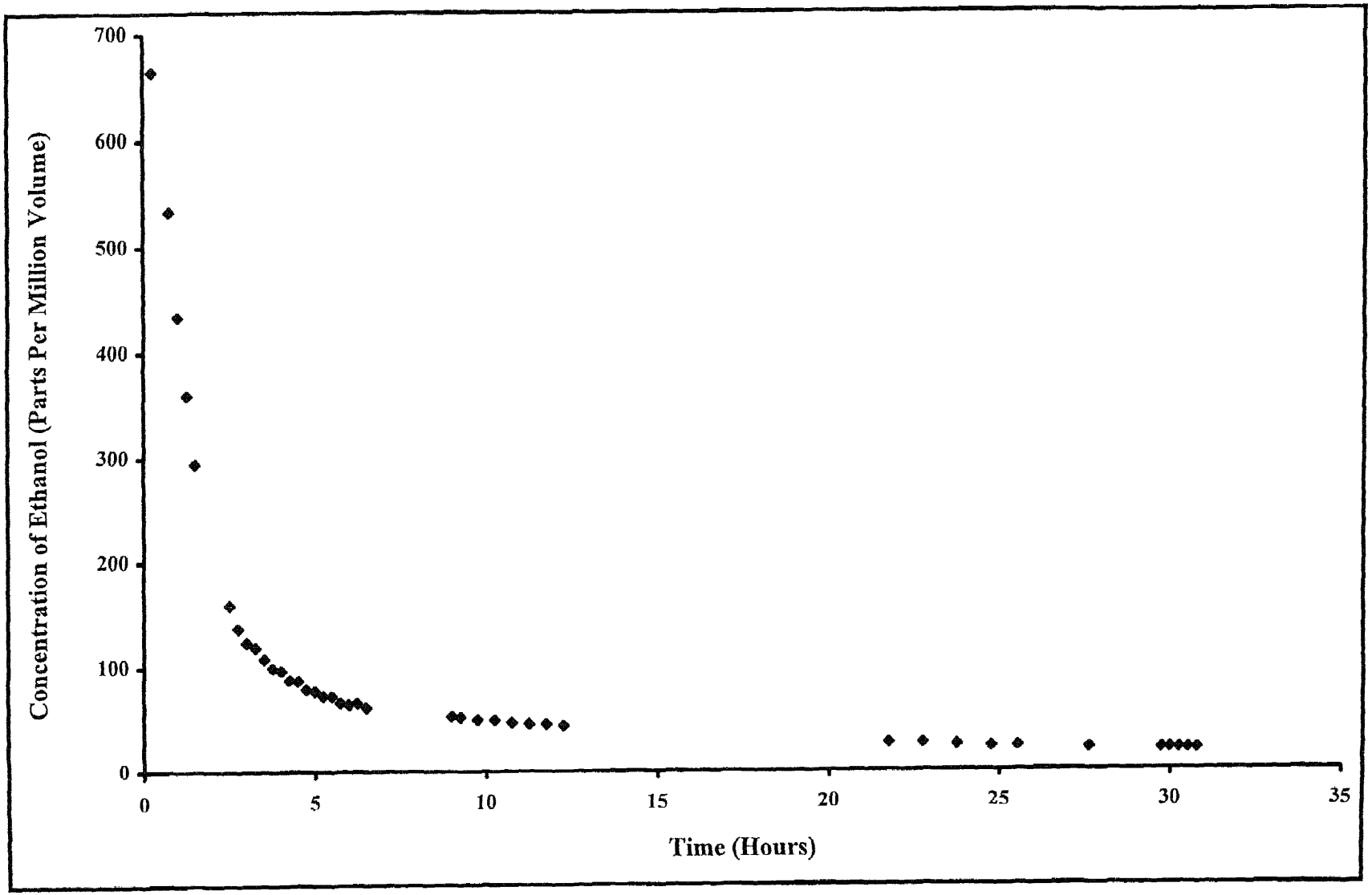

Figure B.1 Measured Data of Concentration of Ethanol Versus Time for Baseline Test (Run 1)

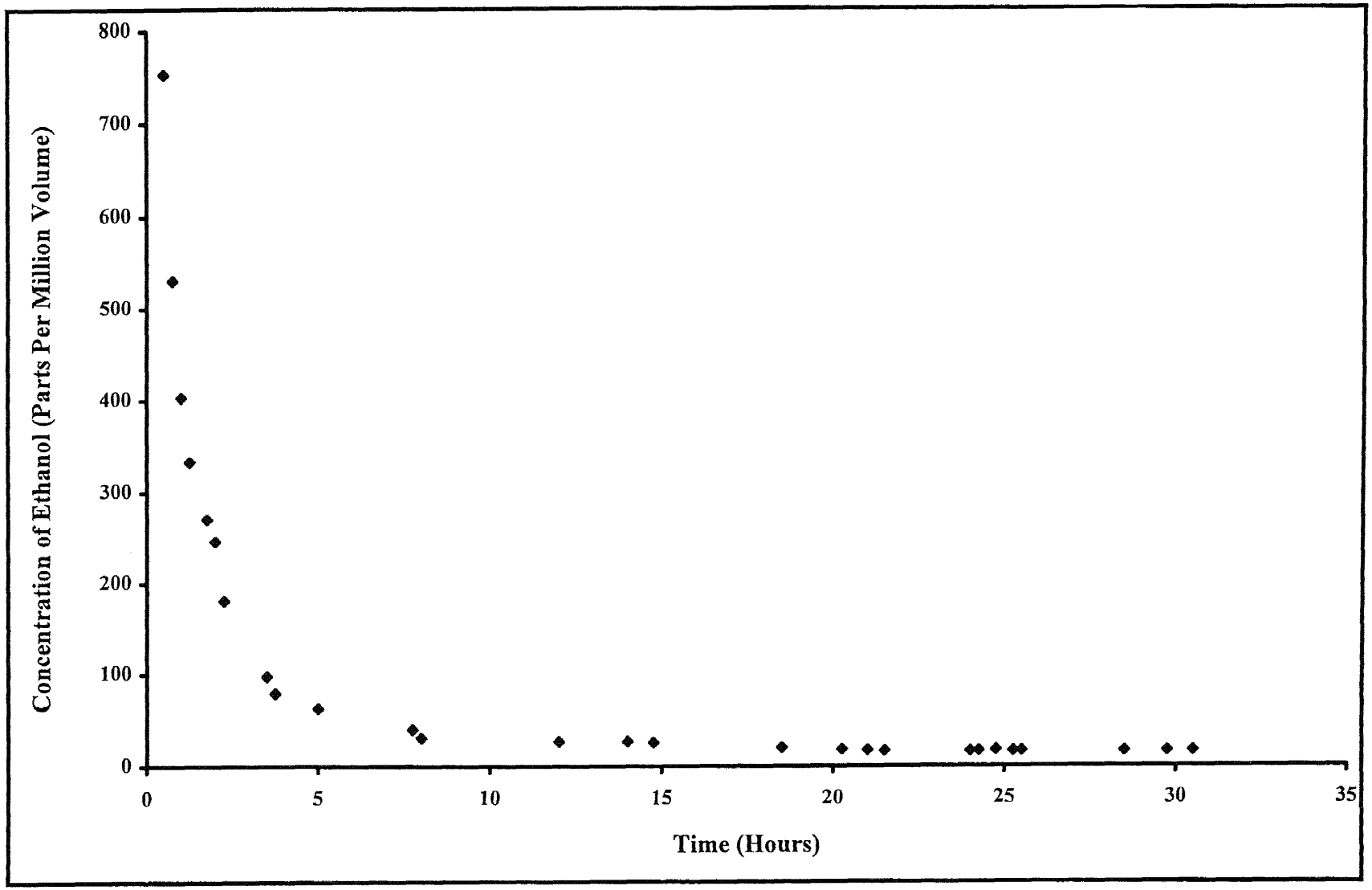

Figure B.2 Measured Data of Concentration of Ethanol Versus Time for Baseline Test (Run 2)

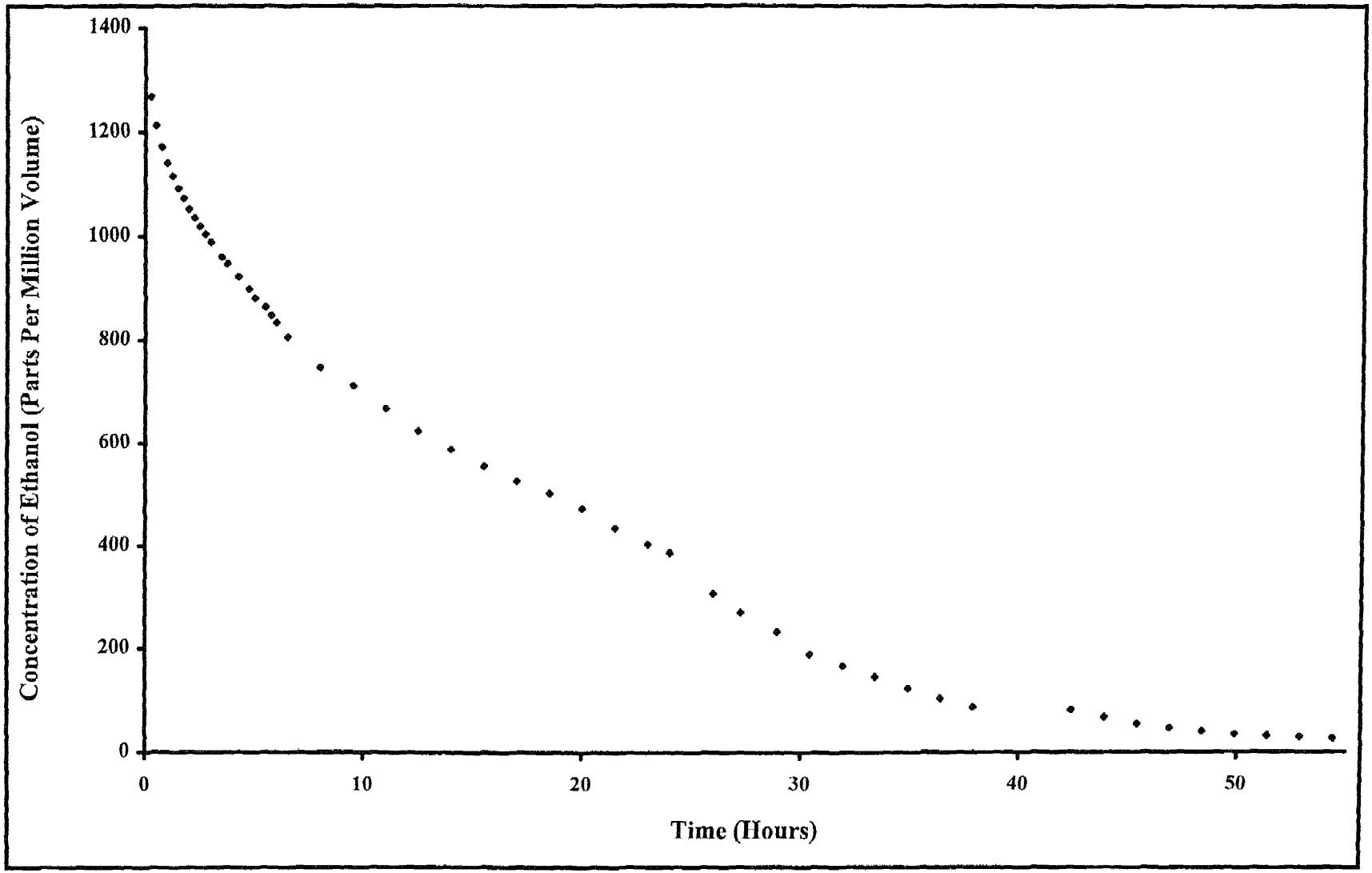

Figure B.3 Measured Data of Concentration of Ethanol Versus Time for a Frequency of 2,957 Hertz (Run 1)

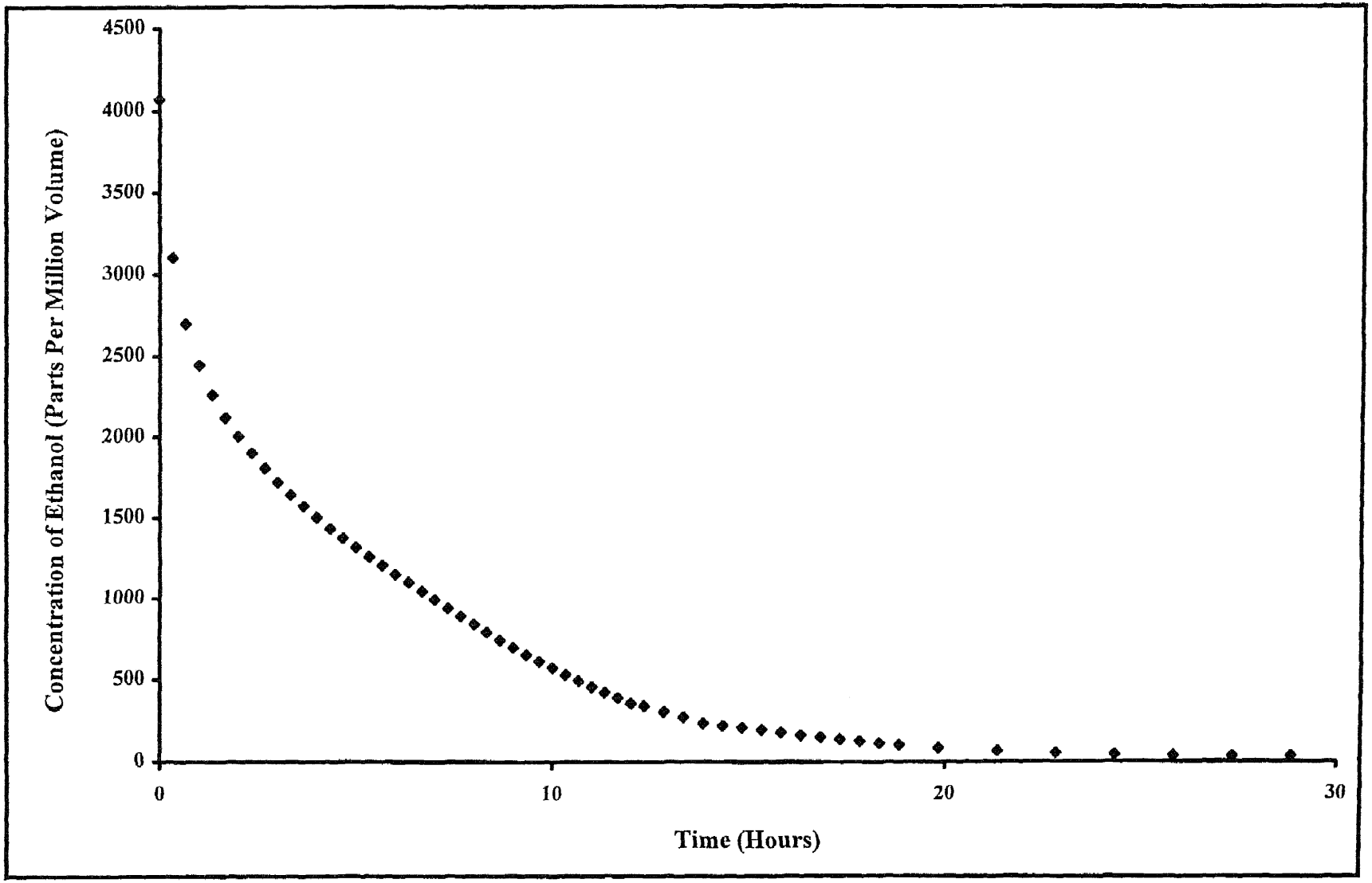

Figure B.4 Measured Data of Concentration of Ethanol Versus Time for a Frequency of 6,637 Hertz (Run 2)

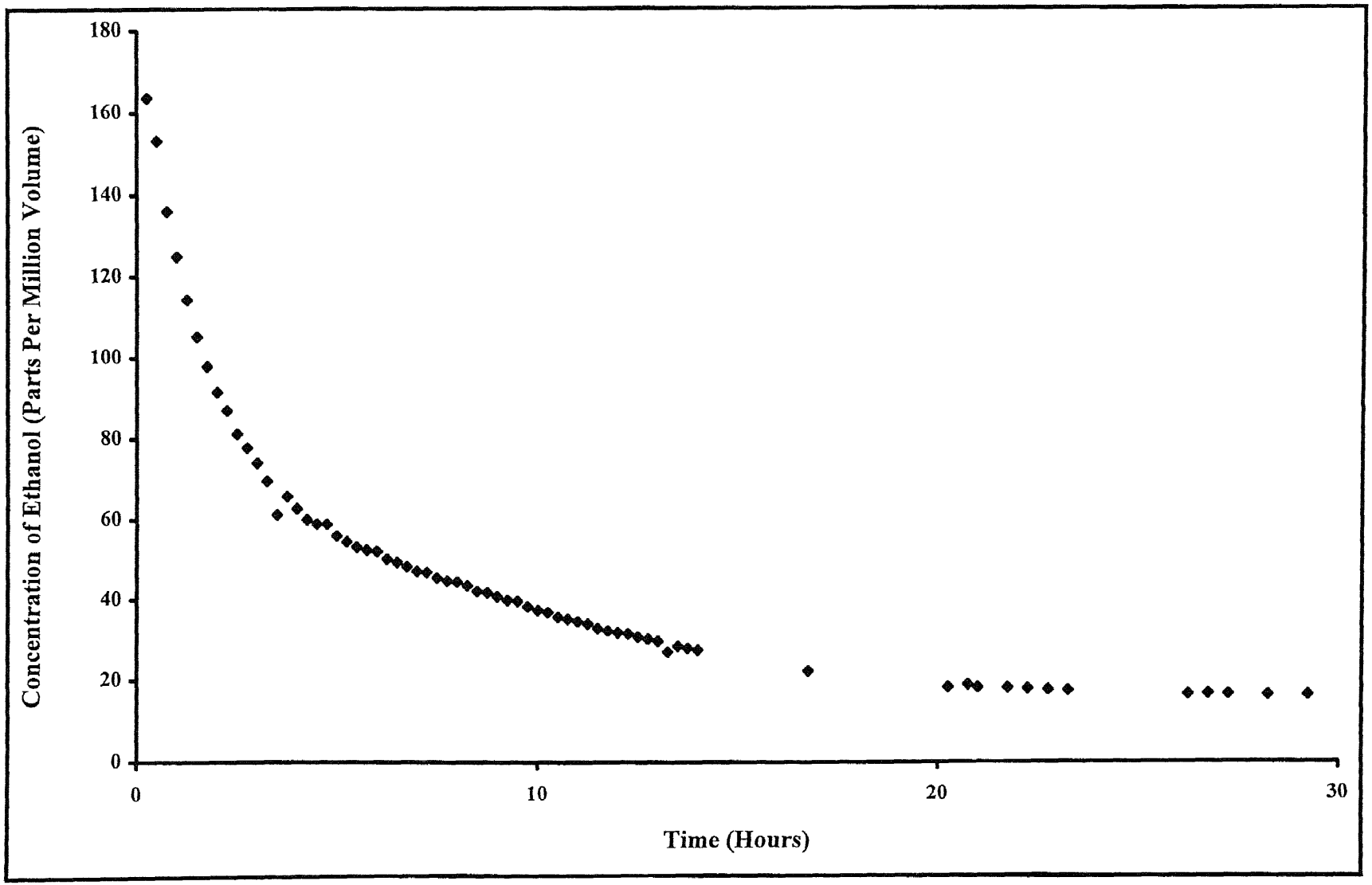

Figure B.5 Measured Data of Concentration of Ethanol Versus Time for a Frequency of 10,317 Hertz

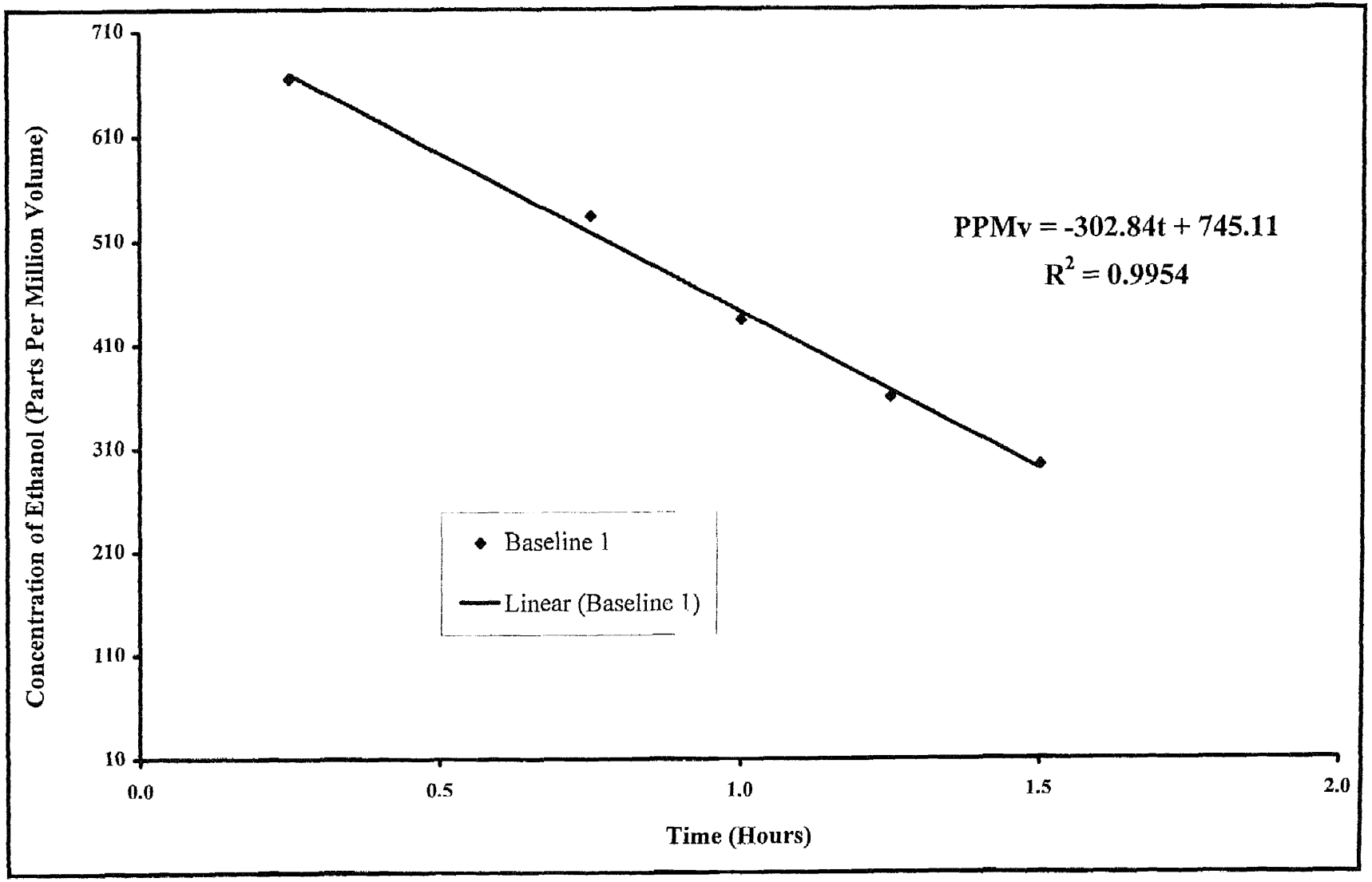

Figure B.6 Arithmetic Plot of Concentration of Ethanol Versus Time in the Constant Rate Region for Baseline Test (Run 1)

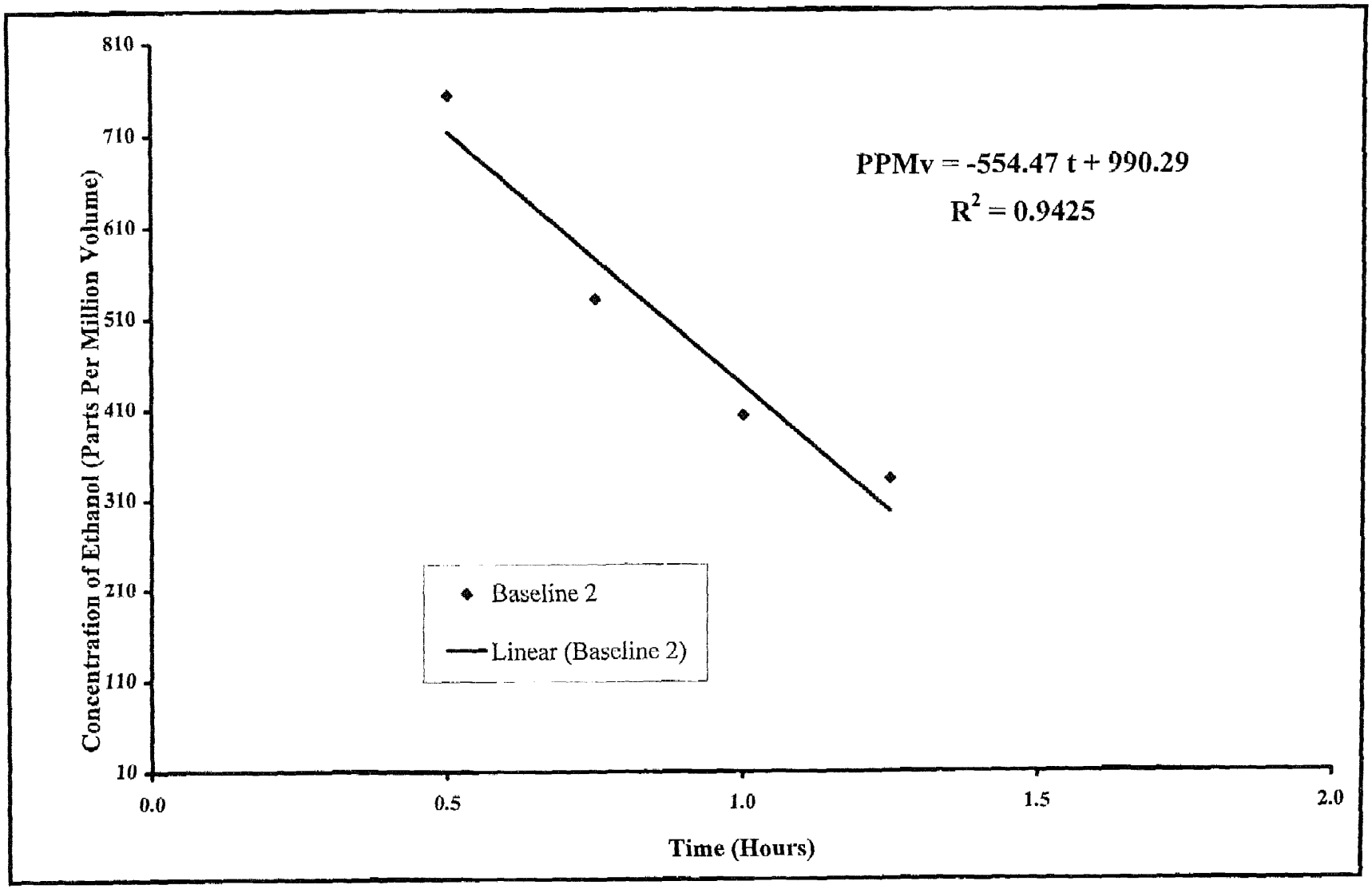

Figure B.7 Arithmetic Plot of Concentration of Ethanol Versus Time for the Constant Rate Region for Baseline Test (Run 2)

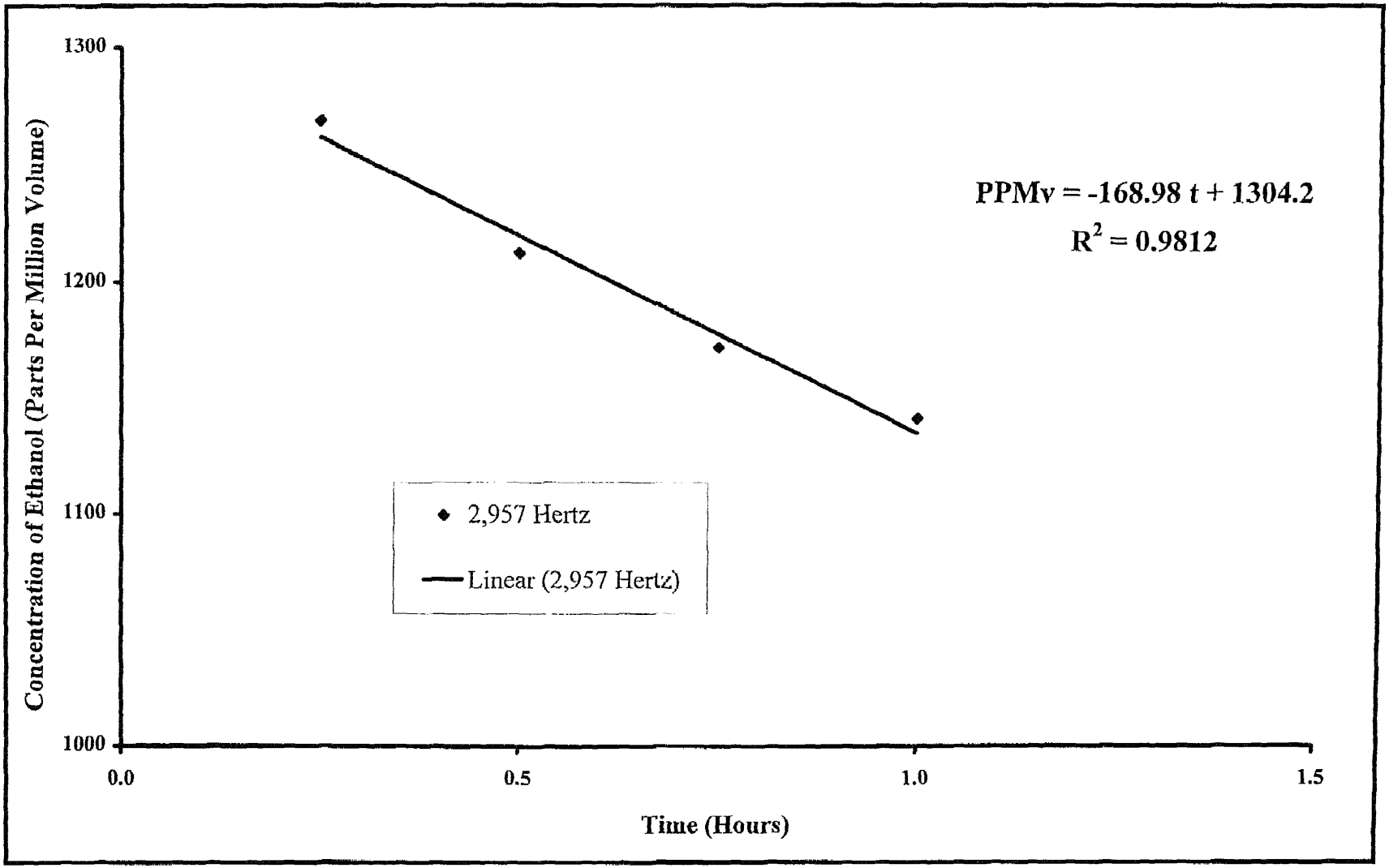

Figure B.8 Arithmetic Plot of Concentration of Ethanol Versus Time for the Constant Rate Region for a Frequency of 2,957 Hertz (Run 1)

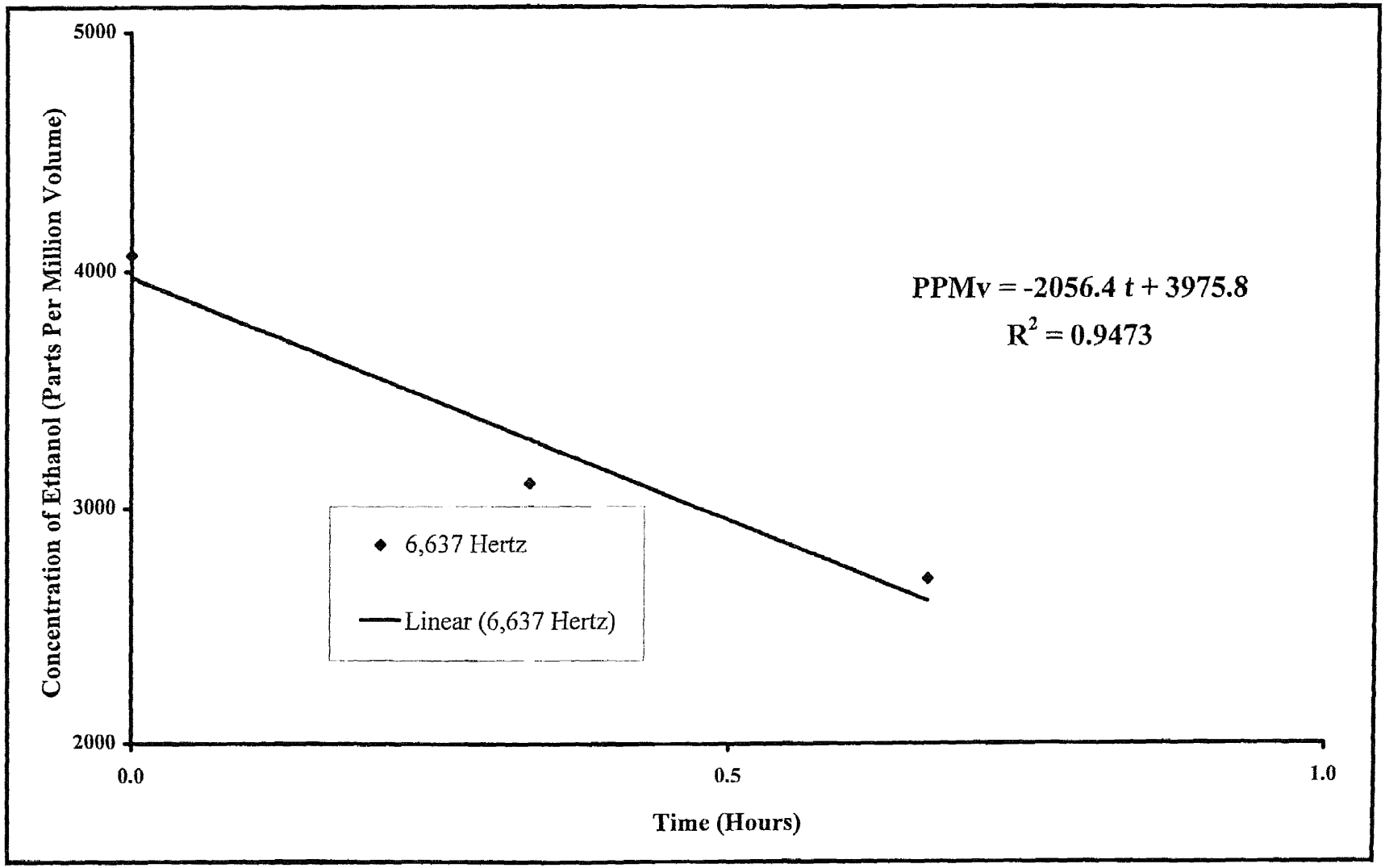

Figure B.9 Arithmetic Plot of Concentration of Ethanol Versus Time for the Constant Rate Region for a Frequency of 6,637 Hertz (Run 2)

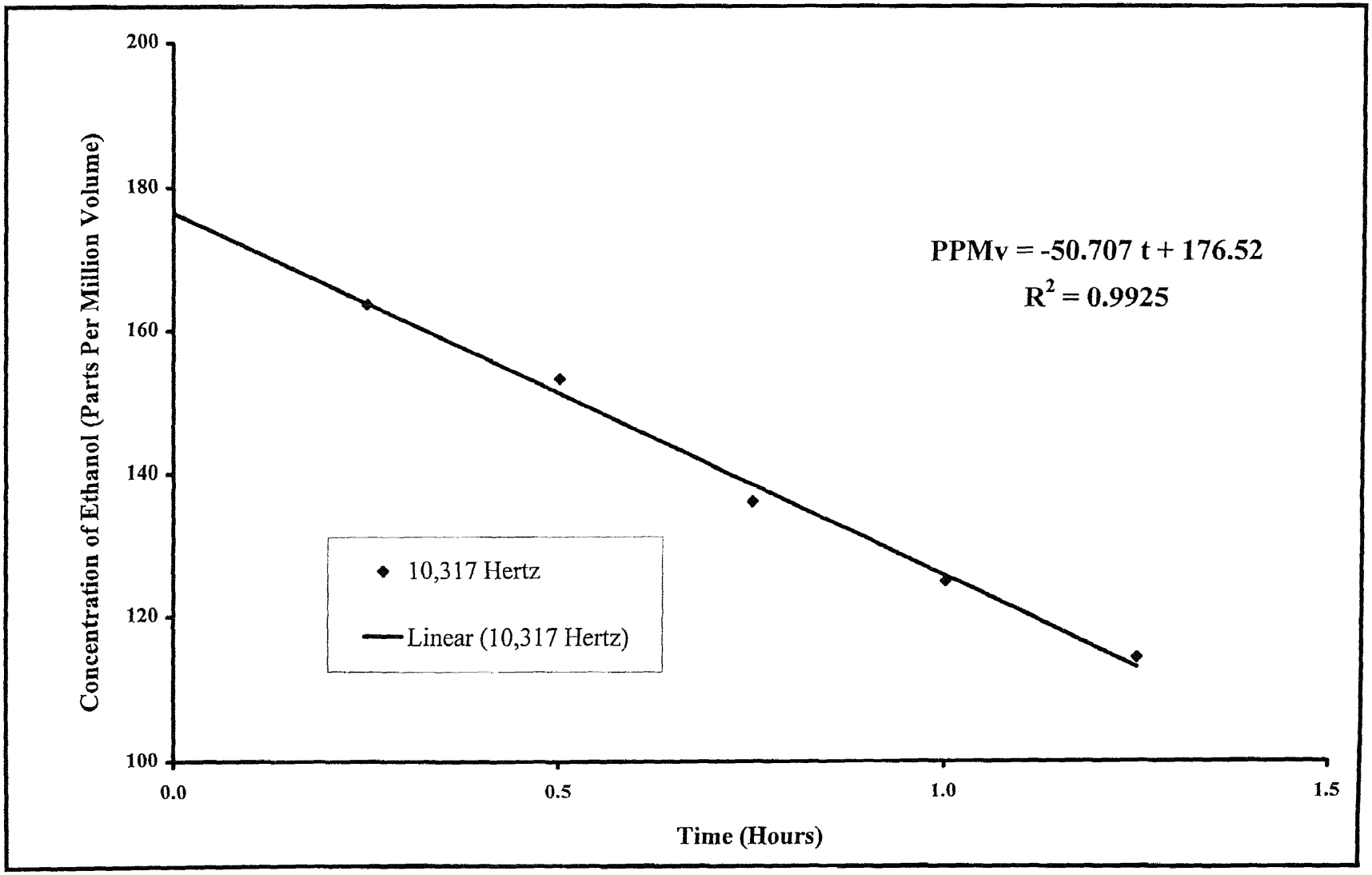

Figure B.10 Arithmetic Plot of Ethanol Versus Time for the Constant Rate Region for a Frequency of 10,317 Hertz

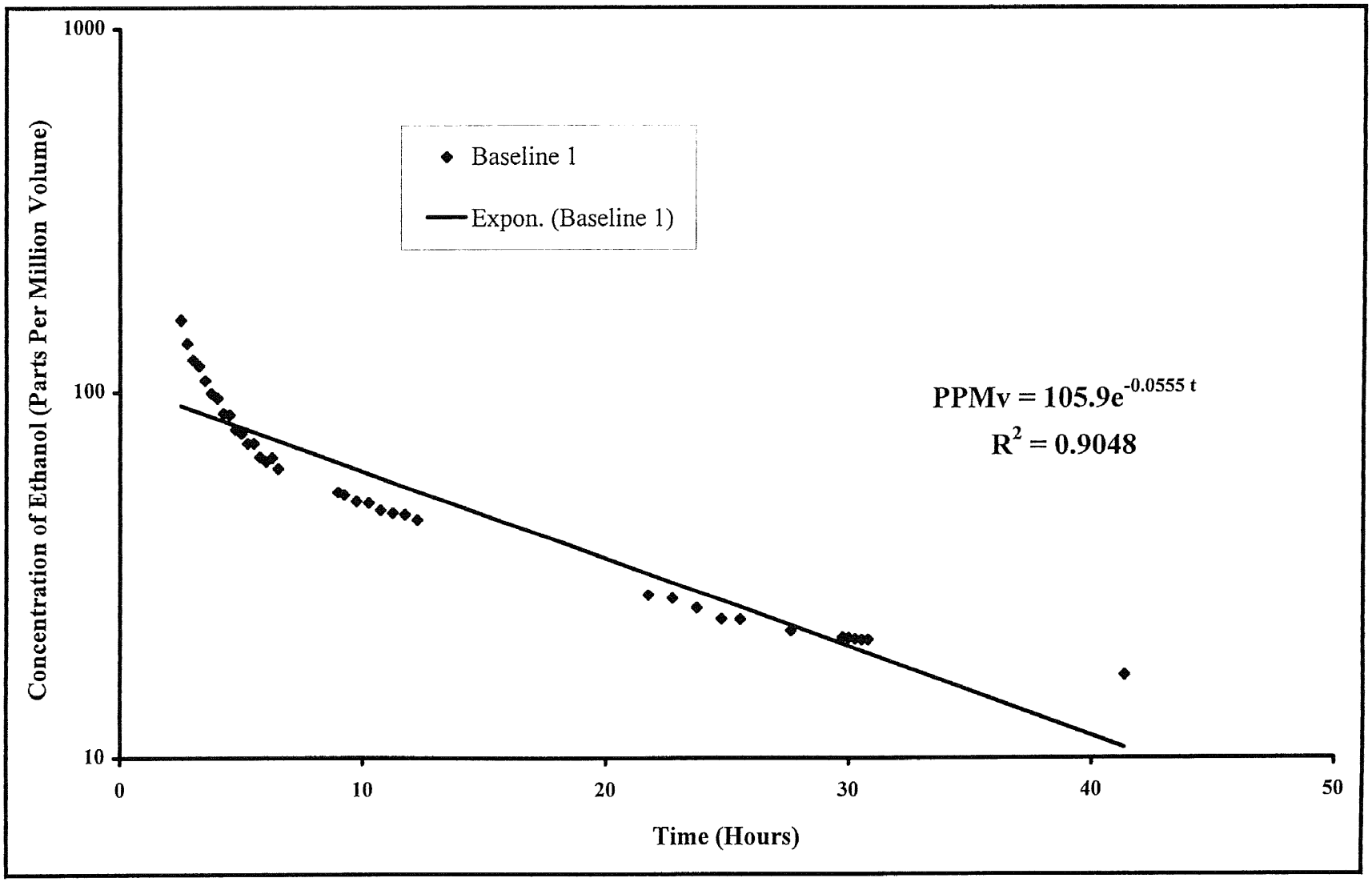

Figure B.11 Semi Logarithmic Plot of Concentration of Ethanol Versus Time for the Falling Rate Region for Baseline Test (Run 1)

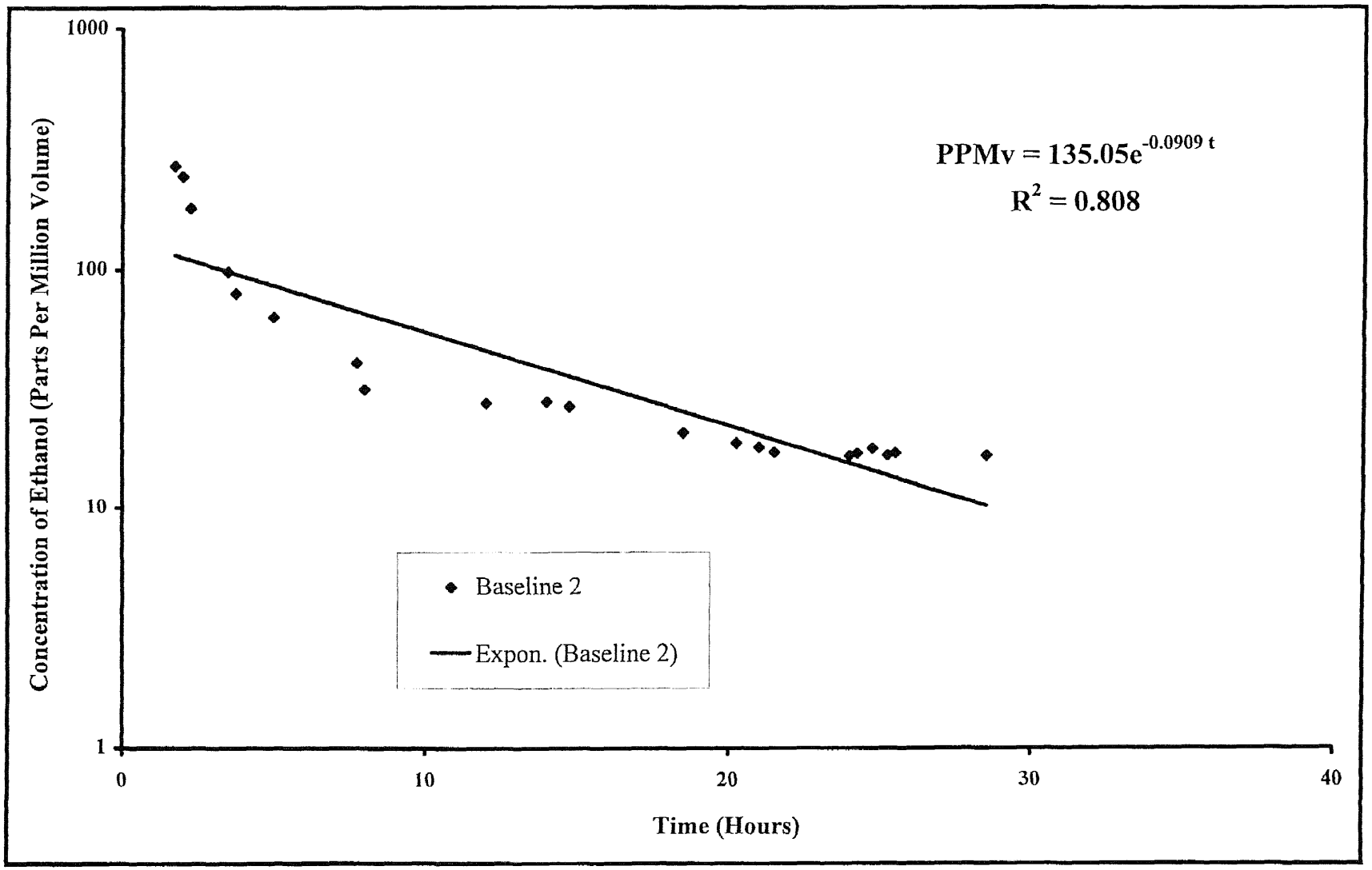

Figure B.12 Semi Logarithmic Plot of Concentration of Ethanol Versus Time for the Falling Rate Region for Baseline Test (Run 2)

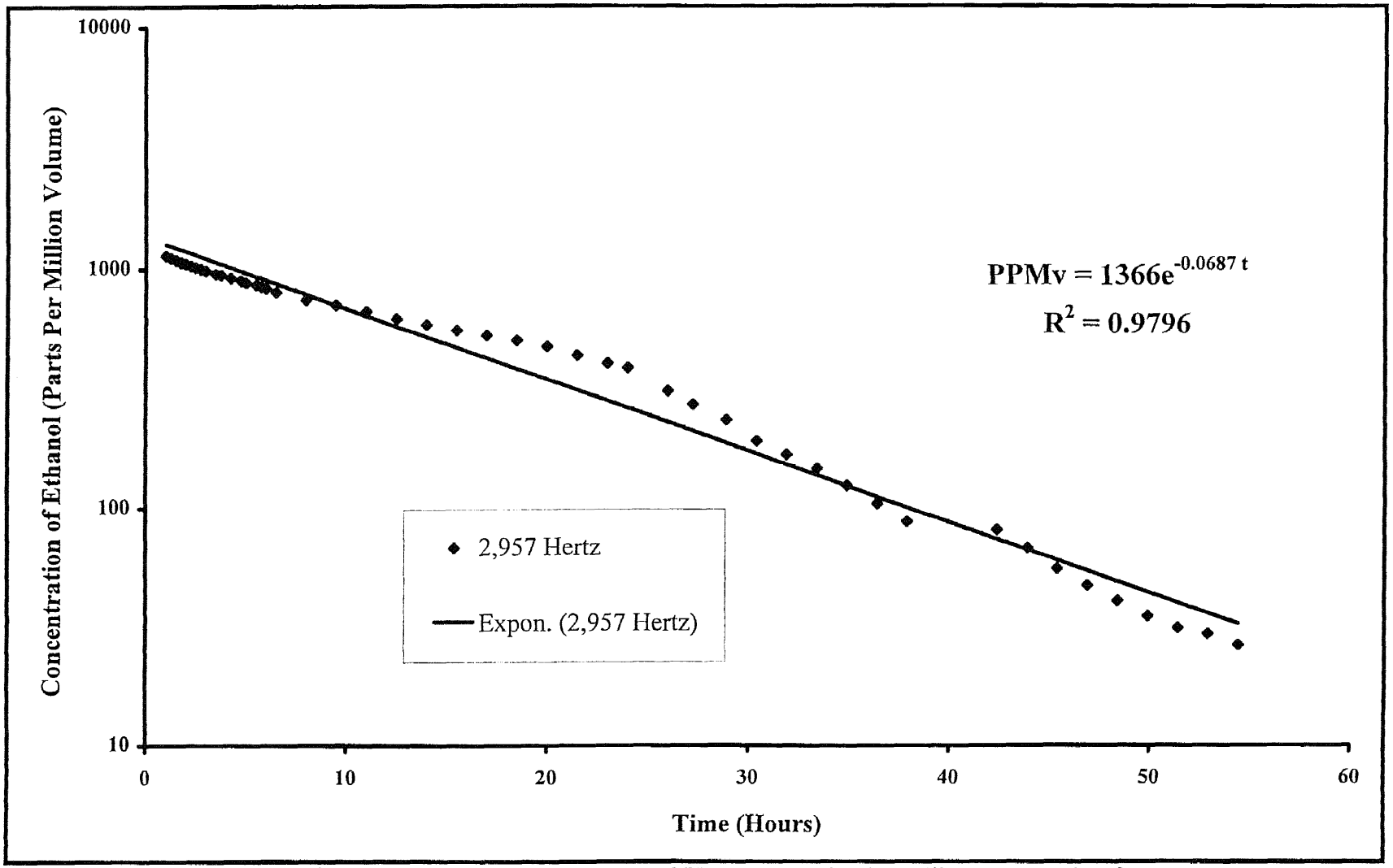

Figure B.13 Semi Logarithmic Plot of Concentration of Ethanol Versus Time for the Falling Rate Region for a Frequency of 2,957 Hertz (Run 1)

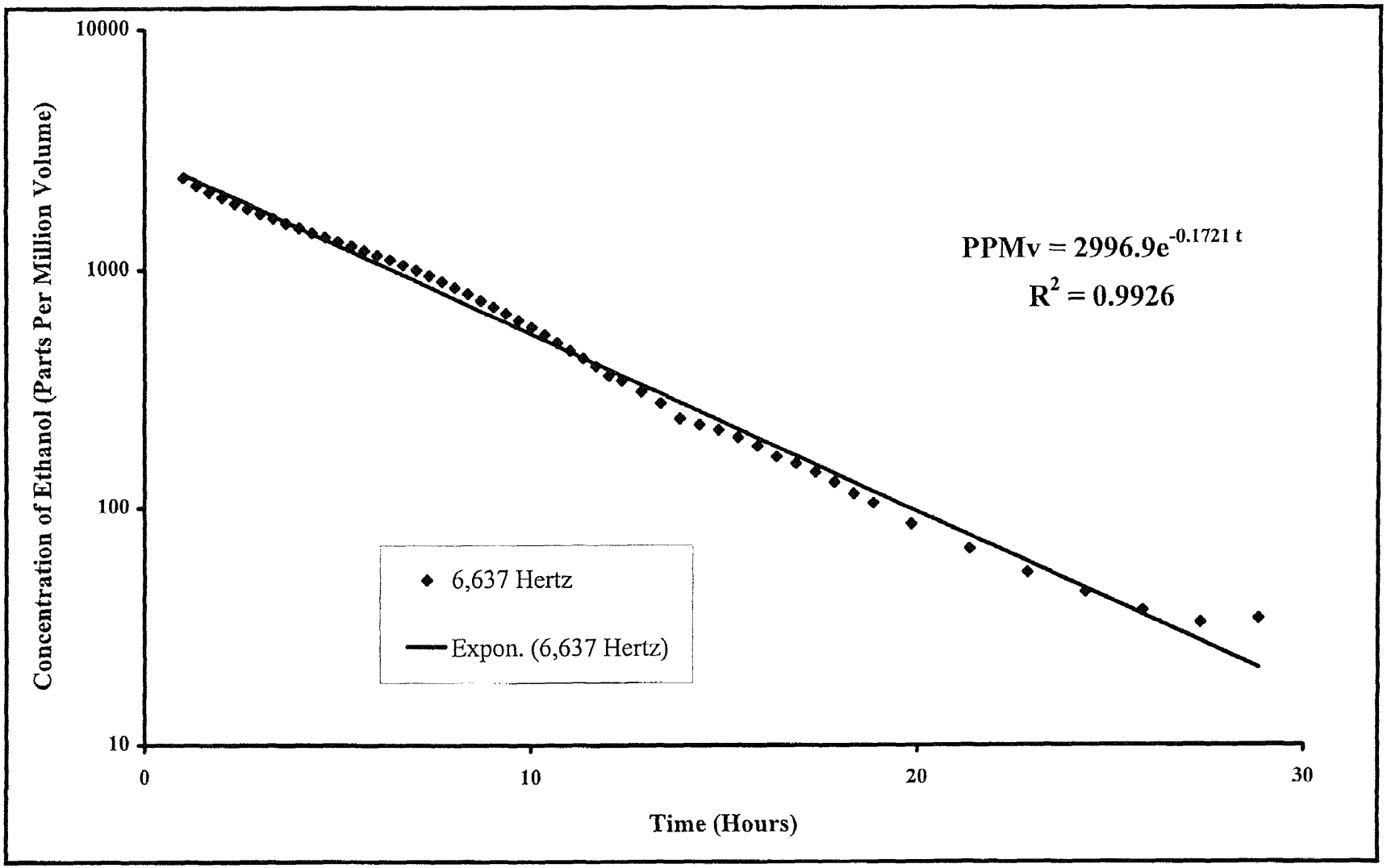

Figure B.14 Semi Logarithmic Plot of Concentration of Ethanol Versus Time for the Falling Rate Region for a Frequency of 6,637 Hertz (Run 2)

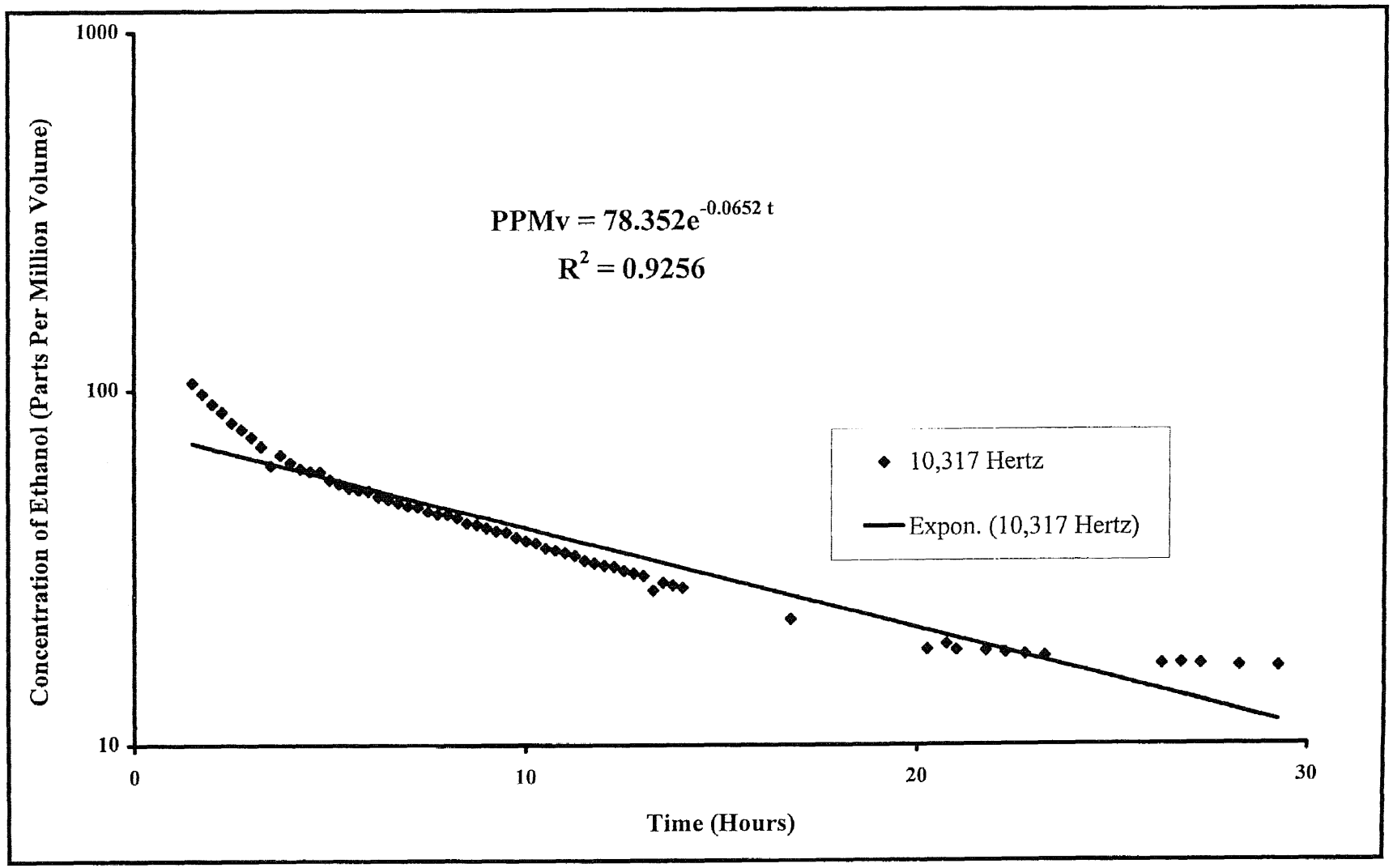

Figure B.15 Semi Logarithmic Plot of Concentration of Ethanol Versus Time for the Falling Rate Region for a Frequency of 10,317 Hertz

APPENDIX C

SAMPLE CALCULATIONS FOR THE DEPTH OF PENETRATION IN DRYING

As discussed in Chapter 4, the equivalent penetration depth of the siren is an important piece of information. Knowing the effective bed drying distance resulting from the sonic energy as an indication of the depth intervals, the sonic device can be placed appropriately in an actual field test to clean a site.

Since the siren is placed in the tank vertically and with the holes aligned to the fracture, 3 inches from the bottom of the tank, the distribution of the sonic energy follows a certain pattern. Figure B.1 shows the pattern of the distribution of dry and wet sand remaining in the tank after asymptotic value is reached.

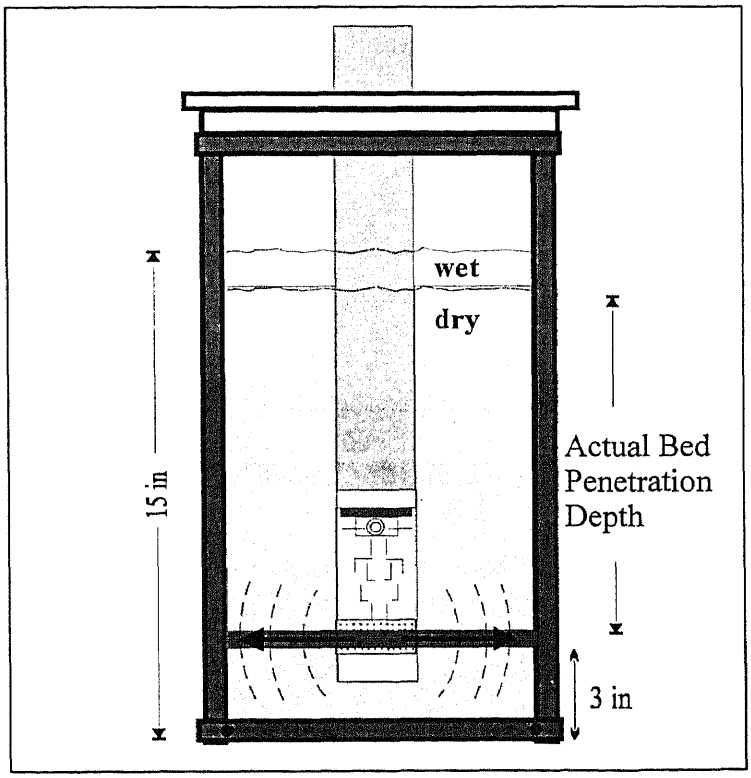

Figure B.1 Distribution of Sonic Energy in the Test Cell

Using data from the Baseline Test (Run 1) as an illustration, to estimate the equivalent penetration depth of the siren, the following information is needed:

- Free moisture level at time zero is 0.05378 lbs of contaminant per pounds of dry sand, this is taken from Table A.3.
- Free Moisture level remaining in the test cell after reaching asymptotic value is 0.009 lbs of contaminant per pounds of dry sand, this information can be found in Table 4.4.
- Measured height of the sand after assembly of the test cell which is 15 inches.

First calculate the weight of the moisture remaining in the test cell at the asymptotic value and its equivalent depth.

$$\frac{\text{total weight of mositure at } t=0}{\text{measured height of sand}} = \frac{\text{weight of moisture removed}}{\text{penetration depth}^*}$$

$$\frac{0.05424}{15} = \frac{0.05424-0.009}{\text{penetration depth}^*} \quad \Rightarrow \textit{Penetration depth} * = 12.511 \textit{ inches}$$

The actual bed penetration depth is the *penetration depth** calculated above minus ½ inch which is the thickness of the artificial fracture minus 3 inches of sand from the bottom of the tank. Therefore, the Actual Bed Penetration Depth is 9.011 inches.

APPENDIX D

DIGITAL VALVE SEQUENCE PROGRAMMER (DVSP)

The DVSP is a timer/programmer that is connected to the GC for its ability to perform remote operation of electrical devices such as solenoid valves. With 4 intervals available in different settable time ranges, the DVSP was very useful in helping the collection of data from the GC simpler (See Table D.1 for specifications).

Table D.1 Specifications of the DVSP (DVSP Manual)

General
3-wire power cord (2 meters)
Externally accessible 2A fuse
95-130 VAC, 25-60 HZ
2 or 4 intervals; settable from 0-99seconds, 0-0.9 minutes, or 0-99 minutes
DPDT relay contacts rated at 3 amps @ 120 VAC resistive load
Elapsed time displayed
Dimensions
11.8" x 6" x 2.4"
weight: 4 lbs
Accuracy
2.16 seconds/day maximum error
Temperature Range
0-70 °C
Power Consumption
110 VAC @ 50 mA
12 VDC @ 200 mA

As discussed in Chapter 3, the analysis of the sample was monitored throughout the experiment. Since the analysis was done in a frequent manner especially at the

beginning of each run, it was very helpful to automate the sequence of the cycles. A typical cycle with 4 sequences is shown in Table D.2.

Table D.2 A Typical DVSP Cycle

Interval	Time	Left Relay Activity	Right Relay Activity
1	15 seconds	Vacuum pump on	Valve to load
2	30 seconds	Vacuum pump on	Close 3-way valve
3	45 seconds	Vacuum pump on	Open 3-way valve
4	14 minutes*	Start integrator	Valve to inject

* Any length of time in the range of 14-99 minutes is advised.

Interval 1 is programmed to have 15 seconds to turn on the vacuum pump and prepare the 6-way valve to load. After the 15 seconds, during interval 2, the vacuum pump remains on while the 3-way valve closes. Then during interval 3, the pump is still on and the 3-way valve opens. Finally, 45 seconds later, interval 4 begins by first turning the pump off. Then, the 6-way valve opens and the sample is injected and the integrator starts integrating signals from the detector in the GC, making 15 minutes as the total time for the cycle. When the DVSP is in the AUTO mode, the cycle continues to repeat itself in the programmed sequence until it is manually turned off.

It is advised that intervals 1 to 3 are set for a short time such as 10-15 seconds each (such period of time is sufficient for their appropriate assigned activities). However, the last interval requires a special amount of time. The reason is that during interval 4, the sample is injected into the column and it requires

approximately 8-10 minutes to complete the analysis (with the GC set at the specified conditions as listed in Table B.3). Therefore, interval 4 can be set at any time range of 10-99, as 99 is the maximum settable time range given by the DVSP.

Since the results follow the trend of the typical drying theory, it is important to gather enough data in the very beginning of the experiment, especially during the constant drying period which is the first 2 to 4 hours as shown on Figures 4.26 to 4.30 (also as discussed in Section 4.1.2).

APPENDIX E

COMPARISON OF GRAIN SIZE AND PARTICLE SIZE ANALYSIS

As discussed in Section 3.2, two different sands were used in the experiment and the purpose of the grain size analysis was to compare the two sands and determine whether the difference in sizes contributed to differences in the results.

E.1 Equipment and Standard Sieve Trays Used

All of the sieve trays used for the analyses were U.S. sieves ranging from sieve number 14 to 200 (opening diameter ranging from 1.4 to 0.075 mm). A balance sensitive to 0.1 grams, an oven to dry the samples, and a mechanical shaker were other necessary items to complete the analysis.

E.2 Procedure to the Grain Size Analysis

The standard method, ASTM D1140-54 was used for the quantitative determination of the distribution of particle size in the soils (for reference, McCabe, Smith, Harriott 1993, was also used). The distribution of the particle sizes was determined by sieving since the particles were larger than 75 μm (retained on the No. 200 sieve). The sieve trays were arranged serially in a stack with the smallest mesh screen at the bottom and the largest at the top. The sample (dry and known weight) is then placed on the top of the first sieve tray and the stack was shaken mechanically for approximately 15 minutes.

The particles retained on each tray were removed and weighed, and the mass (g) of the individual increments are converted to mass percentages of the total sample mass. The particles that passed the finest sieve tray (No. 200) were collected in a pan at the bottom of the stack. The amount of sands used for the analyses were 337.9 g of original sand and 390 g of new sand. Tables E.1 and E.2 list the results of the grain size analyses of both sands.

Table E.1 Results of the Grain Size Analysis of the Original Sand, U.S. Sieve Series

Sieve No.	Sieve Opening (mm)	Mass Retained (g)	Percent Retained	Cumulative Percent Retained	Cumulative Percent Passing Through Screen
14	1.400	0.6	0.2 %	0.2 %	99.8 %
18	1.000	0.1	0.0 %	0.0 %	99.8 %
30	0.600	0.3	0.1 %	0.3 %	99.7 %
35	0.500	40.2	11.9 %	12.2 %	87.8 %
60	0.250	267.9	79.3 %	91.5 %	8.5 %
100	0.150	25.3	7.5 %	99.0 %	1.0 %
200	0.075	3.1	0.9 %	99.9 %	0.1 %
Pan		0.9	0.2 %	100.1 %	-0.1 %
			100.1 %	100.1 %	

Table E.2 Results of the Grain Size Analysis of the New Sand, U.S. Sieve Series

Sieve No.	Sieve Opening (mm)	Mass Retained (g)	Percent Retained	Cumulative Percent Retained	Cumulative Percent Passing Through Screen
14	1.400	0.0	0.0 %	0.0 %	100.0 %
18	1.000	0.0	0.0 %	0.0 %	100.0 %
30	0.600	6.6	1.7 %	1.7 %	98.3 %
35	0.500	196.5	50.4 %	52.1 %	47.9 %
60	0.250	185.5	47.5 %	99.6 %	0.4 %
100	0.150	1.7	0.3 %	99.9 %	0.1 %
200	0.075	0.2	0.1 %	100.0%	0. %
Pan		0.1	0.0 %		0.0 %
			100.0 %		

REFERENCES

Allen, C. H. and B. G. Watters, 1959. "Siren Design for Producing Controlled Wave Forms at High Intensities", *The Journal of the Acoustical Society of America*, 31(2):177:185.

Allen, C. H. and J. Rudnick, 1947. "A Powerful High Frequency Siren", *The Journal of the Acoustical Society of America*, 19(5):857:865.

Fernandez, H.J., 1997. "An Investigation Into the Feasibility of Utilizing Pneumatic Ultrasonic Devices Coupled With Pneumatic Fracturing In Enhancing Removal of Volatile Organic Compounds From Soils", M.S. Thesis, New Jersey Institute of Technology, Newark, New Jersey.

Geankoplis, C.J., 1993 Transport Process and Unit Operations, Fifth Edition, Simon and Schuster, Englewood Cliffs, New Jersey.

Hausman, E., and Slack, E. P., 1939. Physics, Second Edition, D. Van Nostrand Company Inc., New York, New York.

Manthey, W., Kroemer, N. and V. Magori, 1992. "Instrument Science and Technology, Ultrasonic Transducer Arrays for Application in Air", *Measurement Science and Technology*, 3:249-261.

Marks, Peter J., Wujcik, Water J. and Amy F. Loncar, 1994. "Remediation Technologies Screening Matrix and Reference Guide", Second Edition, EPA/542/B-94/013, NTIS PB95-104782, Aberdeen Proving Ground, Maryland.

McCabe, W. L., Smith, J. C., and Harriott, P., 1993. Unit Operations of Chemical Engineering, Fifth Edition, McGraw-Hill, Inc., New York, New York.

Sears, Francis W., Zemansky, Mark W., and Young, Hugh D., 1987. University Physics, Seventh Edition, Addison-Wesley Publishing Co., Reading, Massachusetts.

Walker J. Q., Jackson M. T. and J. B. Maynard, 1977. Chromatographic Systems Second Edition, Academic Press Inc., New York.

Wood, A. B., 1937. A Textbook of Sound, The Macmillan Company, New York, New York.